TECHNISCHE UNIVERSITÄT MÜNCHEN

Lehrstuhl für Ernährungsphysiologie

Transcriptional regulation of the peptide transporter 1 and its role in development in *Caenorhabditis elegans* assessed by proteome analysis

Kerstin Elisabeth Geillinger

Vollständiger Abdruck der von der Fakultät Wissenschaftszentrum Weihenstephan für Ernährung, Landnutzung und Umwelt der Technischen Universität München zur Erlangung des akademischen Grades eines

Doktors der Naturwissenschaften

genehmigten Dissertation.

Vorsitzender:	Univ.-Prof. Dr. D. Haller
Prüfer der Dissertation:	1. Univ.-Prof. Dr. H. Daniel
	2. Univ.-Prof. Dr. B. Küster

Die Dissertation wurde am 19.07.2012 bei der Technischen Universität München eingereicht und durch die Fakultät Wissenschaftszentrum Weihenstephan für Ernährung, Landnutzung und Umwelt am 30.10 2012 angenommen.

„Man muss das Unmögliche versuchen,

um das Mögliche zu erreichen.“

Hermann Hesse

Table of Content

1. Introduction

1.1. The fate of the nutrients

In *Caenorhabditis elegans* (*C. elegans*) a pharyngeal grinder processes the *E. coli* feeding bacteria. Once the food reaches the stomach and the intestine, different proteases initiate the digestion of the protein component. While in higher organisms the intestine is subdivided into different regions with different major functions, in *C. elegans* the intestinal structure is rather simple as it consists of only twenty cells, which are not only involved in absorption but also storage of macromolecules, in immune and stress responses[1]. Nevertheless, in all organisms the main task of the intestine is the digestion and the absorption of nutrients. Therefore, the intestinal epithelium is a highly specialized tissue. The brush border membrane (BBM) of epithelial cells contains various digestive enzymes (e.g.: peptidases) as well as transporters for the uptake of nutrients across the cell membrane[2]. These transporters differ greatly in their transport capacity, in transport mechanism and substrate specificity. Carbohydrates are broken down to monosaccharides by luminal amylases and membrane-bound glucosidases and SGLT1 (Sodium-dependent Glucose Transporter 1) in combination with members of the GLUT family transport the sugars into the cells[3,4]. Fats are first emulsified and provided in mixed micelles to various lipases for hydrolysis into free fatty acids and monoglycerides. Passive diffusion through the non-polar plasma membrane via fatty acid flip flop mechanism is one of the possible entry routes of fatty acids. In addition they can enter the enterocytes via specialized fatty acid transporters [5]. The breakdown of proteins in the lumen and at the BBM results in oligopeptides and free amino acids which are taken up by amino acid transporters and a transporter for oligopeptides designated as PEPT1[6]. While absorption of nutrients mainly occurs in the small intestine of mammals, the large intestine accomplishes electrolyte transport, largely sodium and chloride ions and subsequently water is absorbed[7].

1.2. Functions of the intestinal transporter PEPT1

PEPT-1 mediates the uptake of di- and tripeptides and does not transport any longer peptide-chains[8]. It is a low affinity high capacity transporter; whereas the only second

related transporter PEPT2 functions as a high affinity low capacity transporter with similar substrate specificity. The driving force for the translocation of di-and tripeptides from the gut lumen into the cytosol of the enterocytes is the electrochemical proton-gradient. PEPT1 is directly coupled to sodium movement[9,10] and Anderson et al. (2003)[11] showed the dependence of PEPT1 on the sodium proton exchanger NHE3, which is called NHX-2 in *C. elegans*. These proteins exchange protons for sodium ions in order to maintain the electrochemical gradient[11].

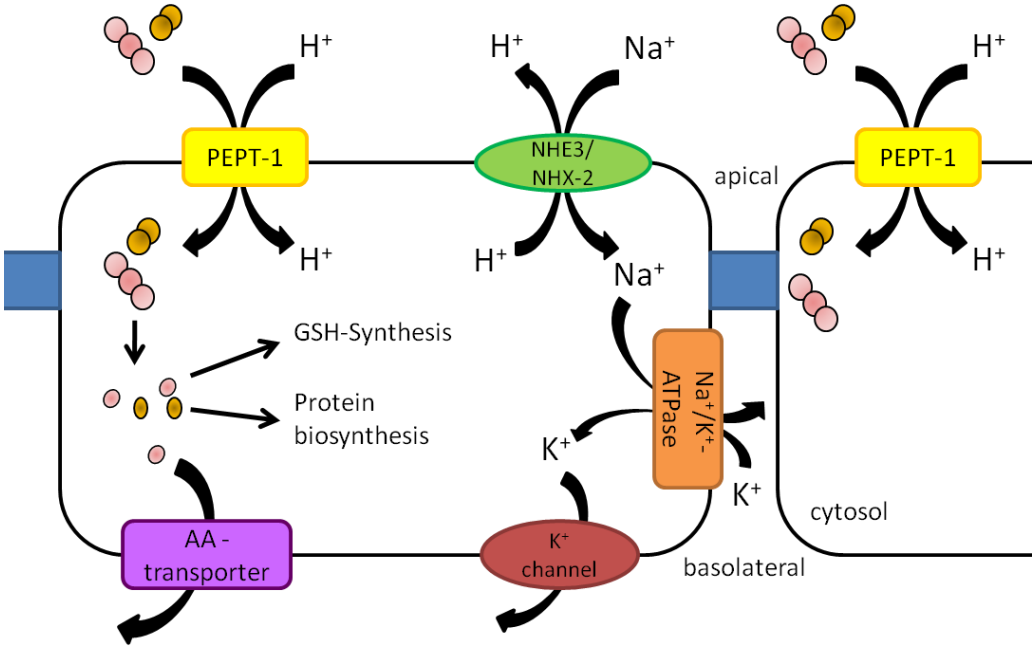

Figure 1: Schematic overview of di- and tripeptide uptake mediated by PEPT-1. In intestinal cells of *C. elegans* its activity is coupled to NHX-2 and in mammals to NHE3

In turn a Na+/K+ ATPase transports sodium ions from the cytosol to the intracellular space and potassium ions vice versa. Potassium ions can leave the cell again via potassium channels in the basolateral membrane (Figure 1) The di-and tripeptides are hydrolyzed by cytosolic peptidases releasing free amino acids of which the majority is exported at the basolateral side into circulation, while the rest is either metabolized or directly used for protein biosynthesis in epithelial cells.

1.3. PEPT-1: from the gene to the protein

In 1994 Fei et al. and Boll et al. reported cloning of the first proton-coupled oligopeptide transporter from rabbit, termed PEPT1[12,13]. Only one year later the rat *pept1* gene was cloned and characterized by Saito et al., while Liang and colleagues published the identification of the human *PEPT1* gene using a human intestinal

cDNA library[14,15]. Since then *PEPT1* has been cloned and/or characterized in various animals including zebrafish, atlantic cod, pig and mouse[16,17,18,19]. The human derived cDNA had a length of 2263 bp, harbouring an open reading frame of 2127bp. The primary amino acid sequence of 708 amino acids results in an assumed molecular weight of 78 kDa. Furthermore the hydropathy plot predicted 12 transmembrane domains (TMDs), with both termini located in the cytosol and a large extracellulare loop between TMD nine and ten. These predicted features were proved by epitope insertion studies[20]. Fei et al. cloned the mouse *PEPT1* gene in 2008[21] and comparison of the retrieved cDNA with its human homologue revealed a rather long 3` untranslated region of almost 1 kb. Otherwise the genes and the proteins show a strong similarity and an identity of about 83 % [16]. This high analogy between mouse and human *PEPT1* genes/ proteins is also observed in the regulation of expression and/ or protein function. Peptide substrates, as well as some amino acids were shown to increase mRNA levels in various species (goat, rat and human intestinal Caco2)[22,23,24]. In addition, hormones like leptin were found to increase *PEPT1* transcription, translation and function in mice, rats and human Caco2 cells (Supplement,Table 19)[25,26,27]. Other findings were more difficult to reproduce in different species, as seen for PPARα, which was proposed to be responsible for abrosia induced up-regulation of *PEPT1* mRNA and resulting protein[28,29]. Especially pharmaceutical companies showed a great interest in deciphering the regulation of PEPT1 protein function, as PEPT1 is responsible for the uptake of a large variety of drugs (for review see [30]). For instance the application of proton delivering polymers was shown to increase the uptake of the antibiotic cefadroxil[31]. Nevertheless, only three transcription factors (SP1, Cdx2 and DBP) were shown to directly bind to the *pept1* promoter, whereby SP1 is believed to drive basal expression in humans[32]. In contrast, control of the *pept-1* gene in *C. elegans* is largely unknown. Only McGhee et al. (2009) proposed a possible involvement of ELT-2 in the expression of *pept-1* during the differentiation of the intestine in worms[33].

Interestingly, PEPT1 abundance seems to be regulated during ontogenesis. Miyamoto et al. (1996)[34] focused on mRNA levels in the jejunum of rats and detected a rapid increase after birth peaking after ten days[34]. Shen et al. (2001)[35] reported similar changes in mRNA and protein levels of PEPT1 in all three segments of rat small intestine. Notably expression of PEPT1 in the kidney only showed a continuous rise, reaching a plateau after 14 days of development. This indicates that regulation

of PEPT1 levels in the small intestine may be of particular importance during ontogenesis[35]. This conclusion is emphasized by the cellular distribution of PEPT1 during ontogenesis. Immunohistochemistry detected PEPT1 not only at the brush border membran but also cytosolic and in the basolateral membrane of rat small intestine at birth[36]. Consistency between species provides a study employing turkey eggs, describing a steep increase of *pept1* mRNA levels at the time of hatching of the animal[37]. This was also seen in *C. elegans*, as highest *pept-1* mRNA levels were detected at the time of hatching followed by a steady decline towards adulthood[38].

1.4. Effects of *pept-1* deletions in mouse and *C. elegans*

Despite the demonstration of a pronounced regulation during ontogenesis, mice lacking PEPT1 did not show any changes in development, body weight and fertility. Neither on mRNA nor protein level compensatory mechanisms for example of amino acid transporters were found in the intestinal mucosa[39]. Interestingly, leptin levels were decreased in *PEPT1*$^{-/-}$ mice, while ghrelin and insulin levels remained unchanged. Metabolic parameters as in weight, food intake and feces excretion only showed genotype specific alterations between knock out and WT when mice were fed a high protein diet. Nevertheless, knock out animals showed changed amino acid levels in blood, which might reflect an altered nitrogen shuttling in liver as suggested by Nässel et al. (2011)[40,39]. In contrast to PEPT1-deficient mice, where plasma amino acid levels were increased, *pept-1* worms showed amino acid deficiencies. In addition, the *C. elegans pept-1* knock out strain (*pept-1(lg601)*) displayed a severe phenotype characterized by delayed postembryonal development, smaller bodysize, reduced brood size in combination with a prolonged reproductive period, elevated stress tolerance and increased fat content mainly consisting of short and medium chain fatty acids[41,42,43]. *De novo* synthesis of long-chain fatty acids was shown to be decreased, while utilizing a fluorescent fatty acid (BODIPY-C12) allowed demonstration of an increased uptake of free fatty acids in the intestine. This was proposed to result from an enhanced entry via the flip flop mechanism due to higher intracellular pH caused by the knock out of *pept-1*[44]. Although studies regarding the altered bodysize of *pept-1(lg601)* were conducted, involvment of DBL-1/TGF-β signaling pathway, a pathway already known to directly regulate bodysize, could not be found[41]. Regarding the elevated stress resistance, an additive effect caused by

the deletion of the insulin receptor gene *daf-2* was observed. Additional knock out of the forkhead transcription factor DAF-16, which is negatively regulated by the Insulin/IGF signlaing cascade reversed additive effects seen in the double knock out of the insulin receptor DAF-2 and PEPT-1.This was also demonstrated for brood size and generation time, implying different signaling cascades to be involved in generating similar phenotypes[41]. Experiments supplying *pept-1(lg601)* worms with additional free amino acids could only partially rescue the observed phenotype. While brood size of knock out animals increased significantly in the presence of free amino acids, postembryonal development time remained unchanged, indicating other factors than amino acid deficiency to be responsible for the delay[41].

1.5. Insulin/IGF-1 like Signaling (IIS)

Mammalian IIS is in the focus of academia and public, as Diabetes mellitus type 2 is emerging as a major chronic disease. Insulin, IGF-1 and IGF-2 can bind to one of the five possible receptor isoforms and therefore activate downstream cascades (Figure 2). Two isoforms of the insulin receptor (a and b) can either form homodimers, similar to the IGF-1 receptor, or interact with the IGF-1 receptor to form a hybrid receptor[45]. Once the ligand is bound to the dimers the tyrosine kinase domains cause autophosphorylation exposing docking sites for various protein substrates. Amongst them IRS-1 and IRS-2, which are to date the best studied. At this point signaling divides into two distinct branches. SOS/GRB2 mediated activation of Ras subsequently leads to the activation of ERK1/2 and therefore to enhanced transcriptional activity, as well as insulin expression in ß-cells[46,47]. In the second branch the phophoinostiol-3 kinase generates PI(3,4,5) triphosphate, which attracts PDK-1 and AKT to the plasma membrane allowing PDK-1 to activate AKT[48]. In turn, a large variety of substrates is phosphorylated by activated AKT, which in the case of GSK3β can lead to its inactivation or as seen for FOXO1 to its cytosolic retention (for review see [49]). The mammalian target of rapamycin (mTOR) and the subsequent regulation of protein synthesis at the step of translation initiation and elongation are regulated via AKT as well, whereas S6Kinase is also a target of PDK1[50].

The genome of *C. elegans* encodes over ten times as many insulin like peptides than are present in mammals but only one insulin like receptor has been identified[51], resulting in a simplified IIS cascade harboring the conserved basic principle. After agonist binding to DAF-2, the PI3K homologue AGE-1 is generating $PI(3,4,5)P_3$ leading to activation of PDK-1 and subsequently to the phosphorylation of a complex consisting of SGK-1, AKT-1 and AKT-2. Both serine/theronine kinases phosphorylate the IIS downstream target DAF-16, the only FOXO transcription factor in *C. elegans*, thus repressing its function[52]. Especially *daf-2* mutant strains evoked great attention as they exhibit up to threefold life span extension depending on the allele[53]. This life span extension can be totally repressed by an additional knock out of *daf-16*. The

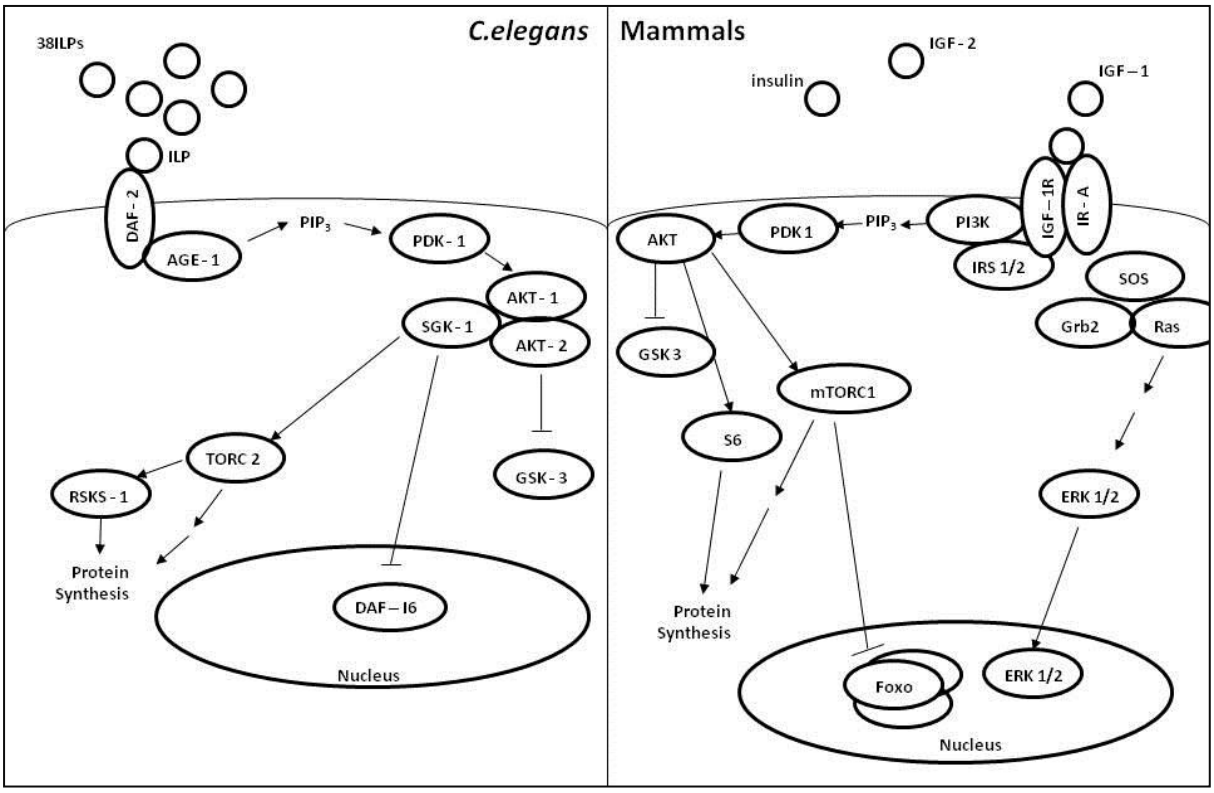

Figure 2: Schematic overview of Insulin/IGF-1 like signaling. On the left components of C. elegans cascade are depicted in comparison to mammalian IIS on the right.

FOXO transcription factor is known to regulate a large number of genes involved in metabolism (e.g. fat-7, gei-7), stress response (e.g. sod-3, ctl-1, gst-4) and aging (e.g. ins-7)[54] and reacts to various environmental factors such as heat shock, oxidative stress and starvation[55]. Constitutive active DAF-16 as seen in *daf-2* mutants results therefore in higher tolerance toward heat and oxidative stress. Interestingly, expression profiles of *daf-2(RNAi)* and *daf-2(RNAi);daf-16(RNAi)* treated worms also showed *pept-1* to be regulated. In addition three potential DAF-16 binding sites were predicted for the *pept-1* promoter[54].

1.6. Oxidative stress response

In *C. elegans,* DAF-16 is one of the major mediators of the oxidative stress response (OSR). The term oxidative stress is widely referred to as the imbalance between the antioxidant capacity and the free radicals and reactive oxygen species (ROS) formation[56]. ROS can either be produced intracellular as side products of the mitochondrial respiratory chain or are derived from exogenous sources. ROS were shown to act as second messengers in e.g. in lymphocyte activation[57,58]. To maintain the balance between the production and the detoxification of ROS non-enzymatic molecules act in conjuction with enzymatic scavengers. Nevertheless, oxidative stress defense can be overcome, leading to the damage of various macromolecules. Especially for molecules with a low turn-over, modification can have fatal effects, as for DNA, lipids or proteins[59,60]. Therefore, oxidative stress is associated with a variety of diseases (e.g. Alzheimer, Parkinson, vascular disease and diabetes)[61,62,63,64]. Several signaling pathways respond to oxidative insult orchestrating the oxidative stress response. Depending on the produced oxygen species, the concentration and the affected cell type, this can have several implications. Generally, low doses appera to increase mitogenic cell division, while intermediate concentrations lead to growth arrest and high doses even to apoptosis or necrosis[65]. In all cases, signaling cascades mainly mediate their response via activation of transcription factors, including NFκB, HSF1, p53, ERK and Nrf2[65,66]. Nowadays Nrf2 (nuclear factor erythroid 2-related factor 2), the so called “master regulator” of OSR, is in the focus of research also as a possible therapeutic target. Nrf2 binds to the antioxidant response element (ARE), which is conserved in the promoter region of a large set of genes encoding antioxidant or detoxification enzymes (e.g. NAD(P)H quinone

oxidoreductase 1 (NQO1) and glutamate-cysteine ligase (γGCS)) as well as proteasomal subunits. Thus, it can regulate their basal as well as stress induced expression[67]. Therefore, control of its activity is rather complex and under vivid investigation, whereas several chemical compounds are identified as Nrf2 modulators (e.g sulforaphane). Keap1, a component of an E3 ubiquitin ligase, directly binds to Nrf2 retaining it in the cytosol as well as targeting it for degradation to the proteasome. Upon oxidation reactive cysteine residues of Keap1 form disulfide bonds, allowing Nrf2 to dissociate and accumulate in the nucleus. Trafficking of Nrf2 is further influenced via phosphorylation by several kinases and acetylation. Protein kinase C acts on Nrf2 at the Ser40 residue influencing the release of Keap1 as well as its transcriptional acitivity[68,69]. While the biological relevance of MAPK dependent phosphorylation is still discussed controversial[70], acetylation of Nrf2 was shown to influence DNA binding specificity[71]. Nrf2 can not only form homodimers but also interact with other bZIP family members adding to the possibility of gene specific regulation of expression[72]. Main interaction partners are the small Maf proteins (MafF, MafG and MafK)[73]. Furthermore interaction of Nrf2 with CBP amplifies transcriptional activation; direct binding of ATF3, however, is able to suppress this effect by displacing CBP form the ARE[74].

In contrast to the mammalian Nrf2, the *C. elegans* homologue SKN-1 binds in a monomeric fashion via its basic region resembling those of bZIP proteins to DNA[75,76,77]. However, the regulation of SKN-1 and identified target genes showed great similarities. WDR-23 interacts with the CUL-4/DDB-1 ubiquitin ligase and targets by direct binding SKN-1 for degradation[78]. In addition phosphorylation by glycogen synthase kinase-3 (GSK-3) retains SKN-1 in the absence of oxidative stress in the cytosol[79]. As seen for DAF-16, activation of IIS results in repressive phosphorylation by the kinase complex SGK1, AKT1 and AKT-2[80]. Additionally other kinases are implicated in the activation of SKN-1 in response to stress. The p38 MAPK pathway induces SKN-1 activation by MPK-1 mediated phosphorylation[81]. Additionally MKK-4, NEKL-2, PDHK-2 and IKKε-1 were shown to positively affect SKN-1 activity[82]. Interestingly, proteasomal dysfunction as well as translational inhibition induce SKN-1 mediated stress responses[83,84]

1.7. Unfolded Protein Response (UPR)

Translational inhibition as well as proteasomal dysfunction are associated with the unfolded protein response (UPR), which is thought to restore ER homeostasis by decreasing the incoming protein load and by up-regulation of ER-protein folding machinery. A connection between OSR and UPR is also implicated by the interaction of ATF4 with Nrf2 in mammals[72]. Accumulation of misfolded polypeptides in the ER as well as in the mitochondria results in the so called unfolded protein response (ER UPR and mtUPR), whereas in the following ER UPR is referred to as UPR. Signaling from the ER to the nucleus is mediated by increased binding of Grp78/BiP to unfolded polypeptides and the subsequent dissociation from the ER-luminal domains of ATF6α/β, IRE1α/β and PERK[85]. Thus, ATF6 translocates to the Golgi complex, where it is cleaved by proteases, releasing the cytosolic bZIP domain. Upon dissociation of Grp78/BiP oligomerization domains like IRE1α/β and PERK are unmasked and undergo homodimerization[86,87]. Active IRE1α/β splices mRNA of *XBP-1*, allowing translation of a functional transcription factor. PERK is on the one hand responsible for the activation of Nrf2[88] and on the other hand inhibits eIF2α action, shutting down global protein synthesis[89] but progressing *ATF4* mRNA

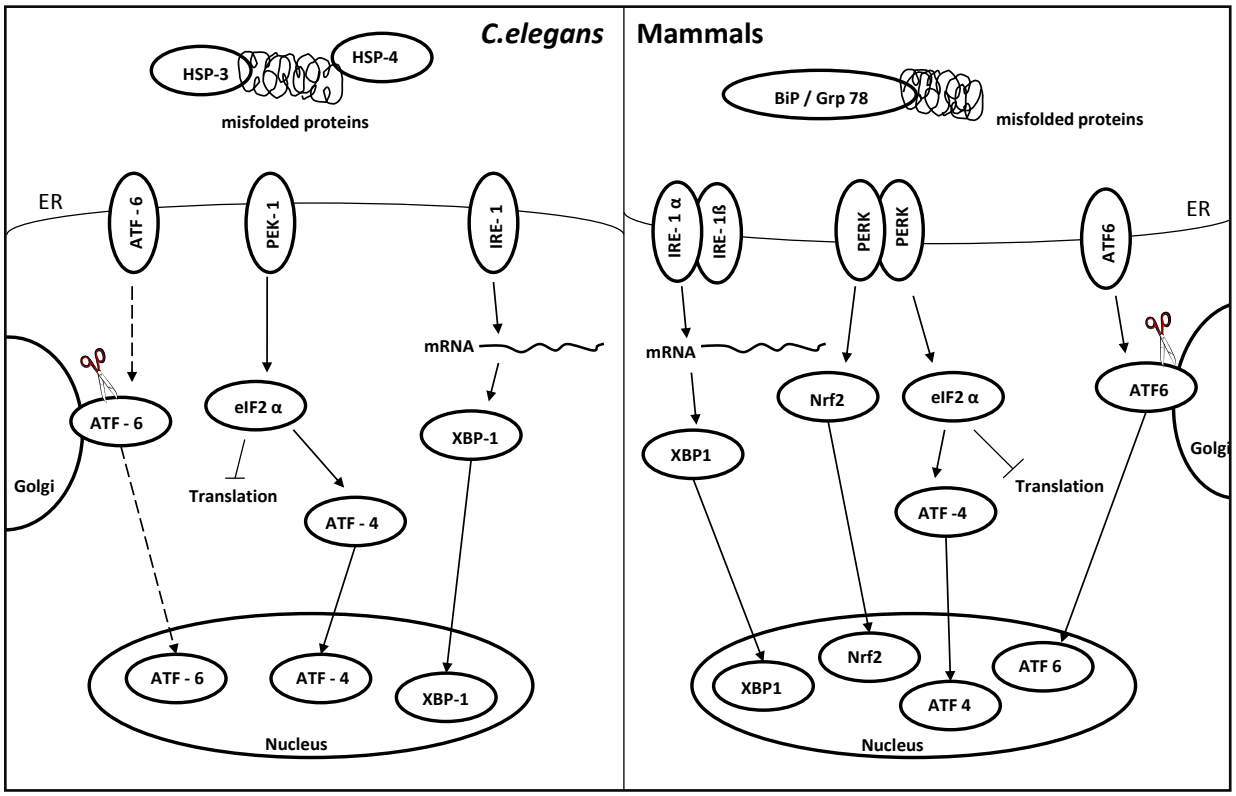

Figure 3: Schematic overview of unfolded protein response. On the left signaling of UPR in *C. elegans* is shown. Dotted line represents proposed mechanism with no experimental evidence. On the right side mammalian signaling cascades involved in UPR are depicted.

translation[90]. Hence, UPR signaling comprises three major branches regulating the expression of a variety of target genes involved in protein folding, ER associated degradation (ERAD I and ERAD II), amino acid metabolism, antioxidant response and lipid synthesis[85]. ERAD I comprises the ubiquitin-proteasomal system for protein degradation, while during ERAD II protein aggregates are degraded by the autophagy/ lysosome pathway[91]. However, ER stress can also result in apoptosis if ER homeostasis cannot be restored. Is this the case, JNK activated by IRE1α/β, inhibits proteins of the anti-apoptotic Bcl-2 family and activates pro-apoptotic BH3 only proteins, while ATF4 up-regulates CHOP expression[92,93,94](Figure 3).

In *C. elegans,* this stress response pathway is largely conserved, as homologues of the major transmitters XBP1, PERK and ATF6 were identified in the nematode as XBP-1, PEK-1 and ATF-6 respectively[95,96]. However, *C. elegans* only expresses IRE-1 while in mammals two isoforms are found (IRE1α and IRE1β). The same is seen for the expression of ATF-6. In contrast two homologues of the chaperone BiP/Grp78 were found in *C. elegans*, namely HSP-4 and HSP-3[97]. As in mammals, nematodes repress overall protein synthesis by phosphorylating eIF2α, which also leads to the induction of *atf-4* mRNA translation[98]. ATF-6 seems to contribute only marginally to the UPR in C. elegans, as the knock down hardly influence the induction of UPR target gene expression[97,99]. Therefore, the main branch of the stress response shifted from IRE-1/XBP-1 in nematodes to ATF6 in mammals, as basal as well as tunicamycin induced *hsp-4* expression is dependent on IRE-1 and XBP-1 in *C. elegans*, while CHOP expression in IRE1 defective cells still responded to ER stress[96,100]. Until now, a homologue of CHOP itself was not identified in *C. elegans*. However, apoptotic pathways, similar in the core mechanisms[101,100], seem only to be active during development of *C. elegans* larvae as well as in the gonad of the adult hermaphrodite. Taking into account that necrotic cell death of intestinal cells was observed after tunicamycin treatment[100] it is unlikely that induction of ER stress results in apoptotic cell death in *C. elegans*.

2. Aim of the work

PEPT1 is the only transporter for di and tripeptides in the intestine of *C. elegans* as well as in mice and humans[41,102]. Its expression was shown to be modulated by a variety of conditions and factors, although the molecular mechanisms are largely not understood. In contrast to mice, *C. elegans* display a very strong phenotype after deletion of *pept-1*. This led to the assumption that the importance of PEPT-1 may extend beyond its role in maintaining amino acid homeostasis in this organism. To assess *pept-1* transcriptional regulation in *C. elegans* initially an *in silico* analysis of the promoter region to identify potential transcription factor (TF) binding sites was performed. In addition, the putative influence of homologues of TF´s already known to regulate *PEPT1* in other species was investigated (see supplement Table 19). *Pept-1* promoter (P*pept-1)* activity was assessed in a P*pept-1*::GFP expressing strain after down regulation of potential TF´s using RNAi. Alterations of mRNA and protein levels were measured and dipeptide uptake was determined for analysis of functional impairments.

To answer the question whether TF´s found in *C. elegans* are also relevant for the transcriptional regulation of PEPT1 in mammals, cell culture experiments, as well as first experiments in mice were conducted. Furthermore, the activity status of candidate transcription factors was modulated by administration of various stimulators.

As amino acid supplementation could not rescue the retarded development of *pept-1(lg601)* worms, *pept-1* might influence signaling cascades by other than those affected by amino acid deficiency. Previously published transcriptomic data of *pept-1(lg601)* and WT did not help to clarify possible mechanisms[103]. Therefore, it was the aim of the present project to identify mechanisms leading to a delay in larval development of *pept-1(lg601)* animals at the protein level. Hence, quantitative proteomics on the basis of ^{15}N metabolic labeling was engaged to study dynamic changes during ontogenesis of WT as well as *pept-1(lg601)*.

3. Results

In the following sections results will always be presented using a color code. Blue represents promoter activity which was determined in *C. elegans* by measuring GFP expression under the control of a 2.4 kb sequence upstream of *pept-1* gene. In HepG2 cells reporter construct assays were employed using various length of the *PEPT1* promoter fused to the luciferase gene. Green depicts mRNA levels detected using qRT-PCR. In all samples of *C. elegans ama-1* was taken as housekeeping gene, while for Caco2 experiments *GAPDH* was used if not otherwise stated. Protein abundance (yellow bars) was measured using Western Blot technique probed either with *C. elegans* specific anti-PEPT-1 or a human specific PEPT1 antibody, both generated in house. Loading control if not otherwise stated was in both cases actin. Transport activity is shown in red and was either measured using the fluorescent dipeptide β-AlaLys-AMCA (*C. elegans*) or by using radioactively labeled ^{14}C-GlySar in Caco2 cells. Corresponding controls for each experiment were set to 1 and changes in *pept-1/PEPT1* expression, abundance or function are depicted as fold change ± SEM. If not stated otherwise at least three independent measurements were performed and statistical analysis was done using unpaired t-test. * indicates $p<0.05$, ** $p<0.01$ and *** $p<0.001$.

3.1. Regulation of *pept-1* expression in *C. elegans*

3.1.1. *In silico* analysis of the *C. elegans pept-1* promoter

In the work of Meissner et al. (2004) a promoter construct of *pept-1* was established to identify organ specific *pept-1* gene expression in *C. elegans*. The gene encoding the green fluorescence protein (GFP) was fused to a 2.4 kb region upstream of the transcriptional start. To determine whether the promoter sequence is conserved, an alignment with related *Caenorhabditis* species was conducted. As the alignment showed best conservation in the first ~ 600 bp upstream of the transcriptional start, transcription factor binding sites were predicted using MatInspector, TRANSFAC and TESS in this part of the sequence. All three software packages identified two possible SKN-1 binding sites. Both showed conservation in all investigated species in the core binding sequence, whereby the second binding site had the highest conservation between related species (Figure 4). These predictions fit well with the observed SKN-1 binding site distribution of two to four in a region of about 1kb upstream of various genes [75], suggesting a possible biological relevance.

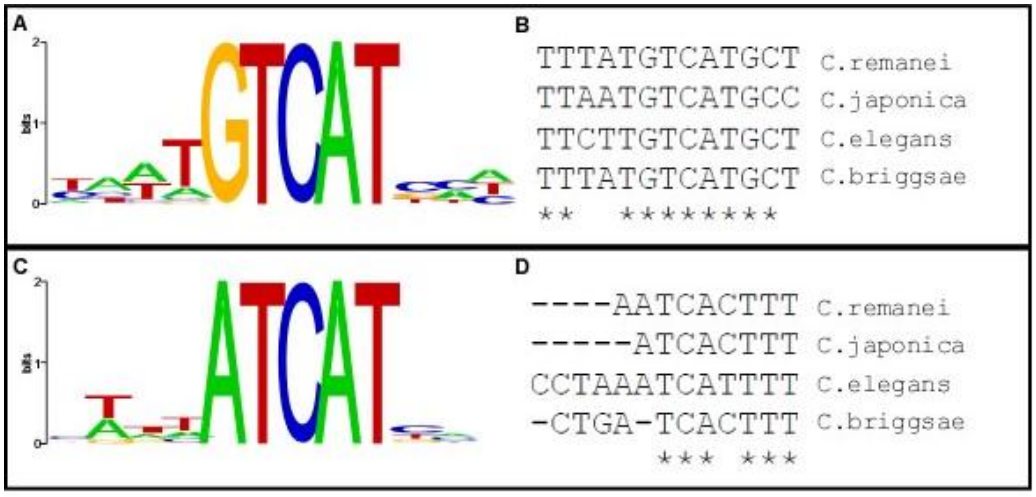

Figure 4: Predicted SKN-1 binding sites in *pept-1* promoter: (A) Matrix of SKN-1 binding site which was **(B)** found to be conserved in related *Caenorhabditis* species. **(C)** Matrix of second predicted SKN-1 binding site **(D)** with conservation between related species. Matrices were retrieved from TESS.

3.1.2. SKN-1 driven *pept-1* expression in *C. elegans*

Analysis of the *pept*-1 promoter revealed two possible SKN-1 binding sites. However, decreased SKN-1 due to *skn-1*(RNAi) did not alter promoter activity of P*pept-1* in relation to vector control (VC) treated worms, neither a change in mRNA nor protein levels was observed. In contrast, an increase in SKN-1 abundance due to down regulation of WDR-23, which is supposed to be part of the CUL-4/DDB-1 ubiquitin ligase complex that subjects SKN-1 to degradation [78], did result in an elevation of *pept-1* promoter activity, increased mRNA levels and protein abundance (Figure 5).

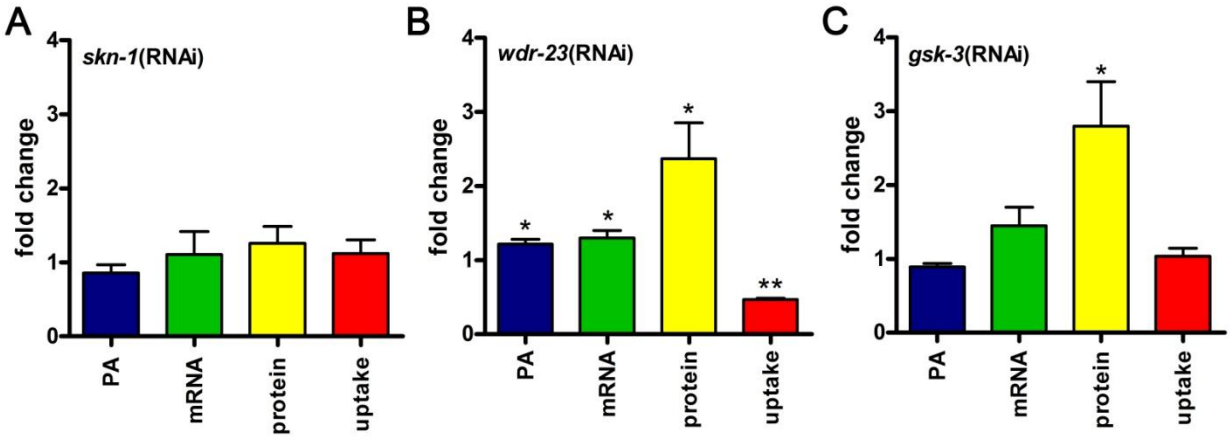

Figure 5: Effect of regulations *of* SKN-1 on *pept-1* expression: N2 or BR2875 P*pept*-1:GFP worms were grown on **(A)** *skn-1*(RNAi), **(B)** *wdr-23*(RNAi) and **(C)** *gsk-3*(RNAi) for 7 days before either promoter activity, mRNA, protein levels or uptake rate of *pept-1* were determined.

Under normal conditions, SKN-1 is inhibited via phosphorylation mediated by GSK-3[79]. Release of this inhibitory influence using RNAi treatment, again resulted in increased mRNA levels and an even higher PEPT-1 abundance, although no change in promoter activity was detectable. However, the function of PEPT-1 employing the fluorescent di-peptide β-AlaLys-AMCA did not show any change after *skn-1*(RNAi) and *gsk-3*(RNAi), while *wdr-23*(RNAi) surprisingly decreased uptake by half (Figure 5).

Upon oxidative stress SEK-1 enhances SKN-1 activity[104]. MPK-1 also positively regulates SKN-1 in response to stress[81] while phosphorylation by AKT-1 has inhibitory effects[80]. Down regulation of these kinases did not alter PEPT-1 protein abundance (Figure 6). As SKN-1 is one of the major facilitators of the oxidative stress response, wild type worms were treated with 10 mM hydrogen peroxide, 1 % sodium azide or as control in M9 buffer for 15 minutes with 4 hrs of recovery on fresh OP50 seeded NGM plates. PEPT-1 protein levels were detected using Western Blot and

revealed for both treatments an increase compared to control, although this change did not reach the level of significance (Figure 6).

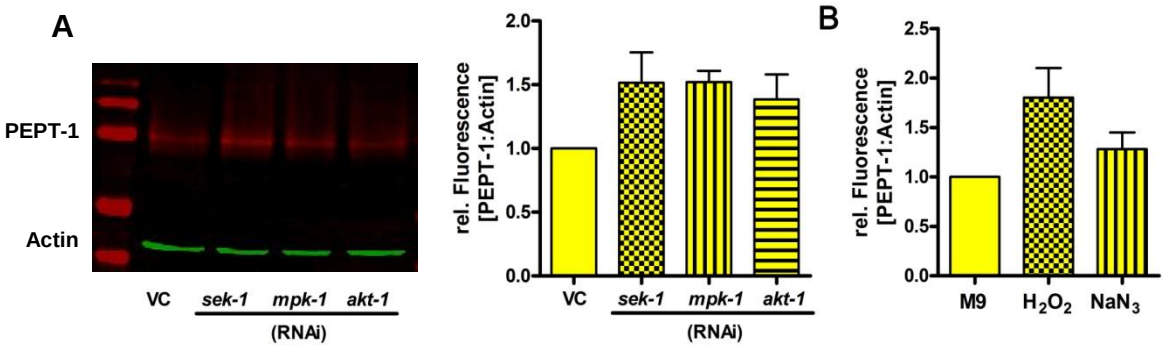

Figure 6: (A) Effect of RNAi of kinases regulating SKN-1 on PEPT-1: PEPT-1 protein levels detected using Western Blot after treatment with indicated RNAi. **(B) Oxidative stress influences PEPT-1 levels:** N2 worms treated for 15 min with 1 mM H_2O_2 or 1 % NaN_3 followed by 4 hrs recovery before protein extraction for western blotting. Two individual experiments are depicted ± SEM

To clarify possible interactions with other transcription factors we tested the influence of *gsk-3*, *wdr-23* and *skn-1*(RNAi) on DAF-16 translocation using a *C. elegans* strain expressing a DAF-16::GFP fusion protein (TJ356). None of the tested RNAi constructs did show any significant change in the localization pattern of DAF-16 (Figure 7).

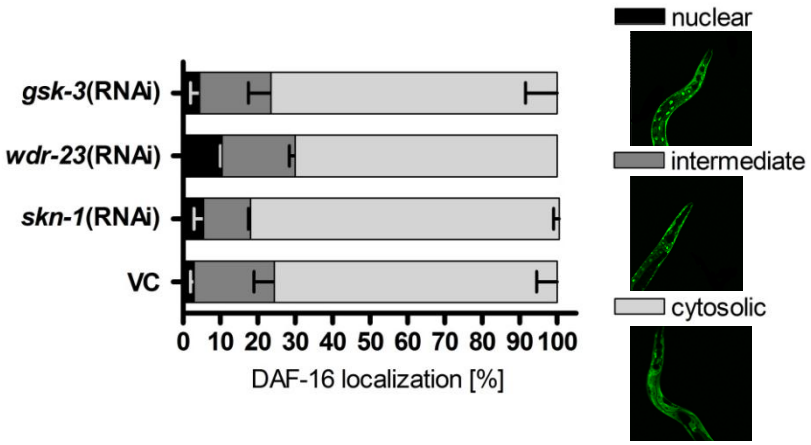

Figure 7: DAF-16 localization after *skn-1, wdr-23* and *gsk-3*(RNAi): TJ356 expressing DAF-16::GFP were grown on indicated RNAi and localization of DAF-16 was at least in 100 animals per experiment scored. Two individual experimets ± SEM

3.1.3. DAF-16 and its capacity of regulating *pept-1* promoter in *C. elegans*

Not only oxidative stress regulates SKN-1 activity but also Insulin/IGF like signaling, whereby phosphorylation of SKN-1 by SGK-1 and AKT-1/2 inhibits its action. It was therefore assessed whether *pept-1* gene expression and corresponding protein levels are changed upon silencing of *daf-2* or in IIS mutant strains. In contrast to the expected elevation due to increased nuclear SKN-1 accumulation in *daf-2(e1370)* or

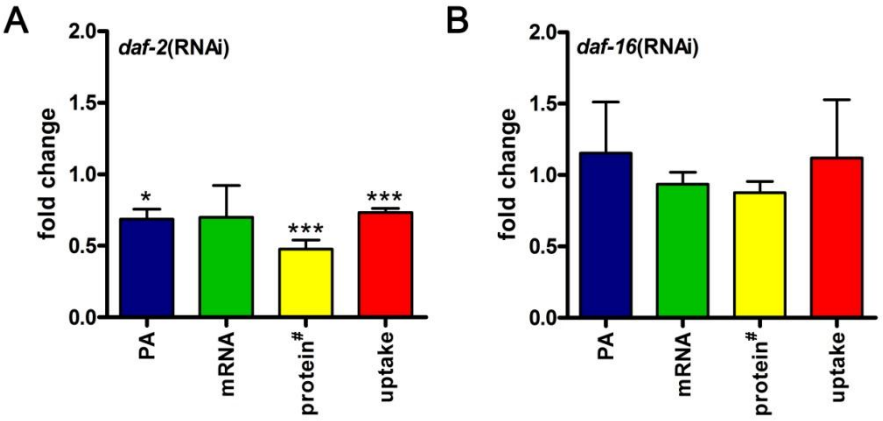

Figure 8: Effect of (A) *daf-2*(RNAi) and (B) *daf-16*(RNAi) on *pept-1* expression: N2 were grown on RNAi for 7 days before P*pept-1*:GFP, mRNA, protein and uptake were determined. Three independent experiments represented ±SEM. # PEPT-1 protein levels were assessed in *daf-2(e1370)* and *daf-16(mu68)* mutant strains. N2 was used as control.

daf-2(RNAi) treated nematodes, promoter activity dropped to about 70 % compared to control. The same was seen for *pept-1* mRNA levels, while protein abundance declined even more leading also to a decreased ß-AlaLys-AMCA uptake (Figure 8).

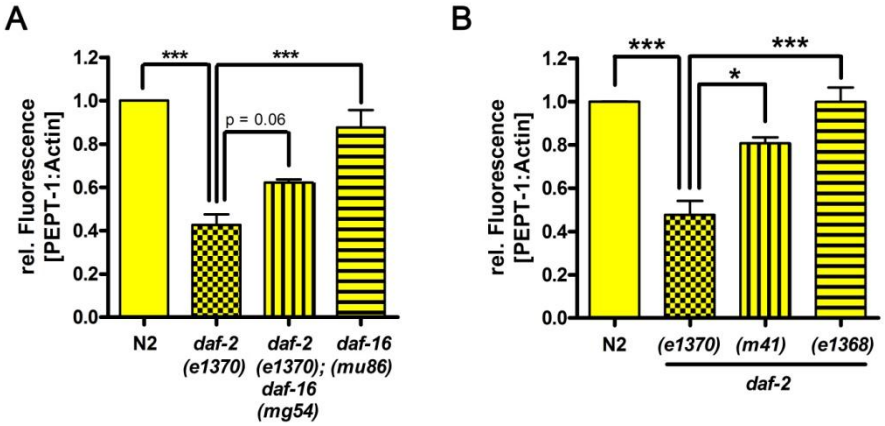

Figure 9: PEPT-1 abundance varies in IIS mutant strains: (A) PEPT-1 abundance depending on DAF-16 **(B)** PEPT-1 abundance depending on *daf-2* allele: Protein was isolated of mixed *C. elegans* culture of depicted strains. At least three independent experiments were analyzed using ANOVA followed by Tukey post-hoc test.

Decreased DAF-16 abundance did not influence promoter activity, mRNA or PEPT-1 protein level (Figure 8). However, additional knock out of *daf-16* in a *daf-2* mutant

background increased PEPT-1 abundance, although the wild-type situation was not reached again (Figure 9). This is in accordance with previously published microarray data showing increased *pept-1* mRNA levels in *daf-2(e1370) daf-16(df50)* compared to *daf-2(e1370)*[105]. The observed decline in PEPT-1 protein abundance was seen to be allele specific, as mutations in other regions of the Insulin/IGF receptor did not show any alterations in PEPT-1 abundance, when compared to wild type (Figure 9).

Subjecting *C. elegans* to glucose stress (2 % Glc) for seven days resulted in a decreased PEPT-1 protein content. This effect was abolished in a *daf-2* mutant background and rather reversed, although not significant, when *daf-16* was eliminated. This is in line with the observed increased nuclear accumulation of DAF-16 assessed by scoring the DAF-16::GFP signal (Figure 10).

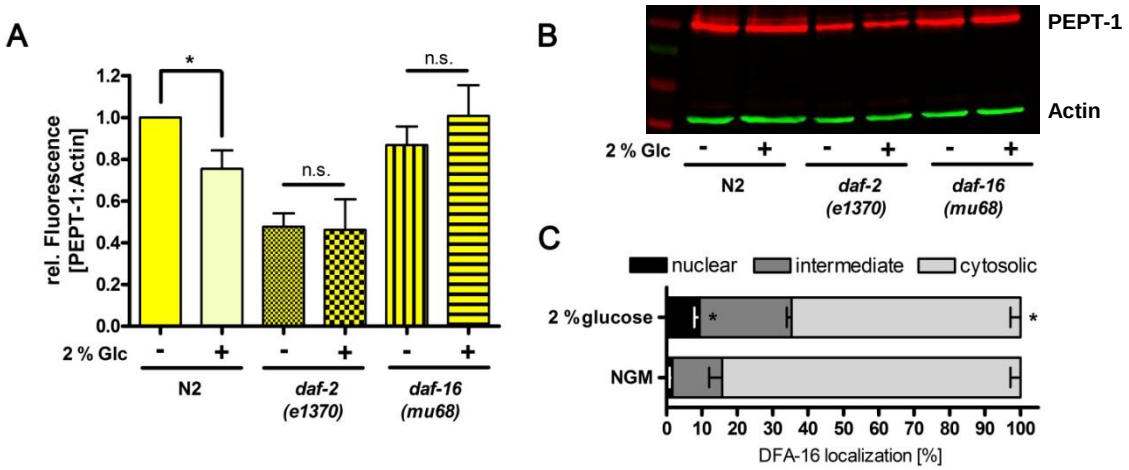

Figure 10: Glucose stress negatively affects PEPT-1 abundance: (A) PEPT-1 levels in N2 and IIS mutants: Nematodes were exposed to 2 % glucose in the NGM agar for 7 days, control worms were grown on standard NGM plates. **(B)** Representative Western Blot depicting PEPT-1 and Actin **(C)** DAF-16 localization after glucose exposure: ZJ356 were grown on NGM plates ± 2 % glucose for 7 days before DAF-16::GFP was detected in at least 100 animals per experiment. At least two independent experiments performed and students t-test was conducted for statistics.

3.1.4. Influence of XBP-1 on PEPT-1 in *C. elegans*

Several stressors including oxidative stress as well as proteasomal dysfunction were shown to activate SKN-1 as well as XBP-1[83,106]. Additionally, Henis-Korenblit et al. (2010) showed XBP-1 signaling to be altered in IIS mutants of *C. elegans*[107]. We therefore asked whether XBP-1 might be involved in the control of *pept-1* expression in *C. elegans.* Down-regulation of *xbp-1* using (RNAi) in *C. elegans* resulted in a significantly reduced promoter activity of *pept-1*. Although mRNA measurements

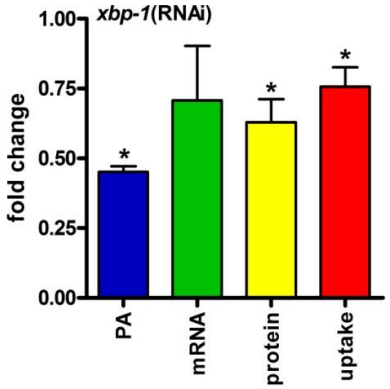

Figure 12: Silencing of *xbp-1* decreases *pept-1* expression: N2 were grown on RNAi for 7 days before P*pept-1*:GFP, mRNA, protein and uptake were determined. Three independent experiments represented ±SEM.

were rather ambigious as seen in the large standard error, a significant decline was observed for protein levels and uptake of ß-AlaLys-AMCA due to *xbp-1*(RNAi) (Figure 12). To elucidate a possible participation of DAF-16 in the decreased *pept-1* expression by *xbp-1*(RNAi), IIS mutant strains were subjected to *xbp-1*(RNAi). While

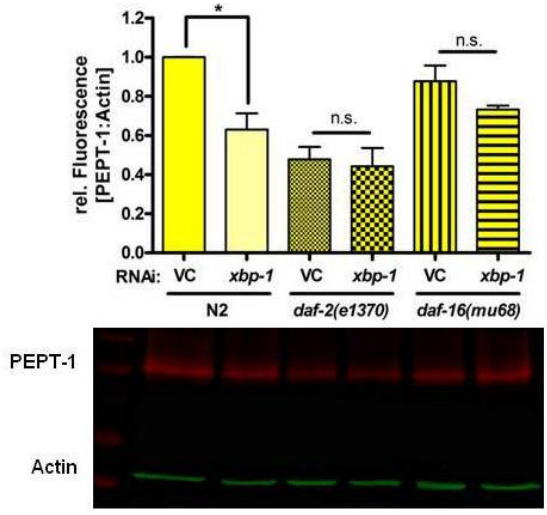

Figure 11: PEPT-1 abundance after *xbp-1*(RNAi) in IIS mutants: N2, *daf-2(e1370)* and *daf-16(mu68)* were grown on either VC or *xbp-1*(RNAi) for 7 days before Western Blot analysis.

PEPT-1 protein levels decreased in N2 due to *xbp-1*(RNAi), protein abundance did not change in *daf-2(e1370)* mutants upon treatment with *xbp-1*(RNAi). In *daf-16* knock out animals a small decrease in PEPT-1 abundance, yet not significant, was observed (Figure 11).

To assess whether *xbp-1*(RNAi) is affecting the IIS signaling cascade DAF-16 localization was probed. Silencing of *xbp-1* resulted in a higher accumulation of DAF-16::GFP in the nucleus with consequently less DAF-16 present in the cytosol. However, this did not cause an up-regulation of mRNA levels of *sod-3,* a known target gene of DAF-16 (Figure 13).

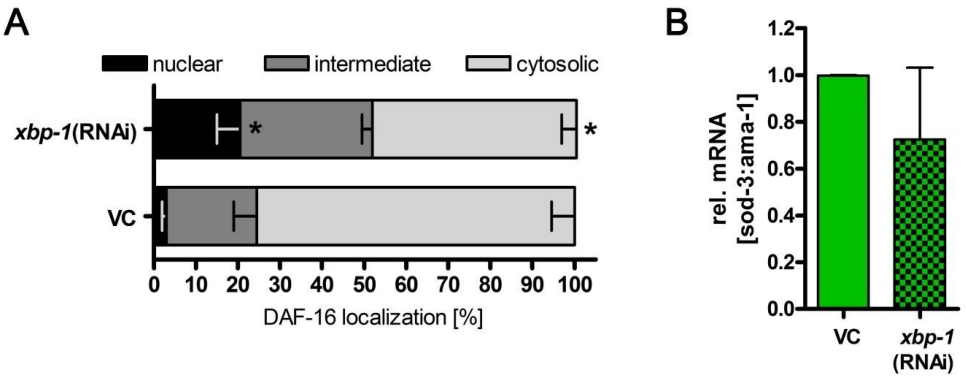

Figure 13: *xbp-1*(RNAi) induces DAF-16 nuclear translocation: (A) DAF-16::GFP was visualized using confocal microscope. At least 100 animals were investigated for DAF-16 localization with two independent experiments. **(B)** Determination of *sod-3* mRNA levels of N2 either grown on VC or on *xbp-1*(RNAi) for 7 days. Bars represent two independent experiments.

3.2. Modulation of TF´s regulating *pept-1* expression and their influence on the *pept-1(lg601)* phenotype

The IIS mutant *daf-2(e1370)* is not only marked by a strong increase in life span but abolished IIS is also accompanied by decreased progeny, elevated stress resistance and increased fat content. Knock out of *pept-1* results in similar phenotypic patterns, although life span extending effects only become visible in the *daf-2* mutant background. Since we herein show significantly reduced PEPT-1 levels in *daf-2(e1370)* mutants, the question arises to which extend phenotypic changes are caused by the reduced PEPT-1 abundance or whether changes in PEPT-1 abundance in WT animals can alter the phenotype.

3.2.1. Determination of fat droplet size

The main storage site of fat in nematodes is the intestine as worms lack specialized adipose tissue. Lipid droplets are surrouded by a phospholipid monolayer and different dyes make it possible to determine their size[108]. In *pept-1(lg601)* knock out animals an increased fat content was determined using sudan black staining as well as GC-MS measurement[44]. This is thought to be caused by the reduced influx of protons due to diminshed peptide coupled proton symport, which in turn increases fatty acid absorption. Such an increased fatty acid absorption was indeed shown by determination of BODIPY-C12 uptake[44]. Hence, we questioned whether indirect up-regulation of PEPT-1 via *wdr-23(*RNAi) and *gsk-3*(RNAi) or down-regulation caused by *xbp-1*(RNAi) would be reflected in fat accumulation in WT animals. Fat content of nematodes was stained using Sudan Black. The diameter of ten fat droplets per

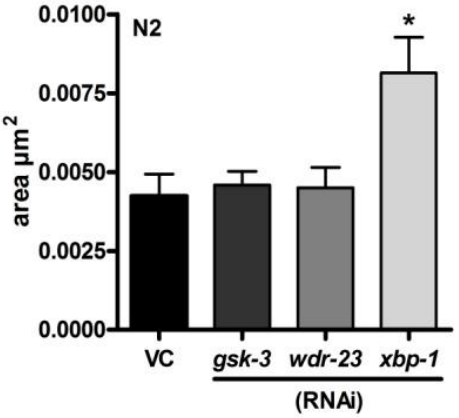

Figure 14: Fat droplet size increases upon *xbp-1*(RNAi): N2 worms were grown on *gsk-3*(RNAi), *wdr-23(*RNAi) or *xbp-1*(RNAi) before fat droplets were stained using Sudan Black Bars represent at least two biological replicates with 10 worms measured per experiment.

animal was measured (Figure 14). Reduction of PEPT-1 by applying *xbp-1*(RNAi) led to a significant increase in fat droplet size, while *gsk-3* and *wdr-23*(RNAi) did not have any influence. Not only *pept-1(lg601)* worms are known to have increased fat levels, but also *daf-2(e1370)* was already shown to have a higher fat content than WT animals[44]. In regard to the strongly reduced PEPT-1 abundance in *daf-2(e1370),* but not in alleles *(m41)* and *(e1368)*, as shown in chapter 3.1.3, fat droplet size was measured in *daf-2(m41)* and *daf-2(e1368).*

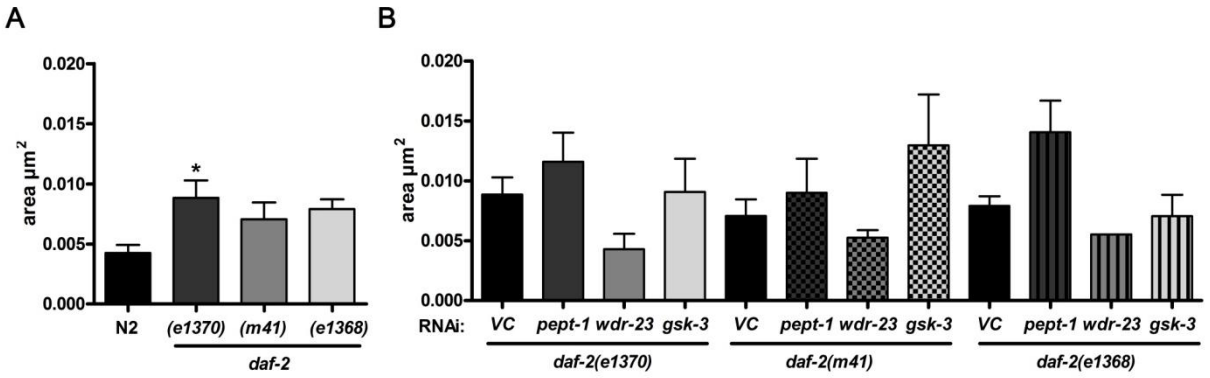

Figure 15: Fat content of *daf-2* mutants: (A) Sudan black staining of *daf-2(e1370), daf-2(m41)* and *daf-2(e1368)*. At least three biological replicates with 10 worms were performed per experiment. One-way ANOVA in combination with tukey post-hoc test was used to calculate significance of differences. **(B)** *daf-2* mutants were subjected to RNAi treatment for 7 days before staining of fat content. At least biological duplicates with 10 animals per experiment, only *daf-2(e1368)* with *wdr23*(RNAi) is represented by single experiment. One way ANOVA for each strain was done with subsequent tukey post-hoc test, but none of the changes had p-values<0.5

Both alleles showed an increase in fat droplet size although not statistically significant. This therefore does not reveal whether the PEPT-1 content in the *daf-2* mutants is responsible for the differences in fat accumulation (Figure 15). To get better insight into its role in altered fat storage in *daf-2* mutants, *wdr-23* and *gsk-3*(RNAi) were used to influence PEPT-1 content in *daf-2* background. Up-regulation of PEPT-1 abundance using *wdr-23* as well as *gsk-3*(RNAi) in the *daf-2* mutant background led only in the case of *wdr-23*(RNAi) to a decrease in fat droplet diameter (Figure 15). Therefore, we tested whether the effect of *wdr-23*(RNAi) is dependent on PEPT-1 by applying RNAi to *pept-1(lg601).* In the same way the effect of *xbp-1(RNAi)* was tested for specificity.

While fat droplets did not further increase after down-regulation of *xbp-1*, their diameter decreased significantly after down-regulation of *wdr-23* (Figure 16). The increase of fat content in WT *xbp-1*(RNAi) animals is therefore dependent on PEPT-1, while fat accumulation seems to be affected by *wdr23*(RNAi) independent on the regulation of PEPT-1 abundance.

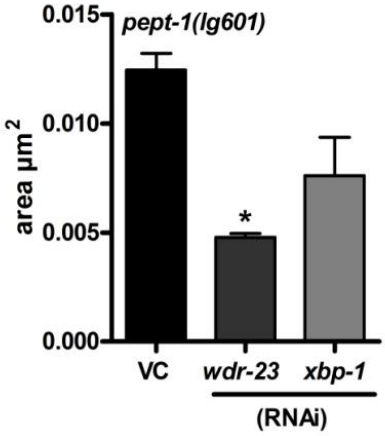

Figure 16: Sudan Black staining depicting fat droplet size in *pept-1(lg601)* after *wdr-23*(RNAi) and *xbp-1*(RNAi): *pept-1(lg60*1) were grown on *wdr-23*(RNAi) or *xbp-1*(RNAi) for 7 days before fat droplets were stained using sudan black. Represented are two biological replicates with 10 worms investigated per experiment. One-way-ANOVA with subsequent tukey post-hoc test resulted in $p<0.05$ in the case of *wdr-23*(RNAi).

3.2.2. Analysis of life span depending on SKN-1 activity

Measurements of fat content in various *daf-2* mutants and/or after RNAi treatment did not clarify whether a reduced PEPT-1 abundance alone is responsible for the increased size of fat droplets. Down-regulation of *pept-1* might also have influence on signaling cascades involved in different stress responses resulting in observed phenotypic differences in *pept-1(lg601).* Deletion of *pept-1* does not affect adult life span but in concert with a diminished IIS, life span of the double knock out almost doubles compared to the already prolonged life span of *daf-2(e1370)*. Therefore, we asked whether the knock out of *pept-1* might influence SKN-1 activity status adding to the pronounced life span increase. To answer this question, life span of WT, *pept-1(lg601), daf-2(e1370)* and *daf-2(e1370); pept-1(lg601)* grown on VC, *gsk-3*(RNAi) or *skn-1*(RNAi) were analyzed. In WT animals life span was significantly shortened due to *skn-1*(RNAi) or *gsk-3*(RNAi) which resulted in median life spans of 12 and 11 days respectively.

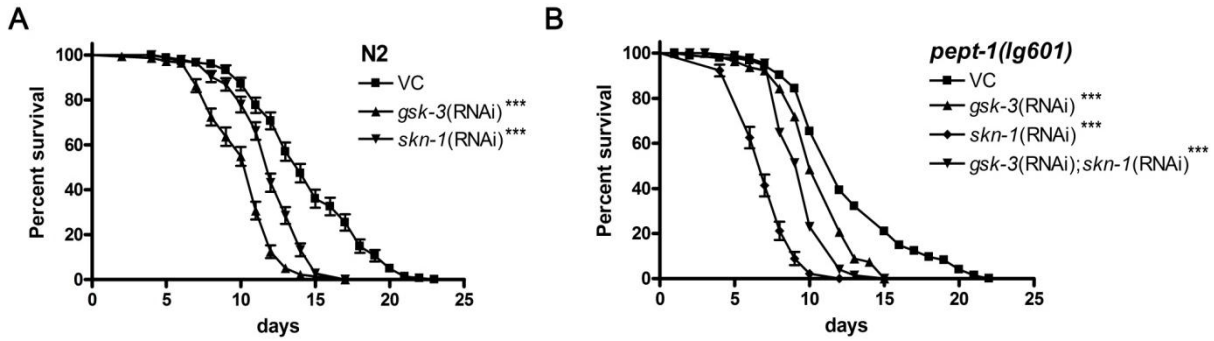

Figure 18: Life span of N2 and *pept-1(lg601)*: (A) Adult life span of N2 worms was determined either on VC, *gsk-3*(RNAi) or *skn-1*(RNAi) **(B)** Adult life span of *pept-1(lg601)* on VC, *gsk-3*(RNAi) and/or *skn-1*(RNAi). Obtained data is depicted as Kaplan-Meier survival curve, statistical analysis was done using log rank test in comparison to control. *p < 0.05; ** p<0.001; *** p<0.0001

Life span of *daf-2(e1370)* did increase due to *gsk-3*(RNAi), while *skn-1*(RNAi) decreased median life span. Double RNAi of *skn-1* and *gsk-3* resulted in equal median life span than *gsk-3*(RNAi) alone but comparison of survival curves did not show any significance anymore. In *daf-2(e1370);pept-1(lg601)* silencing of *skn-1* or *daf-16* decreased life span significantly. However, *gsk-3*(RNAi) did not have any influence on median life span nor on survival.

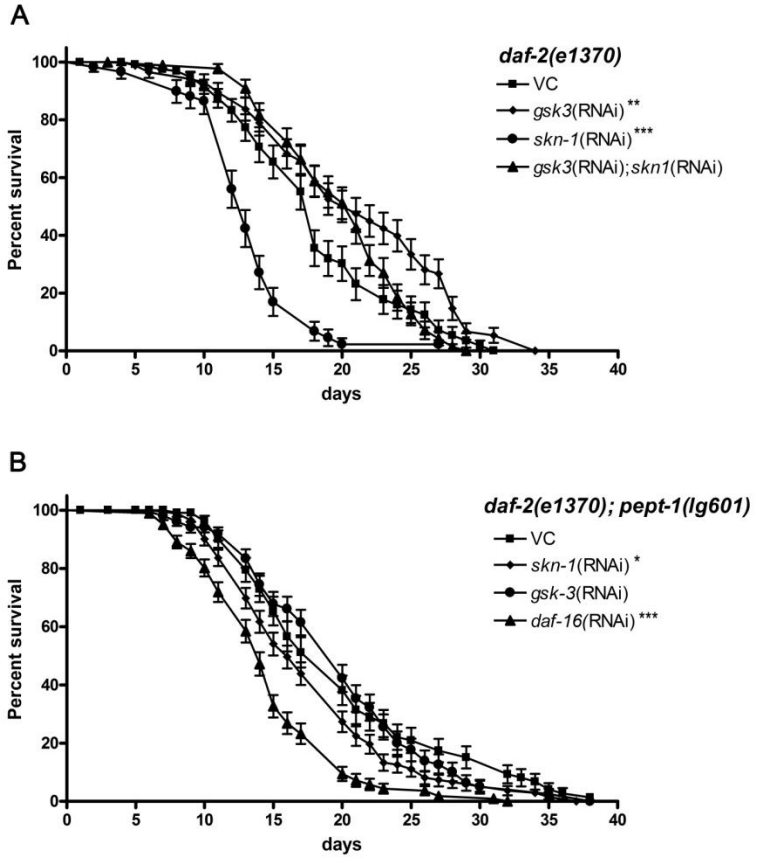

Figure 17: Life Span of (A) *daf-2(e1370)* and (B) *daf-2(e1370);pept-1(lg601)*: Adult life span was determined on VC,*skn-1*(RNAi), *gsk-3*(RNAi) *and daf-16*(RNAi). Obtained data is depicted as Kaplan-Meier survival curve, statistical analysis was done using log rank test in comparison to control. *p < 0.05; ** p<0.001; *** p<0.001

3.3. Identification of regulated proteins during larval development of *pept-1(lg601)*

Abolished di- and tripeptide uptake in *C. elegans* not only leads to the accumulation of fat but also to a slower development and ontogenesis. Amino acid supplementation of *pept-1(lg601)* was not able to rescue retarded postembryonic development although other phenotypic features were at least partially rescued[41]. Therefore, knock out of *pept-1* not only changes amino acid homeostasis but other regulatory mechanisms as well. To identify possible mechanisms responsible for the delayed development of *pept-1* knock out mutant animals the proteome of WT and mutant worms at various times during ontogenesis was profiled.

3.3.1. Evaluation of ^{15}N labeling rate in *C. elegans* culture

Metabolic labeling of *C. elegans* was done by providing ^{15}N labeled *E.coli* OP50 feeding bacteria on agarose plates free of other nitrogen sources. Literature so far reveals only commercially available labeling media. To find a cost-effective alternative we cultured of OP50 bacteria in minimal media containing either ^{15}N or ^{14}N ammonia chloride. To ensure complete labeling, bacterial culture started with a pre-culture over night followed by inoculation in larger volume. After 12-14 hrs at 37 °C, the bacterial suspension was centrifuged and the pellet resuspended in about half of the starting volume. Further *C. elegans* culture was conducted as described in literature [109]. After three generations of *C. elegans* culture on either ^{14}N or ^{15}N labeled bacteria, worms were washed of plates, proteins were extracted and analyzed, either

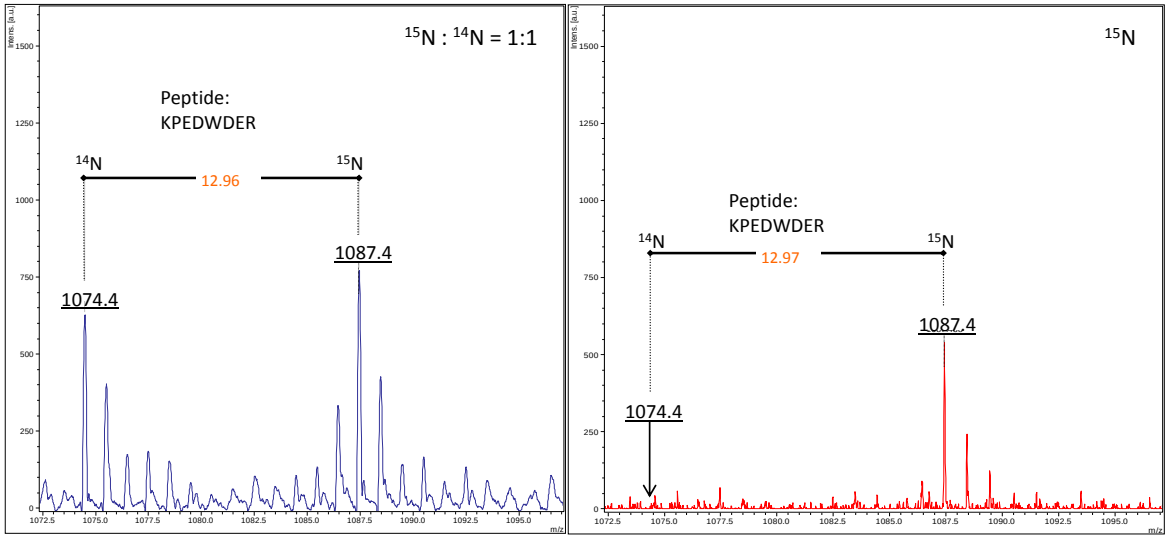

Figure 19: Example of mass spectra obtained by either analyzing tryptic digest of protein spot of a 1:1 mixture of ^{15}N and ^{14}N labeled sample (blue spectra), or only ^{15}Nlabeled protein (red spectra)

combined (1:1 ratio of ^{15}N:^{14}N) or the ^{15}N fraction on its own. Proteins were separated using 2D-PAGE as described in Material and Methods. Randomly picked protein spots were subjected to identification via MALDI-TOF/TOF (Ultraflex 3 by Bruker Dlatonics) analysis and subsequent database search using MASCOT. Identification of proteins was based on spectra of ^{14}N peptides. Figure 19 shows an example of generated mass spectra, whereby peak of ^{14}N peptide is extinct in the ^{15}N mass spectra. Providing MASCOT search results in combination with raw mass spectra to Quantispec [110] theoretical isotope distributions were calculated and matched to the obtained spectra. Thereafter, the labeling rate of each peptide was provided as outcome. By averaging all values of investigated peptides/proteins a labeling rate of 92 % was obtained (Table 1).

Table 1: Overview of randomly picked proteins used for determination of ^{15}N overall labeling rate

Protein	Mascot Score	MW [Da]	Labeling rate [%]	# Peptides
Heat shock protein 90 (Abnormal dauer formation protein 21)	93	80689	96.1	15
Heat shock 70 kDa protein C precursor	81	73093	88	4
Vacuolar ATP synthase catalytic subunit A (EC 3.6.3.14) (V ATPase subunit A) (Vacuolar proton pump subunit alpha) (V ATP	168	66874	91.9	23
Calreticulin precursor	87	45816	93.5	10
Tropomyosin isoforms a/b/d/f (Levamisole resistant protein 11)	169	32984	90.5	15
Kinesin light chain (KLC)	60	60529	87.8	6
Elongation factor 2 (EF 2)	118	95477	93.5	13
Enolase (EC 4.2.1.11) (2 phosphoglycerate dehydratase) (2 phospho D glycerate hydro lyase)	59	46759	93.2	6

3.3.2. Detection of changes in protein abundance during ontogenesis in WT

Quantification of proteins was conducted by using an internal standard consisting of protein extracts of nematodes metabolically labeled with ^{15}N. To ensure integrity of internal standard, ^{15}N protein extracts were generated of all developmental stages and *C. elegans* strains used and combined in equal amounts. Worm culture was

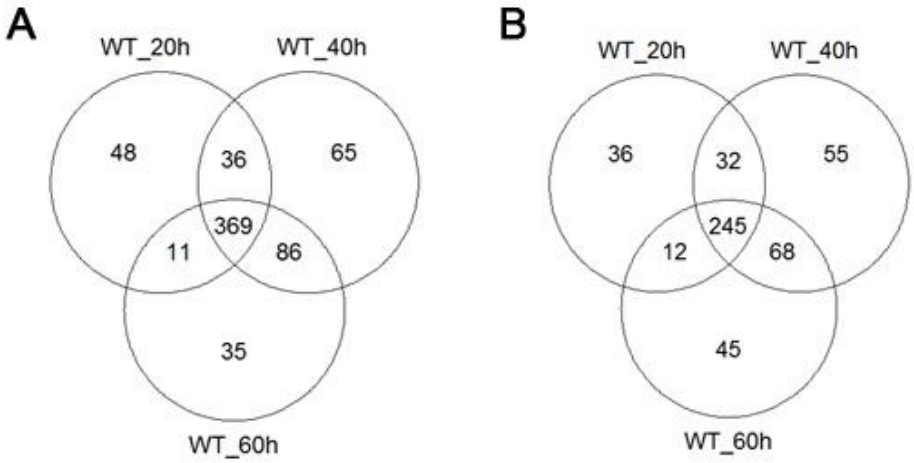

Figure 20: Venn diagram of **(A)** identified proteins and **(B)** identified and quantified proteins in all samples of WT development.

synchronized using hypochloride treatment. L1 larvae were placed on fresh plates and allowed to grow for 20, 40 and 60 hrs respectively. After extensive washing and protein extraction, samples were combined with the internal ^{15}N standard. Protein identification and quantiation was done as described in Material and Methods. Only proteins identified and quantified in each sample of the WT timeseries were taken for further analysis, thereby aiming to reduce false positives. In total 369 proteins were identified in all samples with 245 being also quantified (Figure 20).

To check for reproducibility L/H ratios obtained for proteins in biological replicates at each stage were plotted against each other. Thereby received values show a good

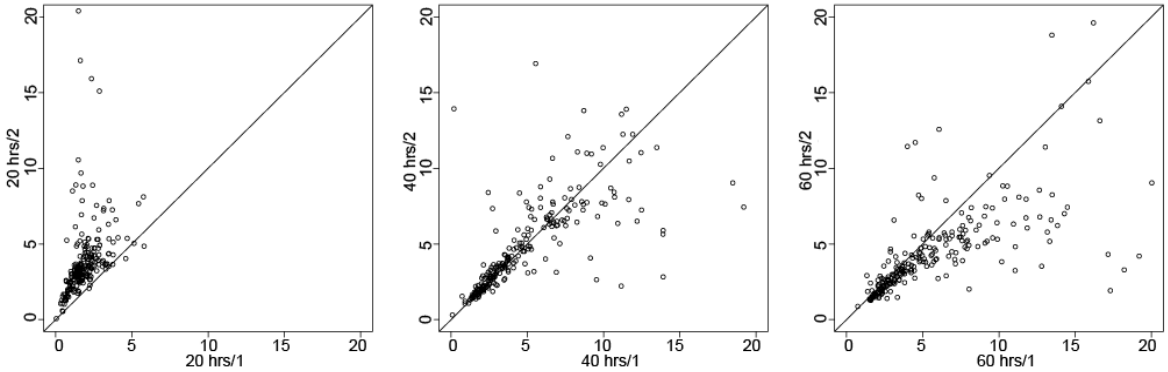

Figure 21: Scatterplot of protein abundances measured in experiment 1 against data obtained during the second experiment.

agreement with data generated in the second experiment for later times of development. However, variability between experiments was seen to be larger in the early stage of development (Figure 21). This might be explained by differences in the developmental processes, which seem to have a stronger impact in the early stages of development. Although the worm population was synchronized, the fertilization of eggs did not occur isochronically, adding further variation which probably aligns during development.

One-way analysis of variance (ANOVA) was done in R, with a subsequent tukey post-hoc test to distinguish between timepoints of development. Provided that p-values are below 0.05, 61 proteins showed a significant regulation (full list see supplement Table 22). Visualization of protein levels of each time point using a

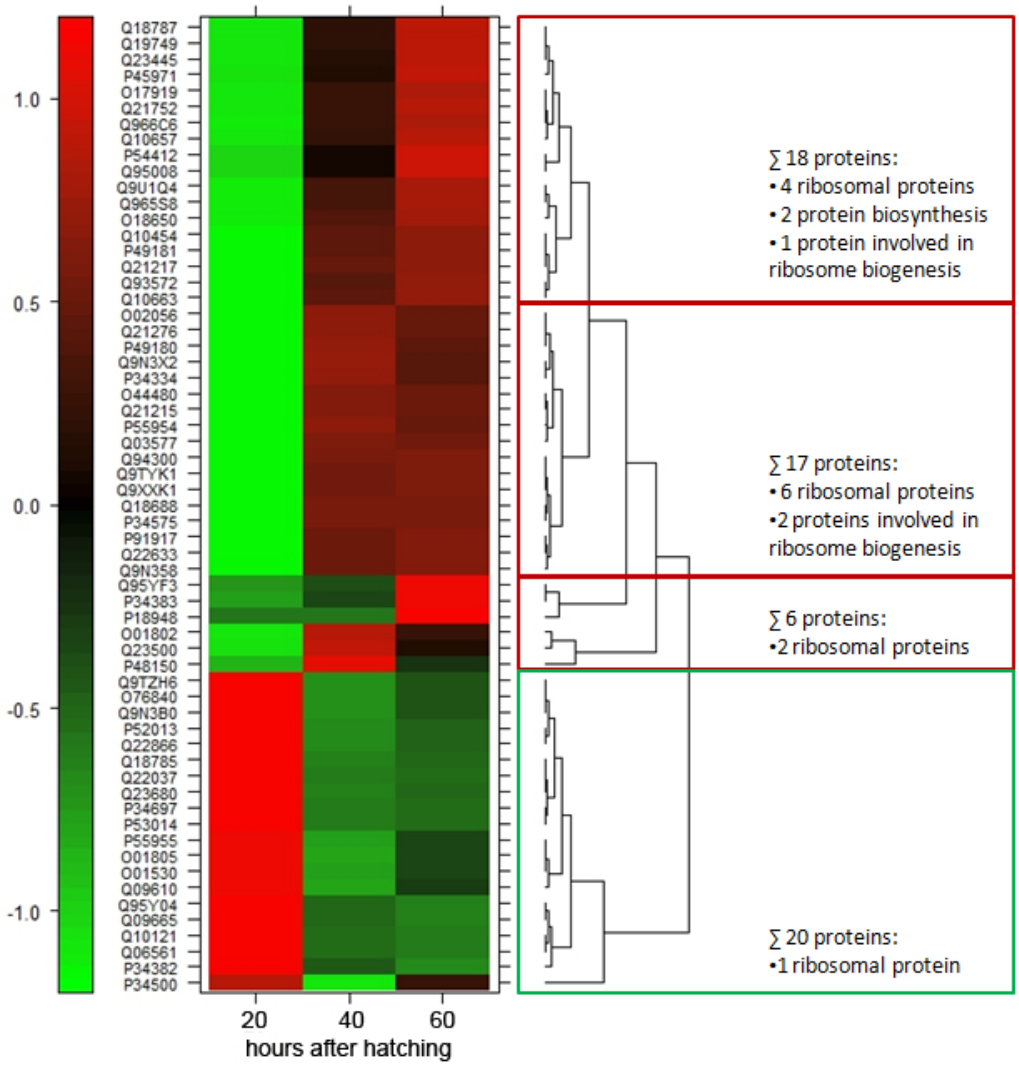

Figure 23: Heatmap of mean L/H ratios. 61 proteins showing significant regulation after 1faq ANOVA are depicted in rows, timepoints 20, 40 and 60 hours after hatching in columns. Hierarchical cluster analysis classifies four groups depending on their expression pattern. Group one stays stable after increase at 40 hours, while group two proteins rise only at 60 hours. Proteins of category three show peak abundances at 40 hours and class four proteins steadily decrease in abundance over time.

heatmap, clearly shows that major changes take place between 20 hrs and 40 hrs of development, while only a few proteins change in abundance between 40 hrs and 60 hrs (Figure 23). Protein abundances over time were hierachically clustered, using an agglomerative approach, to identify possible co-regulations. Four groups emerged from this cluster. The first two clusters compromise proteins with elevated abundances at 40 hrs and either a further increase towards adulthood (group 1) or remaining largely the same at 60 hrs (group 2). The third cluster contains proteins which show a rather unique pattern by either rising very late or decreasing again after a peak at 40 hrs. Of those 41 proteins approximately 40 % are part of the ribosome or involved in protein biosynthesis. Only one ribosomal protein was found to decrease over time (cluster 4). This overrepresentation of proteins involved in protein biosynthesis was also seen in pathway analysis done using KEGG pathway mapper. However, not all ribosomal proteins detected were up-regulated over time, while a large fraction did not show significant alterations some individual ribosomal proteins even decreased (Table 2).

DAVID was used to search for overrepresentations in gene ontology. Taking all regulated proteins as input, the top five terms overrepresented were “translation”, “nematode larval development”, “larval development”, “post-embryonic development” and “growth”. In the functional annotation clustering ribosomal components show highest enrichment (11.01), followed by cluster 2 comprising terms related to larval development with an enrichment of 5.22 (full list see supplement Table 23).

Classification of changes in protein levels between the different time points for significantly regulated proteins as defined by fold-changes with threshold values of ≤0.67 or ≥ 1.5 resulted in a list of 47 proteins. Gradually increasing protein levels which are only significantly changed between the endpoints of the analysis (20 and 60 hours) and proteins with very small changes are thereby excluded. 25 of the residual proteins were up-regulated between 20 and 40 hrs, while 19 showed a decrease and three proteins only increased between 40 and 60 hrs. Molecular functions of proteins increasing in early stages were found to belong to protein synthesis/ ribosome function or metabolic processes such as TCA cycle. Proteins decreasing over time are clearly distinguished in function from the first group as the majority is part of muscle or extracellular protein category.

Table 2: Proteins showing significant regulation between 20 and 40 hrs or 40 and 60 hrs: Proteins were sortet according to regulation and category. FC values in bold represent p<0.05 in tukey posthoc test.

up-regulated 40 versus 20 hours after hatching					
UniProt ID	**Gene name**	**Protein name**	**FC 40-20**	**FC 60-40**	**Category**
O01802	rpl-7; F53G12.10	60S ribosomal protein L7	**3,38**	0,78	ribosome
O02056	rpl-4; B0041.4	60S ribosomal protein L4	**2,77**	0,93	ribosome
O18650	rps-19; T05F1.3	40S ribosomal protein S19[1]	**2,08**	1,13	ribosome
O44480	rpl-20; E04A4.8	60S ribosomal protein L18a	**3,39**	0,95	ribosome
P34334	rpl-21, C14B9.7	60S ribosomal protein L21[1]	**3,98**	0,88	ribosome
P48150	rps-14; F37C12.9	40S ribosomal protein S14[1]	**3,22**	0,53	ribosome
P49180	rpl-33, F10E7.7	60S ribosomal protein L35a[1]	**3,07**	0,92	ribosome
P49181	rpl-36; F37C12.4	60S ribosomal protein L36[1]	**5,17**	1,11	ribosome
Q93572	rpa-0, F25H2.10	60S acidic ribosomal protein P0[1]	**2,24**	1,10	ribosome
Q94300	rpl-11.1; T22F3.4	60S ribosomal protein L11	**2,70**	1,01	ribosome
Q9N3X2	rps-4; Y43B11AR.4	40S ribosomal protein S4	**2,85**	0,89	ribosome
Q21276	K07C5.4	Uncharacterized NOP5 family protein K07C5.4	**7,28**	0,91	ribosome biogenesis
Q9U1Q4	vrs-2; Y87G2A.5	Valyl-tRNA synthetase	**4,57**	1,27	tRNA Synthetase
Q03577	drs-1; B0464.1	Aspartyl-tRNA synthetase, cytoplasmic	**3,76**	0,97	tRNA Synthetase
P34575	cts-1; T20G5.2	Probable citrate synthase, mitochondrial	**3,56**	1,00	TCA cycle
Q23500	aco-1;gei-22; ZK455.1	Probable cytoplasmic aconitate hydratase	**3,17**	0,73	TCA cycle
Q10663	gei-7; C05E4.9	Bifunctional glyoxylate cycle protein[2]	**2,97**	1,11	glyoxylate cycle / TCA cycle
P55954	cco-2; Y37D8A.14	Cytochrome c oxidase subunit 5A, mitochondrial	**1,51**	0,97	oxidative phosphorylation
Q9XXK1	H28O16.1	ATP synthase subunit alpha, mitochondrial	**3,26**	1,03	oxidative phosphorylation
Q19749	F23B12.5	Pyruvate dehydrogenase complex component E2	**2,24**	1,31	pyruvate dehydrogenase
Q22633	hpd-1; T21C12.2	4-hydroxyphenylpyruvate dioxygenase	**3,24**	1,04	amino acid degradation
P45971	T09A5.11	Probable dolichyl-diphosphooligosaccharide-protein glycosyltransferase 48 kDa subunit	**4,95**	1,52	glycosyl-transferase
Q10454	F46H5.3	Probable arginine kinase F46H5.3	**3,78**	1,10	arginine and prolin metabolism
Q18787	rpt-1; C52E4.4	26S protease regulatory subunit 7	**5,73**	1,46	proteasome

UniProt ID	Gene name	Protein name	FC 40-20	FC 60-40	Category
Q21215	rack-1; K04D7.1	Guanine nucleotide-binding protein subunit beta-2-like 1	**3,01**	0,95	small G-protein
down-regulated 40 versus 20 hours after hatching					
O01530	asp-6; F21F8.7	Aspartic protease 6	**0,43**	1,28	extracellular
O76840	mig-6;ppn-1; C37C3.6	Abnormal cell migration protein 6;Papilin	**0,38**	**1,26**	extracellular
P34382	far-1; F02A9.2	Fatty-acid and retinol-binding protein 1	**0,46**	**0,84**	extracellular
P34500	ttr-2; K03H1.4	Transthyretin-like protein 2	**0,25**	**3,09**	extracellular
P55955	ttr-16, Y5F2A.1	Transthyretin-like protein 16	**0,37**	1,39	extracellular
Q9N3B0	Y54G2A.23	ARMET-like protein	**0,53**	**1,13**	extracellular
P53014	mlc-3, F09F7.2	Myosin, essential light chain	**0,57**	1,02	muscle protein
Q09665	tnc-2, ZK673.7	Troponin C, isoform 2	**0,28**	**0,82**	muscle protein
Q18785	mif-2, C52E4.2	MIF-like protein mif-2	**0,28**	1,15	muscle protein
Q22866	lev-11;tmy-1, Y105E8B.1	Tropomyosin isoforms a/b/d/f	**0,39**	1,17	muscle protein
Q9TZH6	pcbd-1, T10B11.1	4-alpha-hydroxy-tetrahydropterin dehydratase	**0,34**	1,31	muscle protein
O01805	acbp-1, C44E4.6	Acyl-CoA-binding protein homolog 1	**0,56**	1,18	lipid transport and storage
P34697	sod-1; C15F1.7	Superoxide dismutase [Cu-Zn]	**0,36**	1,05	oxidative stress response
P52013	cyn-5;cyp-5, F31C3.1	Peptidyl-prolyl cis-trans isomerase 5	**0,42**	1,15	protein folding
Q09610	lec-8, R07B1.10	Probable galaptin lec-8	**0,37**	1,44	carbohydrate binding
Q10121	C23G10.2	UPF0076 protein C23G10.2	**0,51**	**0,97**	translation inhibitor
Q22037	hrp-1;rbp-1, F42A6.7	Heterogeneous nuclear ribonucleoprotein A1	**0,39**	1,08	telomere component
Q23680	vha-9, ZK970.4	Probable V-type proton ATPase subunit F	**0,49**	1,07	ion transport
Q95Y04	rps-28, Y41D4B.5	40S ribosomal protein S28	**0,51**	**0,92**	ribosome
up-regulated 60 versus 40 hours after hatching					
P18948	vit-6, K07H8.6	Vitellogenin-6	3,54	**306**	secreted egg-yolk precursor
P34383	far-2, F02A9.3	Fatty-acid and retinol-binding protein 2	3,14	**3,56**	secreted, lipid transport and storage
P34500	ttr-2, K03H1.4	Transthyretin-like protein 2	**0,25**	**3,09**	secreted, lipid transport and storage

3.3.3. The proteome during ontogenesis in *pept-1(lg601)* animals

Nematodes lacking *pept-1* were grown as described for WT nematodes. Regarding the delayed development of *pept-1(lg601)* an additional sample at 80 hrs after hatching, grossly defined as L4/adult, was generated. Quantification of the proteome was accomplished using the same internal standard as for wild-type, making it possible also to directly compare WT and mutant animals during development (see following chapter). In total 312 proteins were identified in all samples of *pept-1(lg601)* of which 182 were also quantified (corresponding Venn diagrams see supplement Figure 54). Protein levels of 80 hrs time point were compared to protein data of wildtype at all stages to see whether nematodes lacking *pept-1* reach adulthood not only phenotypically but also on a molecular level. Scatterplots of protein abundances of *pept-1(lg601)* 80 hrs on the x- axis and y-axis corresponding to values obtained in wild-type do not show high correlation (Figure 24). Protein abundances at 80 hrs of development in *pept-1(lg601)* do not reach the same level as in wildtype at any time point. Even protein levels detected at 20 hrs in WT are still slightly higher than at 80 hrs in *pept-1(lg601).* This might be an indication for a lower protein biosynthesis rate.

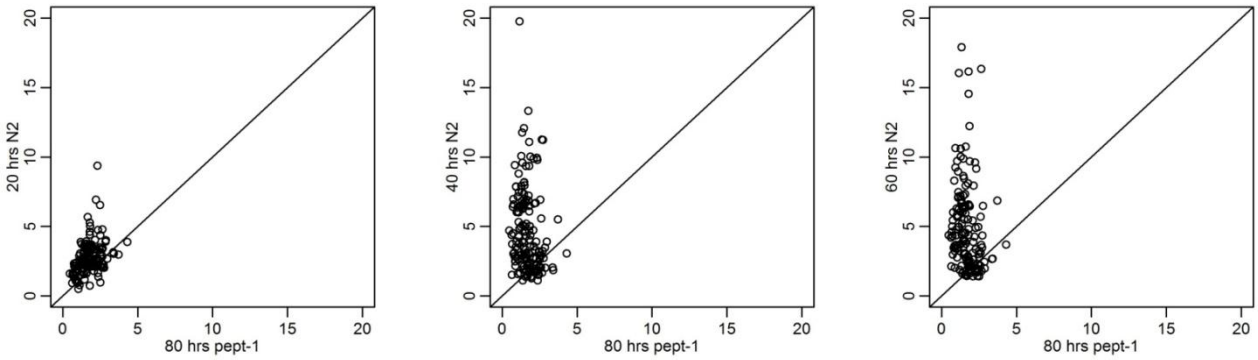

Figure 24: Scatter plots of L/H ratios of proteins identified and quantified in *pept-1(lg601)* at 80 hrs and N2 at 20, 40 and 60 hrs of development.

To test for changes during ontogenesis, a statistical analysis using one-way-ANOVA was performed. Only 16 proteins displayed a p-value below 0.05. Mean values of protein abundances of significantly regulated proteins were depicted in a heatmap after z-score transformation. Hierarchical clustering of protein abundance courses was made to identify possible co-regulations (Figure 25). This resulted in three main groups, whereby the first cluster comprises proteins down-regulated between 20 and 40 hrs followed by rather low protein levels towards adulthood (O45499, P52015, O62327, Q10657, P37806). The second group contains proteins with higher abundances at 20 and 60 hrs, while at 40 and 80 hrs levels were decreased

(P34690, P52275, Q966C6, Q94300, Q9N4G9, P34575, O02639). Proteins of the third group only showed higher levels at 60 hrs otherwise depicting rather low abundances (P47209, P27604, P45971, P02566).

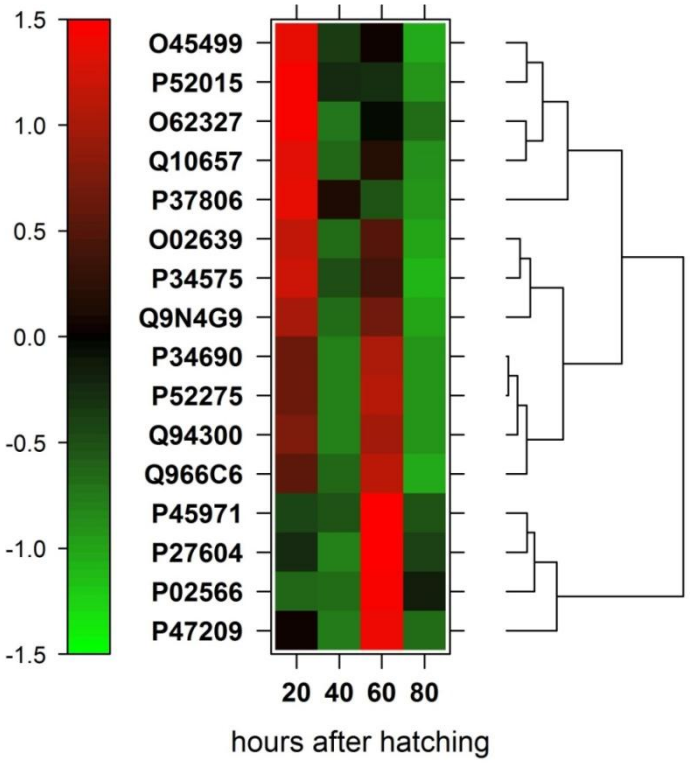

Figure 25: Heatmap of proteins regulated during ontogenesis of *pept-1(lg601):* Table of mean value of protein abundances was sorted in regard to the 20 hrs sample, followed by z-score transformation of values. Protein IDs and colourkey are displayed on the left. Red indicates high abundance and green reflects low levels of proteins. Dendrogram on the right shows a hierarchical cluster analysis of time course of protein abundances.

A tukey post-hoc test revealed changes between individual time points (Table 3). In focussing on proteins which show alterations between time points next to each other (thereby excluding proteins which only show gradual changes) provided a list of significantly regulated proteins with nine candidates. Three of them are part of the ribosome (Q94300, O02639 and O45499). Another three are classified as muscle proteins (P02566, P52275 and P34690) and the remaining three are a hypothetical glutathione peroxidase (O62327), an epsilon subunit of the chaperonin T-complex protein 1 (P47209) and a S-adenosyl-L-homocysteine hydrolase (P27604).

Table 3: List of proteins significantly regulated during ontogenesis of *pept-1(lg601),* obtained by one-way ANOVA, p-Values depicted represent tukey post-hoc test values to distinguish between groups(for full list see supplement). FC values in bold represent p-values < 0,05 for changes between neighboring time points

regulated during development of *pept-1(lg601)*						
UniProt ID	**Gene name**	**Protein name**	**FC 40-20**	**FC 60-40**	**FC 80-60**	**Category**
O02639	rpl-19; C09D4.5	60S ribosomal protein L19	**0,43**	1,84	0,42	ribosome
Q94300	rpl-11.1; T22F3.4	60S ribosomal protein L11	0,45	**2,37**	**0,39**	ribosome
O45499	rps-26; F39B2.6	40S ribosomal protein S26	**0,48**	1,23	0,45	ribosome
P02566	unc-54; F11C3.3	Myosin-4 (Myosin heavy chain B)	0,93	**8,47**	**0,33**	muscle protein
P34690	tba-2; C47B2.3	Tubulin alpha-2 chain	0,48	2,37	**0,39**	cell architecture
P52275	tbb-2; C36E8.5	Tubulin beta-2 chain	**0,47**	**2,47**	**0,36**	cell architecture
O62327	R05H10.5	Probable glutathione peroxidase R05H10.5 (EC 1.11.1.9)	**0,38**	1,52	0,67	oxidative stress response
P47209	cct-5; C07G2.3	T-complex protein 1 subunit epsilon (TCP-1-epsilon)	0,27	**8,02**	0,17	protein folding
P27604	ahcy-1; K02F2.2	Adenosylhomocysteinase (AdoHcyase) (EC 3.3.1.1)	0,60	**3,78**	**0,39**	amino acid biosynthesis

3.3.4. Comparison of the proteome during ontogenesis between *pept-1(lg601)* and wildtype animals

The time-dependent changes in the proteome of WT and *pept-1(lg601)* independently indicate that the proteome of N2 is more dynamic during ontogenesis compared to nematodes lacking *pept-1*. To test for altered protein expression during ontogenesis in *pept-1* worms in comparison to WT animals a two-way ANOVA was conducted with genotype and time of development (20, 40 and 60 hrs) as variables. In total 166 proteins were identified and quantified in all samples of WT and *pept-1(lg601).* Strain dependent differences were found for 49 proteins, while changes solely depending on time were significant for 39 proteins. 35 proteins had a p-value below 0.05 for interaction between strain and time, meaning differential abundances over time course between *C. elegans* strains. A comparison of generated protein lists revealed that 66 individual proteins displayed a p-value < 0.05 with 16 proteins included in all three categories (Figure 26). Proteins that appeared as significantly regulated in strain and strain-time dependent manner were analyzed further only as part of the short list of the strain-time dependent enteties. 35 proteins showed an interaction between time and strain in protein abundances. Therefore, 20 proteins remained in the group of “strain-dependent” regulated. As time specific changes in individual strains were already described in section 3.3.2 and 3.3.3 the focus here is

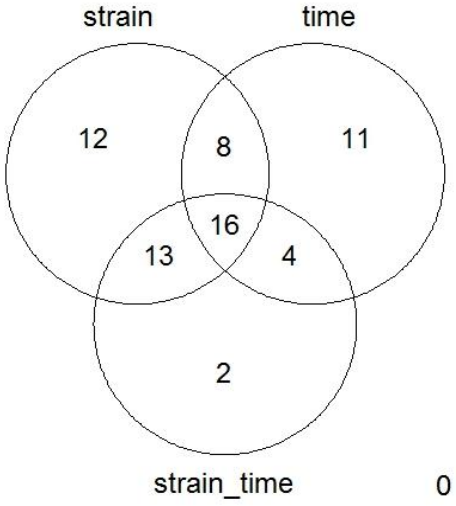

Figure 26: Venn diagram of proteins with a p-value < 0.05 after two-way ANOVA. Protein abundances of all WT and *pept-1(lg601)* for all time points were analyzed for significant changes performing a two-way-ANOVA. List of proteins showing either strain-dependent, time-dependent or a strain-time interaction were compared to retrieve redundant proteins.

on proteins changing in response to genotype and neglected the 11 proteins that only showed time dependent regulations.

3.3.4.1. Regulated proteins depending on the genotype

Proteins that only showed strain specific differences in abundance, are listed in Figure 27 with graphical display of fold-changes of *pept-1(lg601)* versus WT for each time point. The majority of proteins showed lower levels in *pept-1(lg601)* mutant animals compared to wild-type, with only five proteins (O76840, P34328, Q17334, Q21443, Q23680) displaying increased levels with a fold change above 1.3 defined as threshold (Table 4).

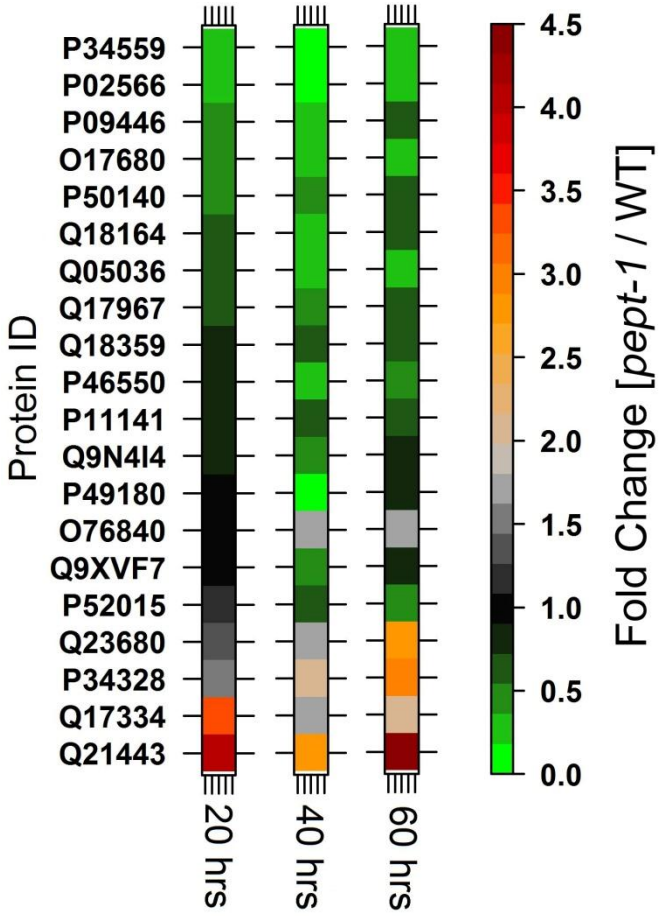

Figure 27: Levelplot of fold changes of protein abundances between *pept-1(lg601)* vs. wild-type. Proteins depicted were seen to be significantly regulated only dependent on genotype with a p-value<0.05 in a two-way ANOVA

Table 4: Proteins showing genotype specific regulation between *pept-1(lg601)* vs. WT: Listed proteins had p-values<0.05 in two-way ANOVA, fold changes were calculated for each timepoint

down-regulated *pept-1(lg601)* versus WT						
UniProt ID	**Gene name**	**Protein name**	**FC [*pept-1(lg601)*/WT]**			**Category**
			20 hrs	**40 hrs**	**60 hrs**	
O17680	sams-1; C49F5.1	Probable S-adenosylmethionine synthase 1 (AdoMet synthase 1) (EC 2.5.1.6)	0,51	0,32	0,31	amino acid and one carbon metabolism
Q18164	dpyd-1; C25F6.3	Dihydropyrimidine dehydrogenase [NADP(+)](DPD) (EC 1.3.1.2)	0,63	0,21	0,59	amino acid and pyrimidin metabolism
P34559	ech-6; T05G5.6	Probable enoyl-CoA hydratase, mitochondrial (EC 4.2.1.17)	0,32	0,14	0,23	amino acid metabolism and lipid metabolism
P02566	unc-45; F11C3.3	Myosin-4 (Myosin heavy chain B)	0,36	0,04	0,26	muscle protein
Q18359	C33A12.1	Probable NADH dehydrogenase [ubiquinone] 1 alpha subcomplex subunit 5	0,73	0,56	0,66	oxidative phosphorylation
P09446	hsp-1; F26D10.3	Heat shock 70 kDa protein A	0,42	0,28	0,60	protein folding/ spliceoseome
P50140	hsp-60; Y22D7AL.5	Chaperonin homolog Hsp-60, mitochondrial	0,53	0,37	0,69	protein folding
P46550	cct-6 F01F1.8	T-complex protein 1 subunit zeta (TCP-1-zeta) (CCT-zeta)	0,77	0,20	0,39	protein folding
P11141	hsp-6; C37H5.8	Heat shock 70 kDa protein F, mitochondrial	0,83	0,57	0,69	protein folding
P52015	cyn-7; Y75B12B.2	Peptidyl-prolyl cis-trans isomerase 7 (PPIase 7) (EC 5.2.1.8)	1,15	0,63	0,45	protein folding
Q17967	pdi-1; C14B1.1	Protein disulfide-isomerase 1 (PDI 1) (EC 5.3.4.1)	0,72	0,48	0,57	protein processing in endoplasmic reticulum
Q9N4I4	rpl-1; Y71F9AL.13	60S ribosomal protein L10a	0,84	0,39	0,73	ribosome
P49180	rpl-33; F10E7.7	60S ribosomal protein L35a	0,90	0,15	0,77	ribosome
Q9XVF7	rpl-2; B0250.1	60S ribosomal protein L8	0,99	0,41	0,81	ribosome
Q05036	C30C11.4	Uncharacterized protein C30C11.4	0,68	0,26	0,26	unknown; HSP70 motif

up-regulated *pept-1(lg601)* versus WT						
UniProt ID	**Gene name**	**Protein name**	**FC [*pept-1(lg601)*/WT]**			**Category**
			20 hrs	**40 hrs**	**60 hrs**	
Q23680	vha-9; ZK970.4	Probable V-type proton ATPase subunit F (V-ATPase subunit F)	1,27	1,76	2,74	oxidative phosphorylation
P34328	hsp-12.2; C14B9.1	Heat shock protein Hsp-12.2	1,45	2,08	2,97	unknown; no chaperonin function
Q17334	sodh-1; K12G11.3	Alcohol dehydrogenase 1 (EC 1.1.1.1)	3,33	1,72	1,99	glycolysis and gluconeogenesis
Q21443	lmn-1; DY3.2	Lamin-1 (Ce-lamin)	4,04	2,73	4,38	nuclear envelope; chromatin organization
O76840	mig-6; C37C3.6	Papilin (Abnormal cell migration protein 6)	0,92	1,80	1,78	secreted protein

DAVID was used to find overrepresentations within groups of down- or up-regulated proteins respectively. Gene ontology search for proteins down-regulated in *pept-1(lg601)* versus WT animals showed enrichment in the categories of “nematode larval development”, “larval development” and “post-embryonic development”. Each category had 11 proteins assigned with p-values of ~$3*10^{-4}$. With a comparable p-value four proteins were grouped in the category of “protein folding”. Further categories retrieved, were “growth”, “regulation of growth rate” and “translation” (Full list see supplement). A functional annotation clustering with high stringency resulted in 6 clusters: cluster 1 comprised heat shock proteins with enrichment score of 4.31, larval development was enriched 3.02 representing cluster 2, nucleotide binding was enriched 2.54 fold (cluster 3), cluster 4 comprised terms of organelle lumen (enrichment score 2.07). Cluster 5 and 6 had enrichment scores below 2 with ribosomal components and regulation of growth as major terms. Search of 15 down regulated proteins using KEGG pathway mapper only found two pathways with more than two matching proteins. Four proteins were grouped into metabolic pathways (Q18164, O17680, P34559 and C33A12.1), while three are allocated to the ribosome (Q9N4I4, P49180 and Q9XVF7). Amino acid metabolism is one of the metabolic pathways, with three proteins involved (O17680, Q18164, P34559), while only one protein is part of the oxidative phosphorylation (Table 4).

3.3.4.2. Regulated proteins that show genotype x time interactions

Dysregulation of gene expression and subsequently of altered protein levels during larval development might be implicated in postembryonic retardation of growth in *pept-1(lg601)*. A two-way ANOVA declared 35 proteins to be differentially expressed during development between WT and knock out mutants (strain*time interaction).

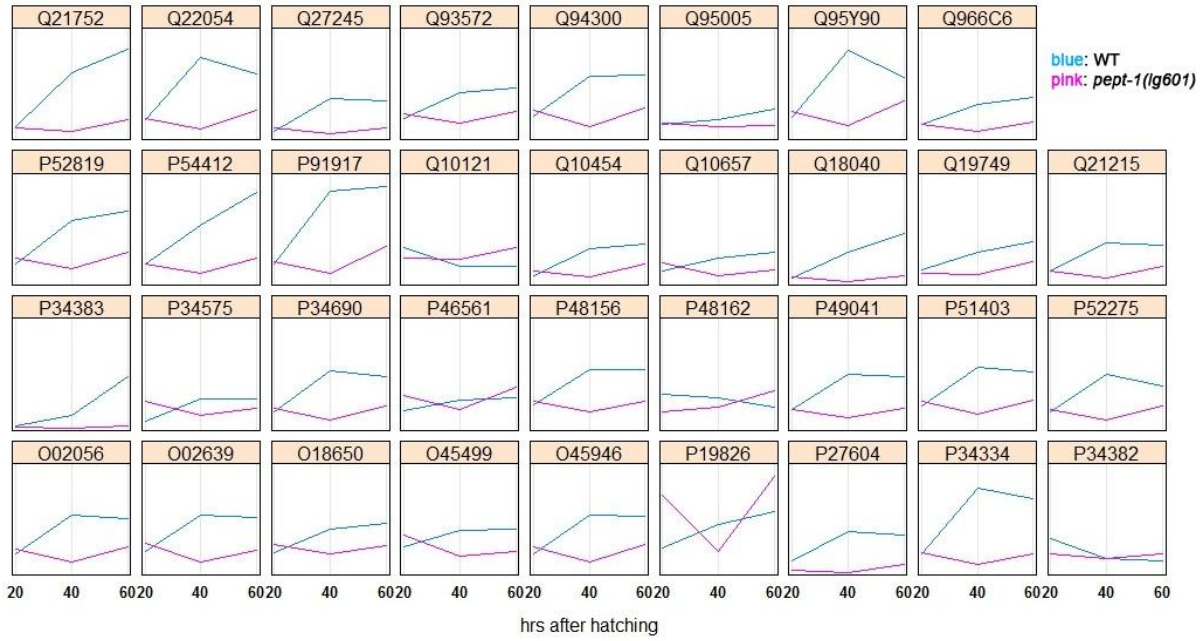

Figure 29: Individual course of protein abundances over time for each protein in WT and *pept-1(lg601)*. Blue lines represent protein abundances in WT, pink lines depict courses in *pept-1(lg601).*

The courses of protein abundances over time for N2 and *pept-1(lg601)* are depicted in Figure 29. In WT animals, the majority of proteins is increasing in abundance during development (Figure 29; blue line) while in *pept-1(lg601)* protein levels remained constant or even decreased at 40 hrs compared to 20 hrs (Figure 29, pink

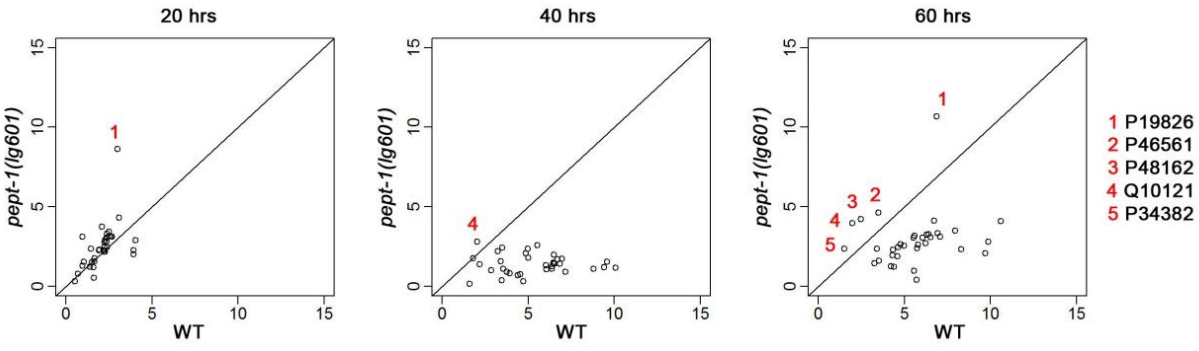

Figure 28: Scatterplot WT vs. *pept-1(lg601):* L/H ratios of WT and *pept-1(lg601)* for each protein were plotted against each other. Proteins with similar abundances in WT and *pept-1(lg601)* are localized close to linear slope. Proteins showing higher abundances in *pept-1(lg601)* are above while those having lower levels are placed underneath. Marked with numbers are proteins having higher abundances in mutant animals.

line). Outliers of this pattern are readily visible in the scatterplot depicting protein L/H ratios at each time point WT versus *pept-1(lg601)* (Figure 28). While at 20 hrs protein abundances are very similar between both strains, differences between genotype become visible during development at 40 and 60 hrs. However, only five proteins show higher abundances at 60 hrs than in WT (Figure 28, P19826, P46561, P48162, Q10121, P34382).

Cluster analysis is used to identify groups of samples which share similar characteristics. Therefore, we used agglomerative hierarchical cluster analysis to identify potential co-regulated proteins. Agglomerative coefficient (AC) describes the strength of clustering structure; whereby values close to one implicate clear structures found in the dataset and values close to zero indicate that data set rather represents only one large group. AC of protein cluster yielding a value of 0.88 denotes rather clear structure. Three main groups were formed with the first one only comprising two proteins (P46561 and P19826). Both proteins showed higher abundances in *pept-1(lg601)* than in WT at 20 and 60 hrs. Proteins in *pept-1(lg601)* depicting only at 60 hrs elevated levels compared to WT were clustered in group 3 (P48162, P34382 and Q10121). Members of cluster 1 and 3 were already highlighted, when raw data was visualized using scatterplot (Figure 28). Remaining proteins were grouped in cluster 2. All tof them showed increasing levels during development in WT animals, while this was not the case in *pept-1(lg601)* (Table 5).

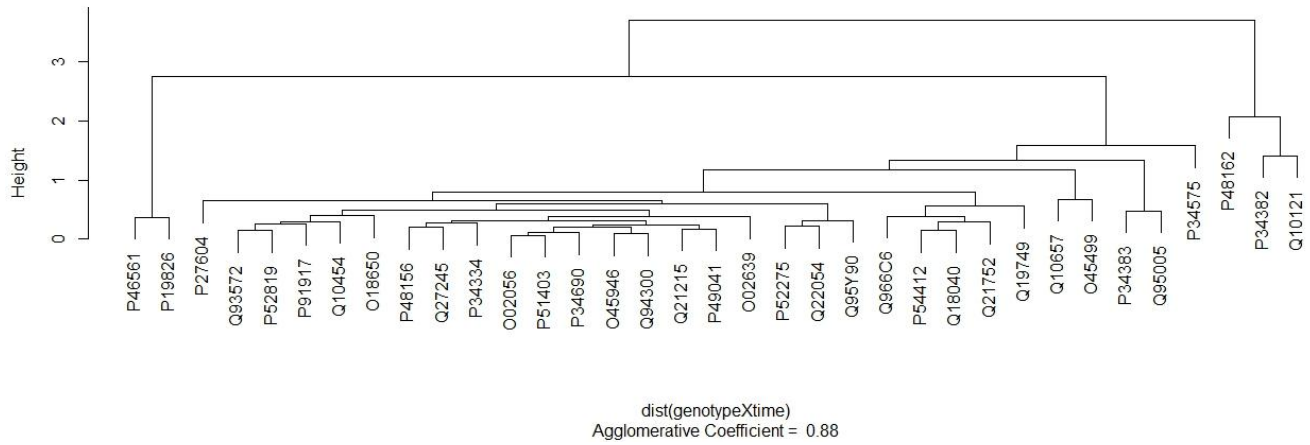

Figure 30: Hierarchical cluster of proteins that show genotype*time interaction: Protein abundances were centered, scaled and transformed into a dissimilarity matrix before subjected to agglomerative hierarchical clustering using R. Agglomerative coefficient reflects strength of clustering structure.

Table 5: Proteins that showed strain*time interaction during ontogenesis: Listed proteins showed p<0.05 in two-way ANOVA, fold changes between 20 and 40 hrs and 40 and 60 hrs are depicted for both genotypes. Table is sorted according to cluster analysis.

UniProt ID	Gene name	Protein name	FC 40-20		FC 60-40		Category
			WT	*pept-1 (lg601)*	WT	*pept-1 (lg601)*	
Cluster 1							
P19826	deb-1; ZC477.9	Vinculin (P107B)	1,85	0,30	1,24	4,14	muscle protein
P46561	atp-2; C34E10.6	ATP synthase subunit beta, mitochondrial (EC 3.6.3.14)	1,54	0,58	1,08	2,12	oxidative phosphorylation
Cluster 2							
P27604	ahcy-1; K02F2.2	Adenosylhomocysteinase (AdoHcyase) (EC 3.3.1.1)	2,93	0,60	0,93	3,78	amino acid biosynthesis
Q10454	F46H5.3	Probable arginine kinase (EC 2.7.3.3)	3,78	0,54	1,10	2,81	arginine and prolin metabolism
Q18040	C16A3.10	Probable ornithine aminotransferase, mitochondrial (EC 2.6.1.13)	4,97	0,47	1,60	2,62	arginine and proline metabolism
P52275	tbb-2; C36E8.5	Tubulin beta-2 chain	3,15	0,47	0,79	2,47	cell architecture
P34690	tba-2; C47B2.3	Tubulin alpha-2 chain	3,26	0,48	0,91	2,37	cell architecture
Q27245	W07G4.4	Putative aminopeptidase W07G4.4 (EC 3.4.11.-)	4,70	0,53	0,96	1,85	glutathione metabolism
Q10657	tpi-1; Y17G7B.7	Triosephosphate isomerase (TIM) (EC 5.3.1.1)	1,99	0,43	1,23	1,57	glycolysis and gluconeogenesis
P34575	cts-1; T20G5.2	Probable citrate synthase, mitochondrial (EC 2.3.3.1)	3,56	0,50	1,00	1,51	TCA cycle
Q19749	F23B12.5	Dihydrolipoyllysine-residue acetyltransferase component of pyruvate dehydrogenase complex, mitochondrial (EC 2.3.1.12)	2,24	0,92	1,31	2,21	pyruvate dehydrogenase
Q21752	R05G6.7	Probable voltage-dependent anion-selective channel	5,12	0,75	1,36	2,29	mitochondrial anion transport
P34383	far-2; F02A9.3	Fatty-acid and retinol-binding protein 2	3,14	0,48	3,56	2,68	secreted, lipid transport and storage
P91917	tag-210; W08E3.3	Putative GTP-binding protein tag-210	4,54	0,48	1,05	3,47	unkown

UniProt ID	Gene name	Protein name	FC 40-20		FC 60-40		Category
			WT	*pept-1 (lg601)*	WT	*pept-1 (lg601)*	
Q95005	pas-4; C36B1.4	Proteasome subunit alpha type-7 (EC 3.4.25.1)	1,31	0,79	1,49	1,05	proteasome
Q21215	rack-1; K04D7.1	Guanine nucleotide-binding protein subunit beta-2-like 1	3,01	0,49	0,95	2,61	ribosomal protein
Q93572	rpa-0; F25H2.10	60S acidic ribosomal protein P0	2,24	0,66	1,10	1,69	ribosome
P48156	rps-8; F42C5.8	40S ribosomal protein S8	2,44	0,63	1,00	1,56	ribosome
O02056	rpl-4; B0041.4	60S ribosomal protein L4	2,77	0,50	0,93	2,18	ribosome
P54412	F17C11.9	Probable elongation factor 1-gamma (EF-1-gamma)	2,81	0,58	1,55	2,21	translation
Q966C6	rpl-7A; Y24D9A.4	60S ribosomal protein L7a	2,26	0,57	1,23	2,10	ribosome
O45946	rpl-18; Y45F10D.12	60S ribosomal protein L18	2,76	0,47	0,99	2,26	ribosome
Q95Y90	rpl-9; R13A5.8	60S ribosomal protein L9	4,05	0,51	0,70	2,65	ribosome
Q22054	rps-16; T01C3.6	40S ribosomal protein S16	4,04	0,49	0,80	2,82	ribosome
P52819	rpl-22; C27A2.2	60S ribosomal protein L22	3,08	0,60	1,14	2,00	ribosome
Q94300	rpl-11.1; T22F3.4	60S ribosomal protein L11	2,70	0,45	1,01	2,37	ribosome
P51403	rps-2; C49H3.11	40S ribosomal protein S2	2,56	0,54	0,94	1,90	ribosome
O02639	rpl-19; C09D4.5	60S ribosomal protein L19	2,58	0,43	0,97	1,84	ribosome
P34334	rpl-21; C14B9.7	60S ribosomal protein L21	3,98	0,48	0,88	1,96	ribosome
P49041	rps-5; T05E11.1	40S ribosomal protein S5	2,74	0,60	0,95	1,82	ribosome
O45499	rps-26; F39B2.6	40S ribosomal protein S26	1,58	0,48	1,02	1,23	ribosome
O18650	rps-19; T05F1.3	40S ribosomal protein S19	2,08	0,72	1,13	1,35	ribosome

Cluster 3							
UniProt ID	Gene name	Protein name	FC 40-20		FC 60-40		category
			WT	*pept-1 (lg601)*	WT	*pept-1 (lg601)*	
Q10121	C23G10.2	RutC family protein C23G10.2	0,51	0,96	0,97	1,42	unkown
P48162	rpl-25.1; F55D10.2	60S ribosomal protein L23a 1	0,89	1,20	0,71	1,74	ribosome
P34382	far-1; F02A9.2	Fatty-acid and retinol-binding protein 1	0,46	0,77	0,84	1,35	extracellular

According to protein function and/or pathways a strong overrepresentation of ribosomal proteins in cluster 2 was observed. As cluster 1 and 3 only consist of two or three proteins respectively, pathway analysis was restrained to cluster 2. KEGG pathway mapper confirmed 15 out of 30 proteins to the ribosome (Figure 31).

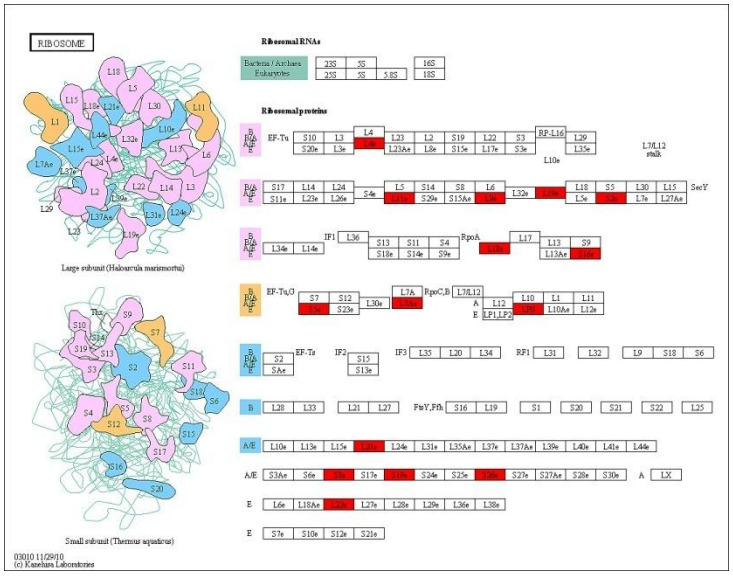

Figure 31: Ribosomal proteins of cluster 2: Red background highlights ribosomal components that show a delayed increase in abundance over time in *pept-1(lg601)* vs. WT done using KEGG Mapper – Search&Color Pathway

Another six proteins were associated with distinct metabolic pathways (Q18040, Q19749, P27604, P34575, Q27245 and Q10657), represented by glycolysis/ gluconeogenesis, TCA cycle and amino acid metabolism. Functional annotation clustering using DAVID resulted in an enrichment score for ribosomal components of 16.22. Components of larval development were found to be enriched by 5.43 fold, and “mitochondrial” associated terms by 2.15 fold. Furthermore terms related to “aging and life span”, as well as “regulation of growth rate” were found to be enriched

(full list see supplement). These clusters were also reflected in an analysis of gene ontology of biological processes. “Translation” showed the lowest p-value ($5.15*10^{-15}$), followed by “larval development” and “post-embryonic development” as well as “aging” and “pyruvate metabolic process”.

3.4. Determination of protein biosynthesis rate

The comparison of the proteome of *pept-1(lg601)* with WT animals at various times during ontogenesis showed major differences in ribosomal components. To elucidate whether this translates into decreased protein biosynthesis, the rate of GFP expression was determined in VC or *pept-1*(RNAi) treated worms. Synchronized worms were either placed on VC or *pept-1*(RNAi) until reaching L4 state. As control, worms grown on VC were pre-incubated on plates containing 7.5 mM cycloheximide (CyX), a protein synthesis inhibitor, for 2 hrs at 20°C before GFP expression was induced using a heat shock for one hour at 34°C. As expected, the rate of GFP expression was significantly reduced after incubation with cycloheximide. The same effect was seen when worms were grown on *pept-1*(RNAi) (Figure 32). The increase in fluorescence per hour dropped to about 50 % of that in VC treated worms, indicating a decreased protein biosynthesis due to *pept-1* silencing.

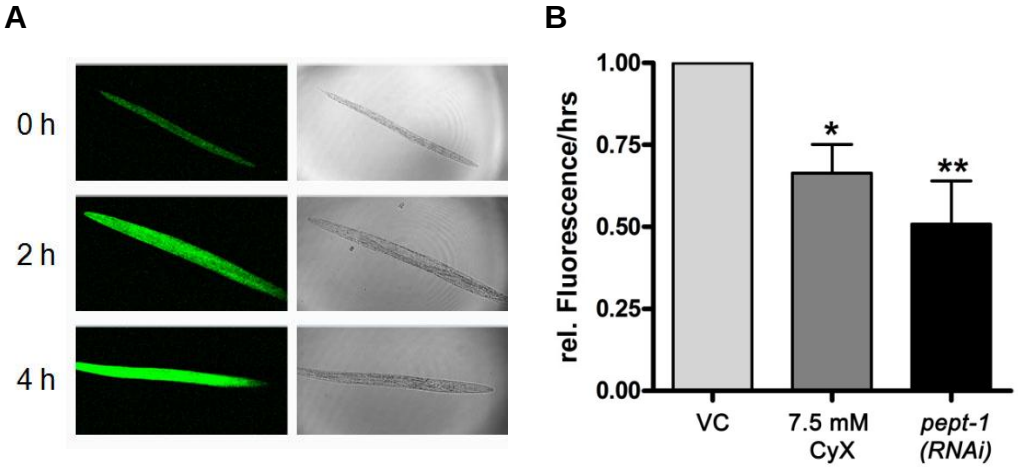

Figure 32: Protein biosynthesis rate of *pept-1(RNAi)*: (A) Determination of induced GFP expression over 4 hrs in CI2070. Representative pictures were taken using a confocal microscope **(B)** Nematodes were either grown on VC or pept-1(RNAi). As control worms grown on VC were pre-incubated with cycloheximide to inhibit protein biosynthesis. Depicted are at least three biological replicates ± SEM. One-way ANOVA in combination with tukey post hoc test was done to determine significance. Depicted are values obtained in comparison with VC.

3.5. Regulation of PEPT1 in mammals

3.5.1. In silico analysis of hPEPT1 promoter

Conservation between *C. elegans pept-1* promoter region and corresponding region of higher organisms like *mus musculus* or human was monitored, but these only showed marginal consent (data not shown). Nevertheless, promoter sequence of human *PEPT1*, published by Urttiac et al. (2001), was screened for potential transcription factor binding sites using MatInspector [111]. Four possible binding sites of Nrf2, the mammalian SKN-1 homolog, were found in the investigated upstream region (Figure 33).

Figure 33: Predicted Nrf2 binding sites in the human PEPT1 promtoer: MatInspector prediction revealed 4 potential binding sites. Core sequences are displayed in the human PEPT1 promoter region

3.5.2. Nrf2 mediated PEPT1 expression in human intestinal Caco2 cells

In mammals oxidative stress response is mediated by NF-E2-related factor 2 (Nrf2), the orthologous protein to SKN-1. MatInspector identified four possible Nrf2 binding sites in the promoter region of h*PEPT1* and therefore 2 kb of the 5` upstream region were amplified from genomic DNA retrieved of Caco2 cells. These upstream regions were fused to the luciferase gene of the pGL3 basic vector using HindIII and BglII restriction enzymes (4 bds construct, contains 4 binding sites). To get more information on the importance of predicted binding sites, the promoter construct was

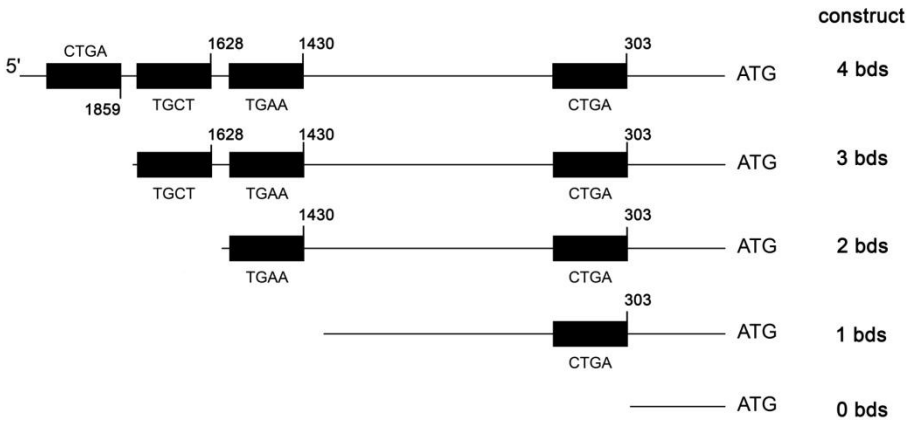

Figure 34: Schematic overview of predicted Nrf2 binding sites in *PEPT1* promoter: Promoter regions were fused to luciferase gene to detect promoter activity depending on promoter region.

shortened by one Nrf2 binding site after the other. Therefore, four different constructs were generated, the shortest containing only ~300 bp of the *PEPT1* upstream region (0 bde construct) (Figure 34).

HepG2 cells were trasfected with the reporter constructs and empty pcDNA3 plasmid. Determination of luciferase activity without any stimulation showed increasing activity with decreasing promoter length. This indicates possible repressive elements to be present. Co-transfection with pcDNA3 containing the *Nrf2* gene[112] elevated luciferase activity in all constructs in relation to co-transfection with empty pcDNA3 plasmid, although this was only significant for constructs with two or one Nrf2 binding site. However, also the shortest construct, not harboring any predicted Nrf2 binding site, showed increased luciferase activity. This indicates Nrf2 to be part of the regulatory network controlling *PEPT1* expression (Figure 35), but the exact mechanism needs further investigation.

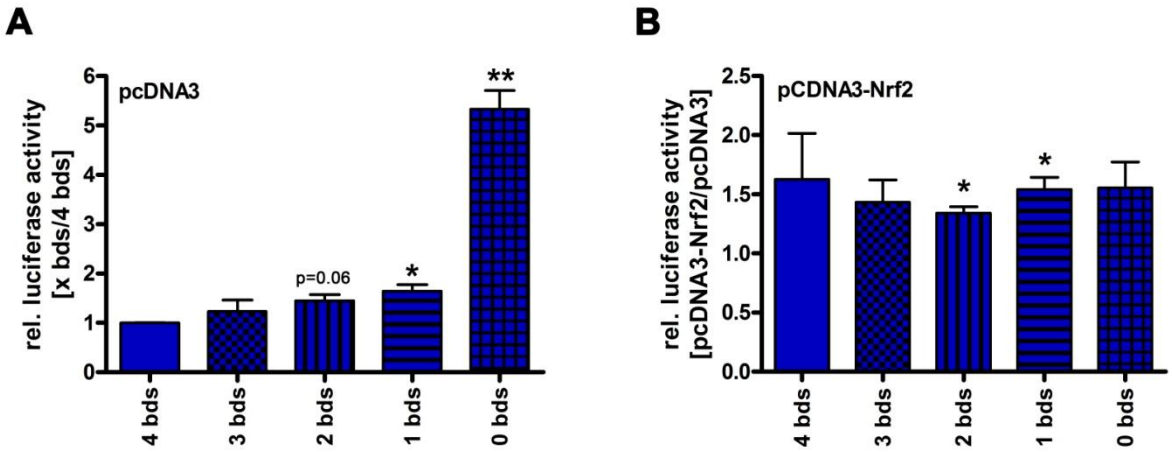

Figure 35: Nrf2 induces *PEPT1* promoter driven luciferase activity: Determination of luciferase activity in HepG2 cells after transfection with reporter constructs. Obtained values were corrected for transfection efficiency using ß-Gal activity measurement. **(A)** basal induction of activity in relation to full length construct **(B)** Stimulation using Nrf2 expression plasmid, results depicted in relation to basal activity. All experiments were done in biological duplicate.

In *C. elegans* Nrf2 is also negatively influenced by GSK3[113,114] and various substances were identified to activate Nrf2. These were in turn applied to stimulate Nrf2 dependent gene expression in Caco2 cells followed by *PEPT1* mRNA and protein level determination. In addition, ^{14}C-GlySar was used as a specific PEPT1 substrate to measure the protein transport function. After 24 hrs of starvation in FCS free medium Caco2 cells were incubated with 30 µM SB-415286, an inhibitor of GSK3, for 4 hrs. To control whether GSK3 activity was inhibited, phosphorylation status of ERK was visualized using Western Blot analysis [115]. As expected,

phosphorylation of ERK was increased, but neither PEPT1 protein nor ^{14}C-GlySar uptake showed any changes compared to control (Supplement, Figure 53)

Resveratrol, a natural occurring polyphenol with antioxidative capacity, was shown to induce Nrf2 mediated target gene expression at a non-toxic concentration of 10 µM in different cell culture systems [116,117,118]. Therefore, Caco2 cells were treated for 3 hrs, 24 hrs and 72 hrs with 10 µM resveratrol or corresponding amounts of ethanol. PEPT1 protein abundance increased over time with a peak at 24 hrs, while at 72 hrs protein levels were back to baseline. To verify induction of gene expression, mRNA levels of *PEPT1* and *NQO1* were measured. *NQO1* mRNA levels after resveratrol treatment confirmed a Nrf2 induction, but mRNA levels of *PEPT1* rather remained unchanged. Surprsingly however, protein abundance increased in line with an increased uptake of ^{14}C-GlySar into Caco2 cells (Figure 36).

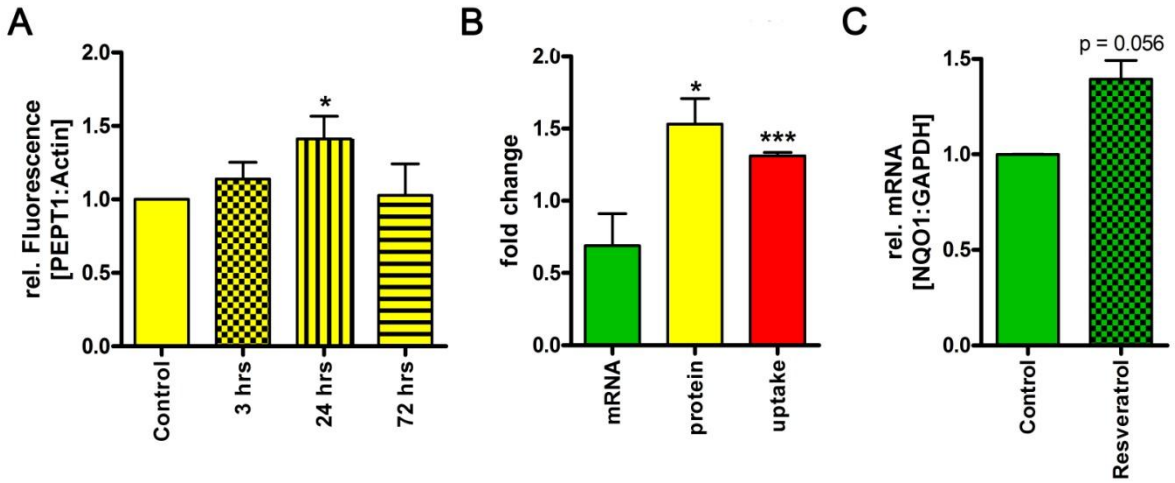

Figure 36: Nrf2 activator resveratrol enhances PEPT1 protein: (A) Effect of resveratrol on PEPT1 level over time: PEPT1 protein level after incubation with 10 µM resveratrol for 3, 24 and 72 hrs. one-way ANOVA followed by Dunnetts test for statistical analysis. **(B)** Effect of resveratrol on *PEPT1* expression: mRNA and protein levels and its uptake capacity after 24 hrs of incubation with 10 µM resveratrol. Values depict at least two experiments ±SEM **(C)** Resveratrol affects *NQO1* mRNA: mRNA of NQO1 after treatment of Caco2 for 24 hrs with 10 µM resveratrol in biological duplicate ±SEM

Menadione like resveratrol was shown to activate Nrf2 and subsequently induce the expression of its target genes [119]. Concentrations used in literature vary greatly from 2,5 µM up to 200 µM [120,119,121]. Since 100 µM decreased the viability of Caco2 by almost 50 %[122], cells were incubated with 10 µM, 30 µM and 50 µM for 24 hrs. As menadione treatment also influences cytoskeletal proteins [123], Na^+/K^+-ATPase was used as reference protein. Only the highest menadione concentration (50 µM) increased PEPT1 abundance (Figure 38).Therefore, cells were exposed to 50 µM

menadione for 24 hrs and *NQO1* and *PEPT1* mRNA levels were determined. However, similar to resveratrol, mRNA levels of *NQO1* approved Nrf2 activation while mRNA level of *PEPT1* was decreased (Figure 38).

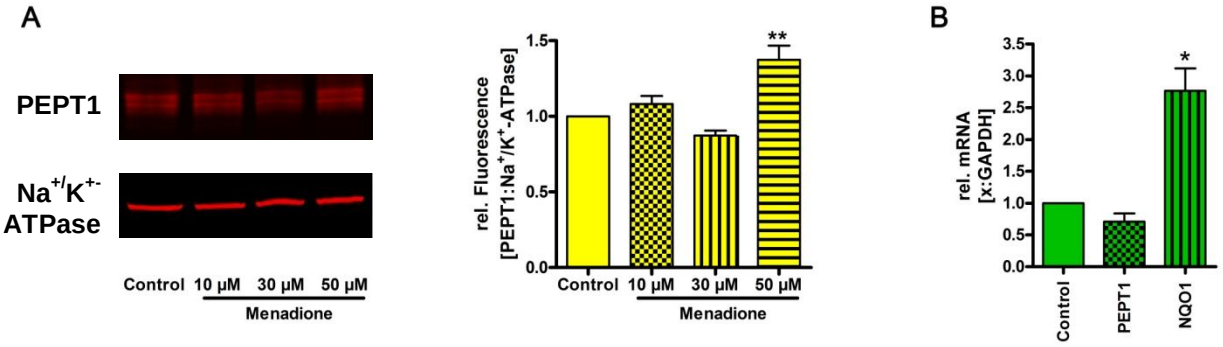

Figure 38: Menadione elevates PEPT1 protein: Effect of **(A)** 24 hrs menadione incubation on PEPT1: Caco2 cells were incubated with 10, 30 and 50 µM. one-way ANOVA followed by Dunnetts test for statistical analysis. **(B)** Detection of mRNA levels of PEPT1 and NQO1 after treatment of cells with 50 µM menadione for 24 hrs.

Another activator of Nrf2 is sulforaphane, a phytochemical derived from broccoli. A concentration of sulforaphane of 10 µM was chosen according to viability tests showing no toxic effects on Caco2[124]. After 24 hrs of incubation with 10 µM sulforaphane, mRNA of *PEPT1* as well as *NQO1* were increased. PEPT1 protein as well as function was determined after 48 hrs in accordance with previous findings of Kipp A. (personal communication). Increase in protein abundance was small but consistent, although transport did not show elevated ^{14}C-GlySar influx (Figure 37).

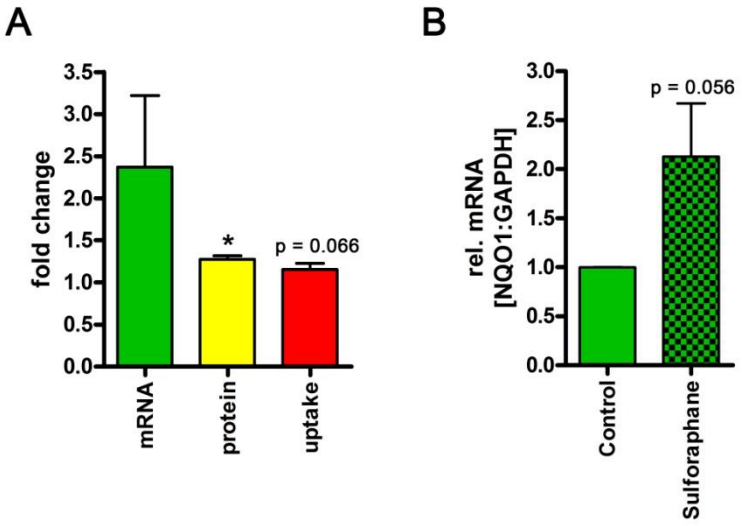

Figure 37: Effect of 10 µM sulforaphane on (A) PEPT1 and (B) *NQO1* mRNA: Treatment of Caco2 cells with 10 µM sulforaphane for 24 hrs for mRNA detection and 48 hrs for PEPT1 levels and uptake assays. Depicted are values of at least three experiments ±SEM. Significance was determined using students t-test

Ebselen is a seleno-organic antioxidant, which has glutathione peroxidase-like activity and its potential as a glutathione peroxidase mimic has been studied in various cell models [125,126,127]. Besides its antioxidant capacity, it was also shown to induce Nrf2 mediated target gene expression possibly by interacting with cysteine residues of Keap1 [125,126].

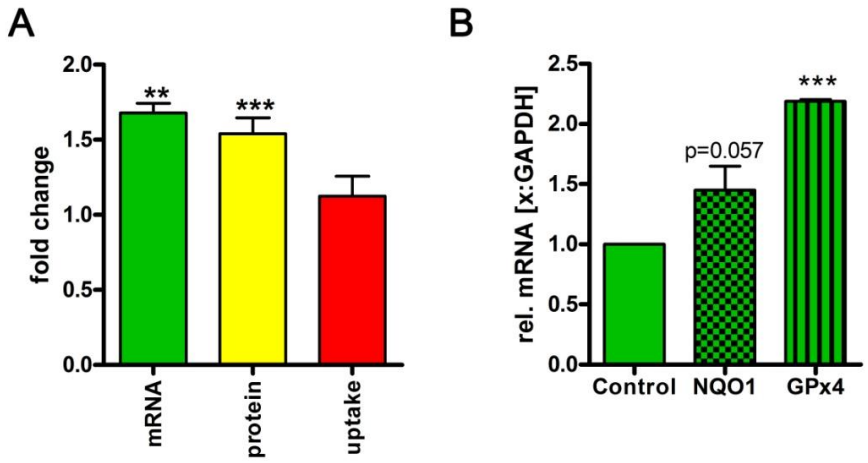

Figure 39: 30 µM Ebselen induced (A) PEPT1 and (B) *NQO1* and *GPx4* mRNA: 24 hrs incubation with 30 µM ebselen. Depicted are values of at least two experiments ±SEM. Significance was determined using students t-test.

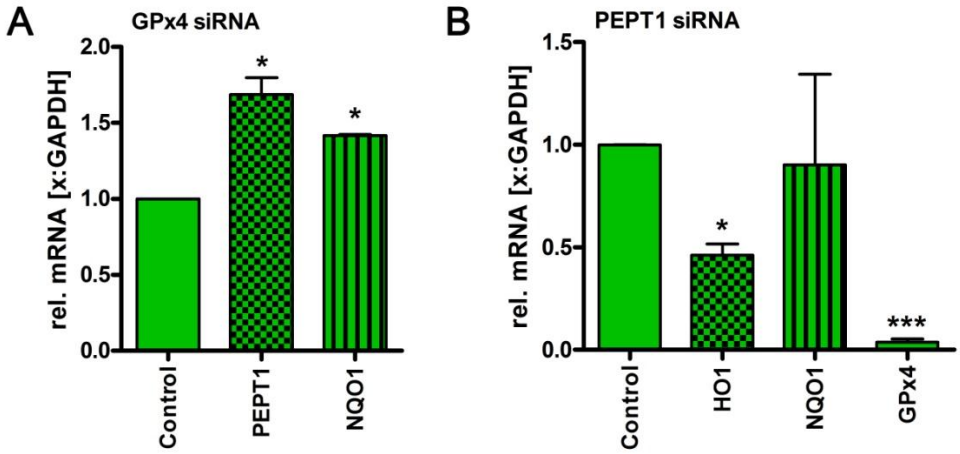

Figure 40: Interplay of PEPT1 and GPx4: (A) Effect of GPx4 siRNA on *PEPT-1* and *NQO1* in Caco2/TC7: Bars represent at least two independent measurements ± SEM. **(B)** Effect of PEPT1 siRNA on *NQO1, HO1* and *GPx4* mRNA: Bars represent at least two independent measurements ±SEM

Incubation of Caco2 with 30 µM of ebselen for 24 hrs resulted in increased PEPT1 mRNA and protein levels, as well as NQO1 mRNA content. Ebselen also induced mRNA levels of *GPx4* (Figure 39).

Benner et al.[42] previously reported a potential GPx4 homologue (F26E4.12) to influence *pept-1* expression in *C. elegans*. As siRNA of *GPx4* on Caco2/TC7 cells increased *PEPT1* mRNA levels as well as PEPT1 mediated di-peptide uptake[128], we asked whether this increase could be mediated by Nrf2. Therefore, we measured *NQO1* mRNA levels in Caco2 cells treated with GPx4 siRNA and found a significant up-regulation. Interestingly, *GPx4* mRNA decreased dramatically in response to a down-regulation of PEPT1 using siRNA. As *NQO1* mRNA levels after PEPT1 siRNA did not clarify whether Nrf2 signaling might be altered, the mRNA of another known target gene, HO1, was determined and found to be repressed by about 50 % (Figure 40).

3.5.3. Selenium dependent regulation of PEPT1 in mice

Nrf2 was already shown to be activated in the intestinte in response to a marginal selenium deficiency[129]. Taking into account that GPx4 is a selenoprotein and its activity or expression is critical for PEPT1 expression we measured *PEPT1* mRNA as well as protein levels in duodenum and/or colon of mice with a marginal selenium deficiency. Therefore, mRNA and protein levels were determined in samples from a feeding trial[129] conducted in the group of Anna Kipp (DIfE; Potsdam-Rehbrücke).

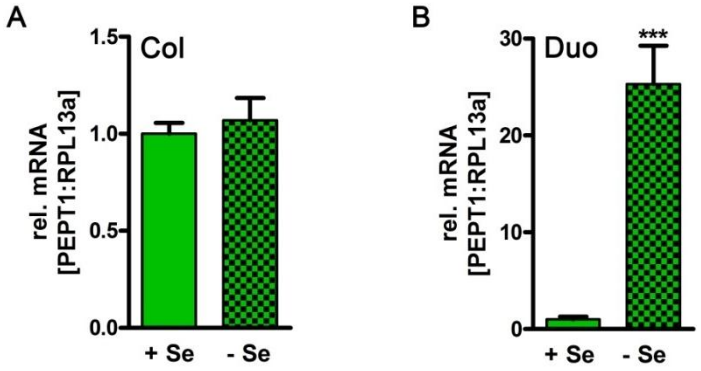

Figure 41: Selenium dependent PEPT1 expression: mRNA levels of PEPT1 in relation to RPL13a. **(A)** colonic tissue of mice fed on diets ± selen for six weeks (n=6) **(B)** tissue of duodenum of 5 mice per group. Students t-test was done for statistical analysis.

Selenium-poor (0.086 mg Se/kg) or selenium-adequate diets (0.15 mg Se/kg) were fed for six weeks to male C57BL/6J mice of 3-4 weeks of age. RNA isolation of intestinal tissues and qRT-PCR was accomplished as described in Muller et al.[129]. In colonic tissues mRNA of *PEPT1* did not change in response to selenium-poor feeding, while mRNA in duodenum increased significantly under selenium-deficiency (Figure 41). These effects were also found on the protein levels. Western Blot analysis of protein extracts retrieved from duodenum revealed elevated protein levels in selenium depleted mice. Immunohistochemical staining which was accomplished by Kipp A. (DIfE; Potsdam-Rehbrücke) showed enhanced PEPT1 abundance in the brush border membrane of epithelial cells (Figure 42).

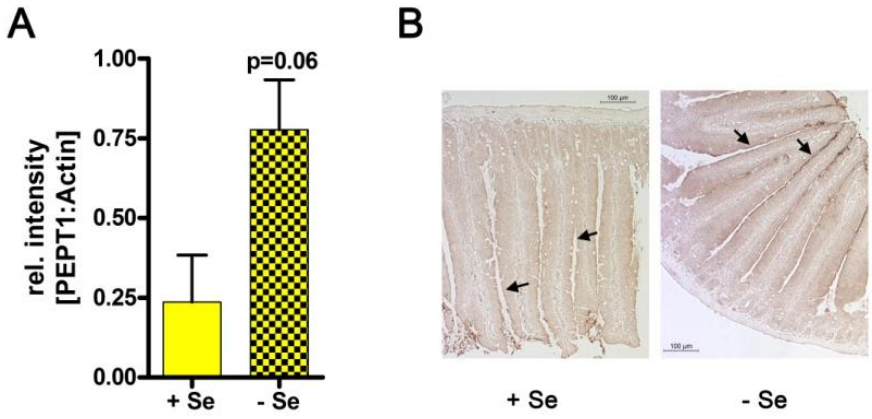

Figure 42: PEPT1 protein is elevated in selenium-poor mice: (A) total protein extracts of duodenum was analyzed using Western Blot analysis (n=3) **(B)** PEPT1 was stained in sections of duodenum from mice either fed a selenium-poor or selenium-adequate diet using immunohistochemistry with a DAB chromogen

To test whether Nrf2 is involved in basal PEPT1 expression, small intestinal mucosa of C57BL6J Nrf2$^{-/-}$ mice and WT C57BL6J was studied. Mucosa of five animals per group was obtained from the lab of Dreger H. (Charité - Universitätsmedizin Berlin). The membrane protein fraction was separated on a SDS-PAGE and PEPT1 and Actin detected using Western Blot technique. However, PEPT1 protein abundance did not change in the small intestine of C57BL6J Nrf2$^{-/-}$ mice as compared to WT C57BL6J (Figure 43).

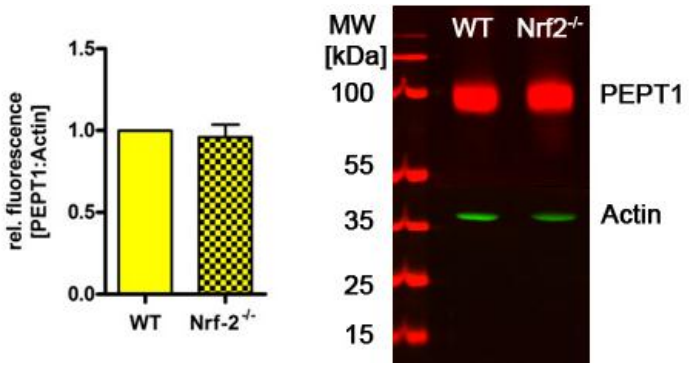

Figure 43: Nrf2 is not involved in basal transcription: Bars represent PEPT1 protein abundance in relation to actin of five animals each. On the right representative western blot depicting PEPT1 in red and Actin in green.

3.5.4. Influence of Glucose stress on PEPT1 in Caco2

To test whether *PEPT1* expression responds to glucose availability, Caco2 cells were grown in DMEM containing either 1 g/l glucose or 4.5 g/l. Caco2 cells were cultured for three passages in corresponding media. To verify whether culture period in different glucose media was long enough to detect adaptional changes, the glucose responsive protein GRP78 was detected in western blot analysis. Protein bands

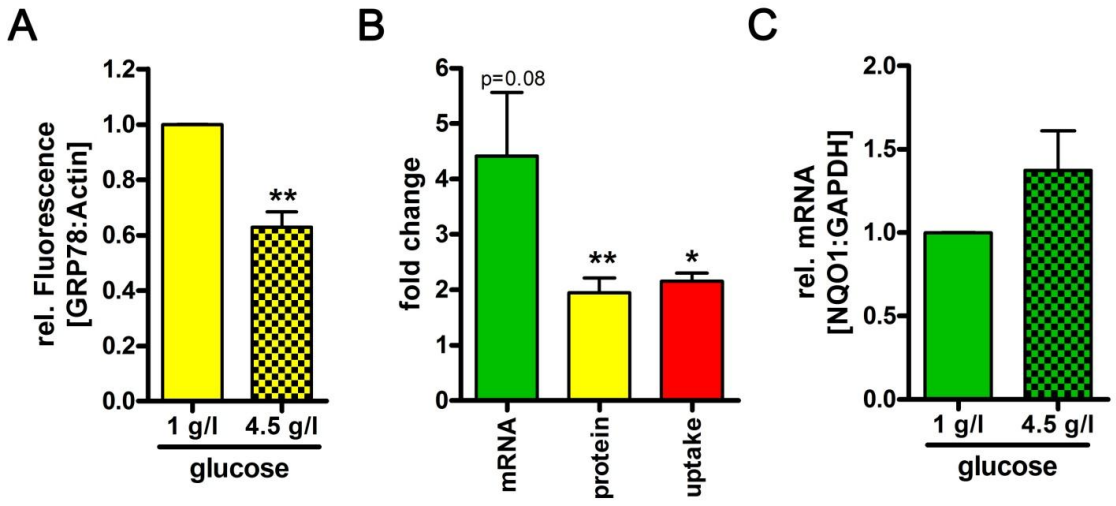

Figure 45: Glucose stress affects PEPT1 abundance in Caco2: Culturing Caco2 in media containing 1 g/l glucose or 4.5 g/l for three passages (14 days): **(A)** GRP78 protein abundance is higher under glucose deprivation **(B)** Effects on *PEPT1* mRNA, protein levels and uptake capacity in relation to standard culture media containing 1 g/l glucose **(C)** Determination of *NQO1* mRNA abundance.

revealed more prominent bands in samples from cells grown in DMEM containing only 1 g/l glucose (Figure 45), as was expected[130]. Under high glucose conditions mRNA levels of PEPT1 increased about four-fold and this translated into elevated protein abundance and function. Nrf2 target gene (*NQO1*) expression was also higher in Caco2 cells when cultured in media containing 4.5 g/l of glucose.

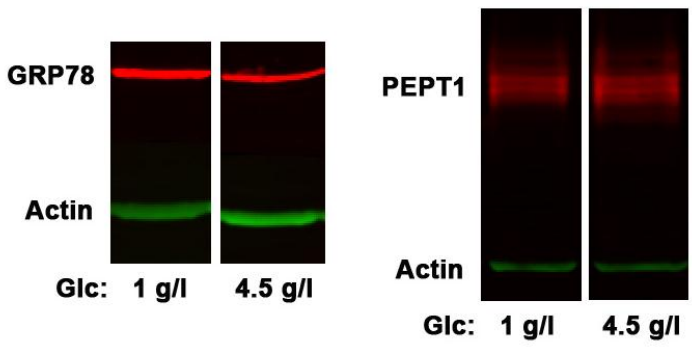

Figure 44: Representative Western Blot of GRP78 and PEPT1: Caco2 cells were cultured in media containing 1 g/l glucose or 4.5 g/l for three passages (14 days)

3.5.5. Induction of ER stress in Caco2

ER stress is initiated by the accumulation of unfolded/misfolded polypeptides in the ER lumen. Tunicamycin, an antibiotic, is causing ER stress by inhibiting N-linked glycosylation. As it is also causing cell cycle arrest, tunicamycin was added to Caco2 cells 5 days after confluency. To test efficiency of ER stress induction we first measured Grp78 mRNA expression after 24 and 48 hrs of treatment with 1 µg/ml Tunicamycin. 48 hrs of incubation resulted in ~ 3 fold increase of Grp78 mRNA level, and consequently experiments were performed after 48 hrs of tunicamycin treatment. As PEPT1 is glycosylated during its migration through the ER, we detected not only PEPT1 protein in its glycosylated form (protein G) but also after de-glycosylation

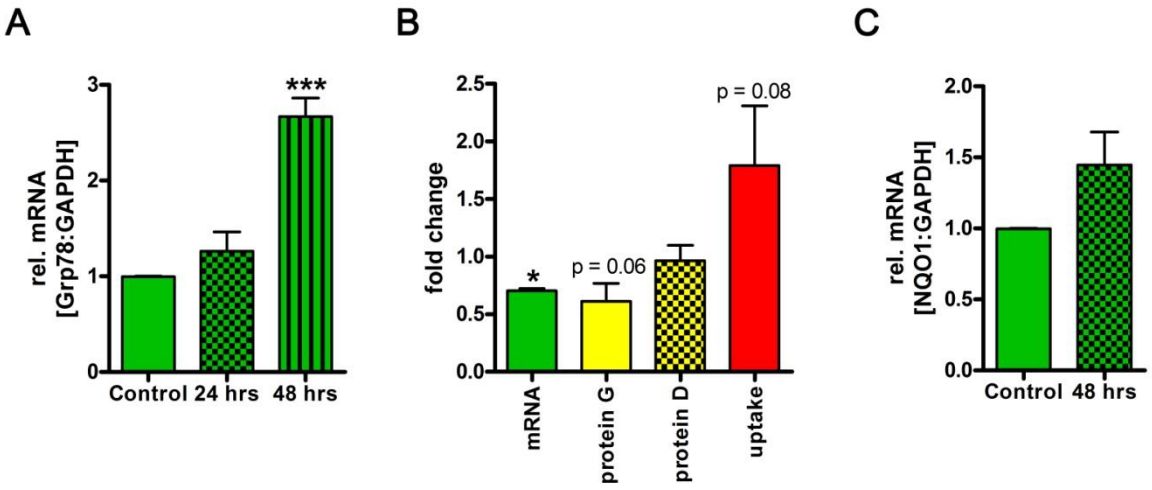

Figure 46: Inhibition of protein glycosylation using Tunicamycin has controverse effects on PEPT1: (A) Grp78 mRNA was measured as control of ER stress induction upon incubation with 1 µg/µl tunicamycin or DMSO control. **(B)** Effect on PEPT1 expression and function after 48 hrs of tunicamycin incubation **(C)** To estimate Nrf2 activity NQO1 mRNA was determined. Experiments were done in triplicate and bars represent mean ±SEM. For statistical analysis of time dependency (A) one-way ANOVA was done, otherwise students t-test was applied.

(protein D) using PNGaseF. In contrast to the observed increase of ^{14}C-GlySar uptake, overall PEPT1 abundance remained constant with a decreased fraction of the glycosylated protein. The mRNA level of *PEPT1* was even decreased, while *NQO1* mRNA increased slightly but not significantly (Figure 46).

3.5.6. Induction of autophagy modulates PEPT1 protein and function inversely

Oxidative stress induces expression of protective genes and increases autophagy to remove protein aggregates and damaged organelles. Resveratrol, menadione and sulforaphane not only activate Nrf2 but also affect autophagy[131,132,133]. Thus, we treated Caco2 cells for 24 hrs with MG132, a widely used inhibitor of the ubiquitin

proteasome system, to induce autophagy[134]. This resulted in elevated PEPT1 protein levels. However, transport rate decreased significantly (Figure 47).

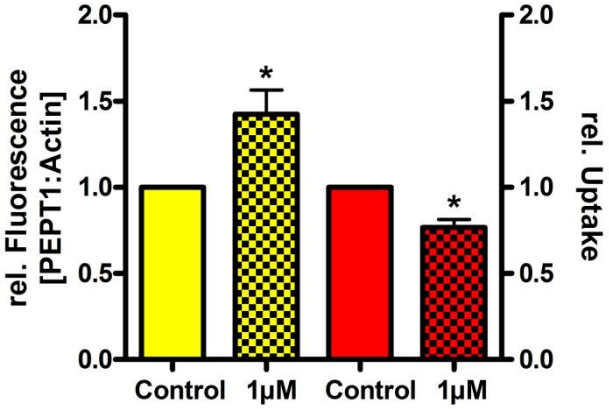

Figure 47: Autophagy inversly regulates PEPT1 protein and function: Caco2 cells were incubated for 24 hrs with 1 µM MG132 or EtOH as control. Graph depicts two or three independent replicates of uptake measurement and western blot analysis respectively.

4. Discussion

4.1. SKN-1 mediated regulation of *pept-1* ensures GSH precursor availability in *C. elegans*

Various transcription factors were already shown to regulate *PEPT1* expression in mammals (Table 19), yet *C. elegans* homologues did not affect *pept-1* expression in nematodes. However, *in silico* analysis of the promoter region of *C. elegans* revealed possible SKN-1 binding sites, with conservation between different *Caenorhabditis* species (Figure 4). Accumulation of SKN-1 by inhibiting its degradation increased the promoter activity as well as mRNA levels resulting in an elevated PEPT-1 protein abundance (Figure 5). Down-regulation of *skn-1* using RNAi did not alter *pept-1* expression at any stage (promoter activity, mRNA, protein or function), indicating SKN-1 dependent expression to be part of a stress response mechanism. Oxidative stress activates SKN-1 via reduced degradation and increased nuclear accumulation due to phosphorylation[75,64]. In *C. elegans* PEPT-1 increases in response to hydrogen peroxide treatment (Figure 6), providing enhanced capacity for the uptake of amino acids in peptide bound form, amongst them cysteine, glutamate and glycine. These amino acids serve as precursors for glutathione biosynthesis and especially cysteine availability is thought to regulate *de novo* synthesis [135]. The rate limiting formation of γ-glutamylcysteine is catalyzed by γ-glutamyl cysteine synthetase (γ-GCS)[136]. In a second step, GSH synthetase (GS) fuses glycine to the γ-glutamylcysteine resulting in GSH. Glutathione itself acts as antioxidant and serves as a substrate for various antioxidative enzymes[136,137]. Hence, up-regulation of PEPT-1 might indirectly contribute to the antioxidative stress response in *C. elegans* by providing precursors for glutathione synthesis. Contrary to expectations, *pept-1* knock-out worms exhibit an increased tolerance to oxidative stress, increased intracellular glutathione levels[138] and decreased mitochondrial ROS levels. We have previously shown that GSSG reductase activity as well as mRNA levels of γ-glutamyl cysteine synthetase and M176.2 (the homologue of GSH synthetase) are unaltered in *pept-1(lg601)*[139]. In addition, amino acid pools in *pept-1(lg601)* animals are decreased[44], limiting the substrates for *de novo* synthesis. Therefore, mutant worms cannot rapidly access amino acid pools and subsequently *de novo* synthesis of glutathione in response to stress might not be sufficient anymore to balance oxidative impact. Besides the tight

regulation of GSH synthesis intracellular GSH pools are also controlled by transport and degradation processes[135]. Extracellular degradation of GSH is mediated by γ-glutamyl transpeptidase (GGT), which catalyzes the transfer of γ-glutamyl to an acceptor amino acid. In a second step, cysteinyl-glycine is cleaved by a membrane bound dipeptidase to yield glycine and cysteine[140]. Nitrogen starvation in yeast leads to the storage of GSH in the vacuole and to longer half-lives of GSH[135]. In regard to the lower amino acid and therefore nitrogen levels of *pept-1(lg601)* it seems plausible that a similar mechanism might be responsible for the elevation of GSH pools, ensuring quick reaction on oxidative impact. Knock out of GGT in mice resulted in elevated plasma GSH levels, decreased concentrations in liver and pancreas, while small intestine and kidney were not affected. Interestingly, these knock out animals displayed severe retardation of postembryonic development[141] a phenotype also observed in *pept-1* deficient *C. elegans*.

4.2. Nrf2, the mammalian homologue of SKN-1, affects *PEPT1* expression in Caco2

Interestingly, *in silico* analysis of the human *PEPT1* promoter revealed four potential binding sites for Nrf2, the mammalian homologue of SKN-1. As found in *C. elegans*, over-expression of Nrf2 in a human intestinal cell line, directly or indirectly, also lead to increased *PEPT1* promoter activity (Figure 35). Analysis of PEPT1 levels in the intestine of *Nrf2*$^{-/-}$ mice did not reveal alterations, confirming the observations made in *C. elegans* (Figure 43),. Therefore, it is proposed that SKN-1/Nrf2 mediates the expression of *PEPT1* as part of an evolutionary conserved mechanism in response to stress. Previously shown regulatory mechanisms in mammals might therefore have developed later in evolution. Promoter activity assays indicate possible repressive elements upstream of 1628 bp of the promoter since constructs with shorter promoter sequences showed elevated activity compared to the full length promoter (Figure 35). Over-expression of Nrf2 induced luciferase expression regardless of the length of the promoter region, with the shortest construct harboring ~ 300 bp of the *PEPT1* promoter (Figure 35). These findings implicate a rather complex regulation of PEPT1 expression. Nrf2 contains a basic-leucine zipper domain[142], which allows dimerization with various proteins. However, none of the transcription factors, which have predicted binding sites in the region ~ 300 bp upstream of *PEPT1* are known to interact with Nrf2. Besides small Maf proteins (MafF, MafK and MafG), Nrf2 also

binds to CREB binding protein (CBP)[74,142], a co-activator of transcription, which has non-specific DNA binding capacity itself[143]. To exclude possible indirect actions of Nrf2 on reporter gene constructs, either by non-specific binding via dimerization with CBP or up-regulation of other transcription factors, chromatin immunoprecipitation (ChiP) would be necessary.

4.2.1. Induction of autophagy affects *PEPT1* expression in mammals

Even though mice lacking PEPT1 do not show any severe phenotype similar to *C. elegans pept-1(lg601)*, stress induced regulation of PEPT1 via Nrf2 is conserved. Nevertheless, human Caco2 cell line exhibit diminished PEPT1 levels upon incubation with hydrogen peroxide[144] in contrast to the results obtained in *C. elegans*. However, stimulation of Caco2 with Nrf2 activators resulted in elevated mRNA, protein and function of PEPT1 as observed for sulforaphane (Figure 37). Interestingly, also between different Nrf2 activating substances differences in the response in mRNA, protein or transport rate of PEPT1 were seen. Resveratrol and menadione led to a significant induction of protein and/or uptake rate but did not change *PEPT1* mRNA levels (Figure 36, Figure 38). On the contrary, mRNA and protein levels increased by treatment with ebselen, while uptake rate remained unaltered (Figure 39). These observations may lead to the conclusion that stress induced PEPT1 expression mediated by Nrf2 in mammals is not part of the oxidative stress response, but might be embedded in other protective response mechanisms, as autophagy. Autophagy in combination with the ubiquitin-proteasom system (UPS) and the chaperone system is responsible for the maintainance of protein homeostasis[145]. In addition, damaged organelles as well as protein aggregates can be removed by autophagic processes. In a first step, a membrane separates damaged components from the cytosol by, forming the autophagosome, which fuses with a lysosome to yield the autophagosome[145]. Degradation products, like amino acids or small peptides are retrieved by various transporters into the cystosol. PEPT1 has already been detected as one of these transporters in hepatic lysosomes of rats[146] as well as other cell types[147,148] . Components of both degradation pathways are regulated by Nrf2, linking Nrf2 activity to the removal of damaged proteins as well as organells[149].

Although resveratrol, menadione, sulforaphane and ebselen activate Nrf2 by diverse mechanisms, all of them were shown to interact with autophagic processes[133,132,131,150]. Additionally, *in vivo* experiments conducted in mice and rats revealed increased PEPT1 mRNA and/ or protein levels after strarvation[151,152,153], a condition with increased autophagic processes[145]. To dissect whether alterations in autophagy are responsible for PEPT1 regulation a specific inhibitor of the UPS (MG132) was used to up-regulate autophagy[134]. This resulted in elevated PEPT1 protein levels in conjunction with decreased transport activity (Figure 47). In addition, GlySar uptake studies conducted in Caco2 cells after treatment with stimulators of Nrf2 did either not show any induction or lower induction than seen for PEPT1 protein abundance. These differences in induction of protein abundance and observed uptake capacity might be indicative for intracellular rather than apical PEPT1 location. Thus, we speculate that under conditions with enhanced autophagy PEPT1 expression is up-regulated, possibly by the transcription factor Nrf2. Data indicates

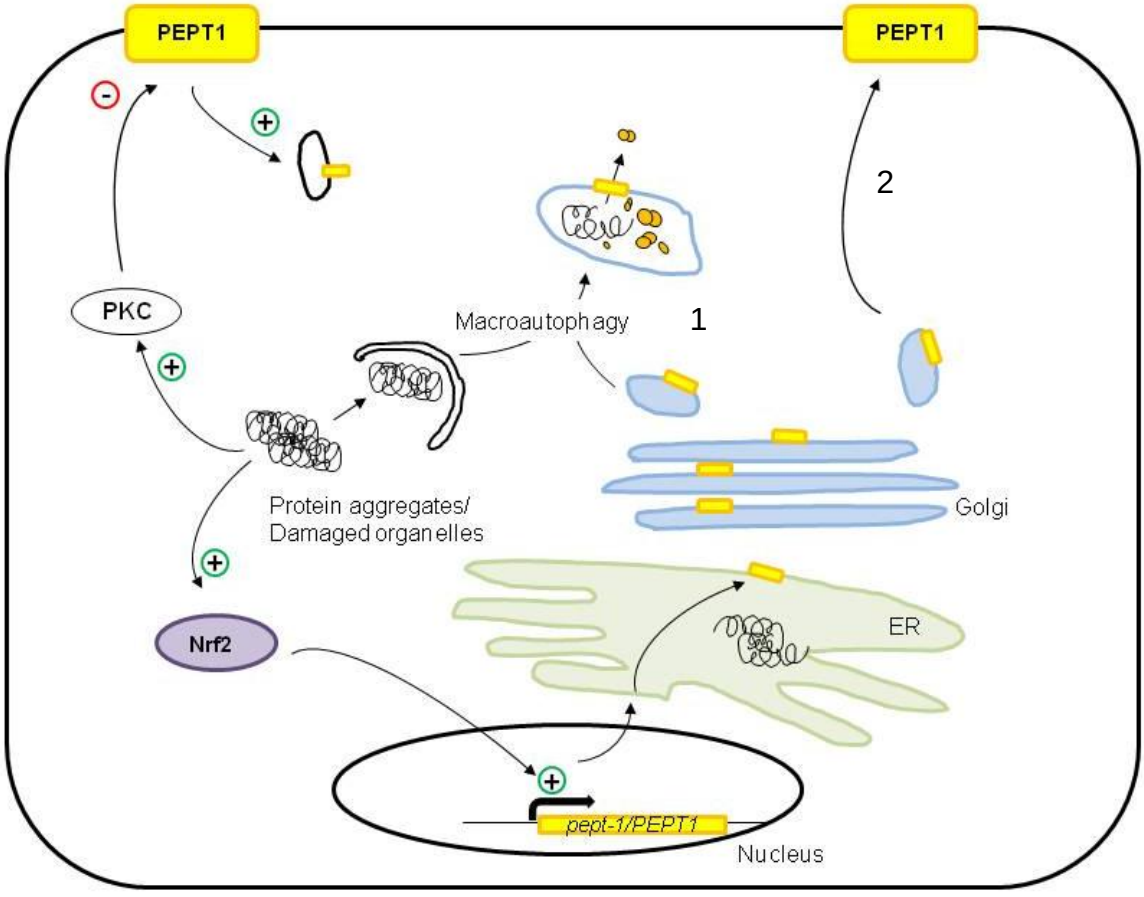

Figure 48: Model of pept-1/PEPT1 regulation upon autophagy: Autophagy is induced by various stressors. This results in activation of PKC, in turn inhibiting PEPT1 mediated uptake and trigger its retrieval from the plasma membrane. Additionally, Nrf2 is activated to mediate *PEPT1* gene expression. Thus, protein levels of PEPT1 are increased to retrieve peptides produced in lysosomes during macroautophay (1) and to restore PEPT1 in the plasma membrane (2).

that under these conditions more PEPT1 resides in the lysosomal membrane rather than in the apical membrane. This might be due to the activation of PKC, which subsequently results in the retrieval of PEPT1 from the apical membrane[154]. Additionally, newly synthesized PEPT1 might be shuttled to lysosomal compartments. Furthermore, increased expression might also restore apical PEPT1 population. Engulfed proteins are degraded by hydrolases, which require an acidic environment. This acidification of the lysosome provides the electrochemical proton-gradient for PEPT1 mediated retrieval of generated di- and tripeptides. Thus, regulation of *PEPT1* expression in connection with autophagy might ensure complete retrieval of di- and tripeptides from lysosomes.

4.2.2. Autophagy links GPx4 activity to PEPT1 expression

Not only xenobiotics are known to stimulate Nrf2 dependent gene expression but also electrophilic products that are generated during lipid peroxidation[155]. Generally GPx4, the sole phospholipid hydroperoxide glutathione peroxidase, protects phospholipid membranes from oxidative damage[156]. Hence, knock down of GPx4 results in elevation of lipid peroxidation products, while intracellular ROS levels remaine unchanged[157]. In addition, siRNA on GPx4 was found to induce *PEPT1* gene expression as well as uptake function in Caco2/TC7[128] and as shown here also to increase *NQO1* expression (Figure 40). Thus, up-regulation of PEPT1 in response to down-regulation of GPx4 might be mediated by activation of Nrf2 due to increased lipid peroxidation. Reactive aldehyde products of lipid peroxidation are able to modify proteins covalently. Although the mechanisms for the removal of those adducts are still under investigation, involvement of lysosomal degradation seems likely. On the one hand proteasomal activity was shown to be inhibited by reactive lipid species (RLS) like 4-hydroxynonenal (4-HNE) either by direct modification or indirect via protein-RLS adducts[158,159]. In addition, cell culture experiments proved lysosomal degradation to be essential for viability and removal of adducts during 4-HNE challenge[160,161]. Nevertheless, preliminary experiments using 1 µM 4-HNE did not alter PEPT1 protein after 3 hrs of incubation (data not shown). As this substance is rather unstable, longer incubation times were not employed. Yet, prolonged incubation with repeated addition of 4HNE might show the expected effects on *PEPT1* expression.

A low selenium status in mice was shown to decrease glutathione peroxidase activities with corresponding activation of Nrf2 target gene expression in duodenum as well as colon[129,162]. Thus, the observed increase in PEPT1 mRNA and protein levels in the duodenum of these mice is not surprising. However, PEPT1 did not respond to selenium depletion in colon, irrespectively of the decreased GPx function and Nrf2 activation, raising the question of further biological implications of PEPT1 in selenium-dependent regulation. One possibility could be the uptake of peptide-bound selenium (Se-Met, Se-Cys) and selenodicysteine, which is build spontaneously with cysteine[163].

4.3. Different effects of IIS and glucose stress on *pept-1/PEPT1* expression in *C. elegans* and mammals

Various studies on PEPT1 regulation in diabetic models and/or insulin treatment in rats and Caco2 cells have been published[164,165,166,167,168,169]. Insulin treatment of Caco2 cells increased the apical fraction of PEPT1, but did not change mRNA levels[168,165]. Results obtained in streptozotocin treated rats and mice show rather contradictory effects (details see Table 19). Genetically induced diabetes models such as Zucker (fa/fa) and Goto-Kakizaki mice with hyperinsulinemia and peripheral insulin resistance showed increased PEPT1 mediated uptake in the duodenum. Increased uptake was due to higher apical abundance of PEPT1 rather than via *de novo* synthesis as mRNA levels remained unchanged[167]. Microarry analysis of worms with reduced IIS (*daf-2(e1370)*) reported decreased *pept-1* gene expression[170]. However, *in silico* analysis using various bioinformatic tools did not predict a binding site for DAF-16, the major TF downstream of the insulin receptor. Nevertheless, experiments in *C. elegans* identified in accordance with microarray data DAF-16 as a repressor of *pept-1* gene expression (Figure 8, Figure 9). The reduced PEPT-1 level in *daf-2* mutants depends only partially on DAF-16 since double knock out did not fully restore PEPT-1 levels (Figure 9). Thus, insulin action leading to an inhibition of DAF-16/FOXO would result in increased *pept-1/PEPT1* transcription, constituting a negative feedback loop. In cell culture models insulin treatment only enhanced uptake rather than transcription[165]. Nevertheless, a possible repressor function of FOXO in mammals cannot be excluded on the basis of previous literature. Therefore, *C. elegans* as well as Caco2 cells were exposed to high glucose levels. While *C. elegans* showed a DAF-16 dependent down-regulation of PEPT-1 (Figure 9), *PEPT1*

expression (mRNA, protein, uptake function) increased in Caco2 cells (Figure 45). Expression of other nutrient transporters such as SGLT1 were not altered or even decreased (GLUT-1) in cell culture models in response to long term glucose exposure, showing that observed effects are specific for PEPT1 [171,172]. High glucose concentrations in cell culture are also associated with increased lipid peroxides[172,173] as well as PKC activated gene expression[174] giving rise to a possible Nrf2 involvement. This is supported by the fact that glucose stress in *daf-16* deficient worms rather increased PEPT-1 protein, uncovering SKN-1 driven gene expression. In addition, *NQO1* expression in Caco2 was slightly elevated in response to high glucose levels. However, the primary response in WT *C. elegans* does not mimick the effects seen in Caco2 cell culture. This could either be due to evolutionary differences, or might be explained by *C. elegans* representing the response of a whole organism to long-term glucose exposure which may result in insulin resistance while cell culture only reflects cellular mechanisms. As nutrient uptake naturally comprises proteins, carbohydrates and fat it seems plausible that uptake and metabolism of all components are regulated by similar if not the same mechanisms. Insulin is not only secreted in response to glucose but also amino acids can trigger an insulin release from the pancreas, providing a positive feedback loop on amino acid uptake in peptide bound form. Additionally, insulin stimulates leptin secretion, which seem to enhance PEPT1 expression (mRNA, protein and transport)[27] contributing to the positive feedback loop. During fasting, insulin and leptin levels are decreased, suggesting a decrease in PEPT1 expression[175]. However, fasting of mice as well as rats was shown to increase PEPT1 in mRNA and protein abundance[152,151,176,153], which might be attributed to a higher rate of autophagy and a subsequent Nrf2 mediated induction of PEPT1 expression.

4.4. Possible participation of XBP-1 in expression control of *pept-1/PEPT1*

DAF-16 was here identified as a repressor of *pept-1* expression in *C. elegans*. However, the double knock out of insulin-like receptor *daf-2* and the FOXO homologue *daf-16* did not result in full recovery of PEPT-1 levels, implicating additional mechanisms involved in *pept-1* expression. Henis-Korenblit et al. (2010)[107] proposed the interaction of DAF-16 and XBP-1 to regulate a gene named *dox-1*, encoding a protein probably functioning in RNA splicing. In addition, interaction of

XBP-1 with a FoxO family member, namely FoxO1 was previously shown to regulate glucose homeostasis in mice[177]. Taking these results into account the possible role of XBP-1 in *pept-1/PEPT1* gene expression was studied. In *C. elegans* silencing of *xbp-1* resulted in decreased *pept-1* expression (promoter activity, mRNA, protein and uptake function, Figure 12), while tunicamycin treatment provoked elevated mRNA levels of *pept-1* (personal communication, Blackwell K.). Silencing of *xbp-1* caused DAF-16 translocation into the nucleus, but mRNA levels of established DAF-16 target were not altered (Figure 13). Furthermore, *daf-2* mutants were shown to have an improved ER homeostasis accompanied with a low level of *xbp-1/ire-1* pathway activity[107]. Thus, *xbp-1*(RNAi) was not able to further decrease PEPT-1 content in *daf-2(e1370),* while in *daf-16* mutants still a small decline was observed (Figure 11). Therefore, activation of the repressor DAF-16 in combination with a decreased activity of the activator XBP-1 accounts most likely for the reduced *pept-1* expression in *daf-2(e1370)*. The XBP-1/ IRE-1 signaling pathway is not only of great importance during ER stress, but also under physiological conditions to maintain ER homeostasis[178]. Microarray analysis of L2 larvae harboring defects in *xbp-1*, *ire-1* or *atf-6* revealed regulation of a large set of genes, involved in metabolism, gene expression and signal transduction[95]. However, this data set only showed minor changes in *pept-1* expression with fold changes > -2. Only tunicamycin treatment in *xbp-1* mutant animals showed a more than 2 fold reduction of *pept-1*[95]. As the role of the UPR under physiological conditions is not yet understood, the biological role of XBP-1 as an activator of basal *pept-1* gene expression remains elusive. ER stress induced PEPT-1 expression might be linked to the UPR via the protein degradation pathways (ERAD I and II). Accumulation of malfolded proteins in the ER induces ERAD to remove polypeptides from the ER. In a first step, misfolded proteins are translocated into the cytosol. Subsequently ubiquitinylation results in hydrolysis by the proteasome. If degradation via the proteasome is not sufficient, aggregates undergo macroautophagy[91]. Thus, it might be speculated that in *C. elegans* PEPT-1 is localized in the apical membrane of intestinal cells as well as in lysosomal membranes as proposed in mammals.

Preliminary experiments utilizing tunicamycin for the induction of UPR in Caco2 cells did not give a clear picture on possible regulation of *PEPT1* expression. Uptake of the PEPT1 substrate GlySar, however, was increased after treatment of Caco2 cells with tunicamycin. Fully glycosylated PEPT1 protein content was decreased,

suggesting other mechanisms than expressional changes to be responsible for enhanced uptake (Figure 46). As the main branch of the unfolded protein response shifted from IRE-1/XBP-1 in nematodes to ATF6 in mammals, it is not surprising that these regulatory mechanisms cannot be transferred to mammals[95,100].

4.5. Dynamic proteome analysis links *pept-1* expression to overall proteostasis in *C. elegans*

Proteome as well as transcriptome analysis of intestinal mucosa of control and PEPT1 deficient mice did not uncover any evidence for compensatory mechanisms[39]. However, in *C. elegans* transcriptomics as well as quantitative proteomics revealed major alterations in worms lacking *pept-1*. During the ontogenesis of WT nematodes a large quantitiy of proteins rise in their abundance. Of 25 proteins up-regualted at 40 hrs after hatching compared to 20 hrs, 12 are either ribosomal proteins or involved in ribosome biogenesis (Table 2, Figure 23). One protein showing a decreased content is also part of the ribosome (Q95Y04). The overrepresentation of “translation” is therefore found in gene ontology analysis. Although, it is not very surprising that protein biosynthesis is one of the most important processes during larval development and growth, differences in the proteome of developmentally retarded mutant worms compared to WT are impressive. The retardation of development in *pept-1(lg601)* animals is mirrored in a rather static proteome. While in WT worms 61 proteins were differentially expressed only 16 proteins were found to change during ontogenesis of *pept-1(lg601)* indicating altered protein synthesis and/ or turn-over (Figure 25). This is supported by the finding that only three out of these 16 proteins are part of the ribosome compared to 13 out of 61 in WT. A direct comparison of genotypes further illustrates decreased protein synthesis capacity in *pept-1(lg601)*. Out of 35 proteins showing strain*time interaction, 17 proteins are part of the ribosome (Table 5). Except for P48162 (RPL-25.1), the remaining 16 proteins displayed a delayed increase in abundances in *pept-1(lg601)* compared to WT animals. Three ribosomal proteins were decreased regardless of larval stage depicting a genotype-specific change. Measuring protein synthesis by GFP fusion construct proved a slower rate in agreement with a decreased ribosomal function (Figure 32). Thus, the loss of PEPT-1 results in a lower expression level of ribosomal proteins and hence to a decreased overall protein synthesis rate. Whether the lower expression of ribosomal proteins is a consequence of lower amino acid

concentrations with subsequent decelerated protein synthesis remains elusive. Amino acid supplementation in *pept-1(lg601)* did not cause a rescue of the phenotype[138]. However, expression of ribosomal proteins is regulated via the TOR signaling pathway[179,180]. As Meissner et al. (2004)[138] proposed altered TOR signaling in *pept-1(lg601)* worms*,* altered TOR signaling in *pept-1(lg601)* might be causative for the down-regulation of ribosomal proteins. As TOR signaling is known to regulate cell proliferation and growth, retarded development might as well be directly linked to it. A direct correlation of protein synthesis rate and ribosomal content was already observed in the developing liver of mice accompanied by slower protein degradation rates during liver growth[181]. Unfortunately determination of protein degradation rates were not possible, as radioactive pulse-chase experiments failed. Thus, we can only speculate that protein degradation might be altered in *pept-1(lg601)*. Indeed, a proteasomal component (Q95005; PAS-4) was detected with lower abundance in *pept-1(lg601)* as compared to WT animals. In addition, the transcriptomics data set[44] perviously generated revealed a small but consistent down-regulation (-1.2 to -1.65 fold) of various proteasomal proteins including *pas-4* (-1.4 fold). Based on these data it is suggested that the protein turn-over is severly impaired in *pept-1* knock out worms. However, proteostasis is not only regulated by the rate of protein synthesis and degradation but also by proper protein folding.

After the synthesis of polypeptide chains a characteristic three dimensional structure is formed by interaction of amino acid residues. This process is called protein folding. Only properly folded proteins are functional, while misfolded proteins can be harmful for the cell. Thus, protein misfolding and aggregation is implicated in various diseases[85]. To circumvent the accumulation of misfolded proteins chaperones help polypeptide chains to adopt their functional conformation. Previously published microarray data[139] on *pept-1(lg601)* revealed a more than 3 fold down-regulation of five transcripts encoding for chaperones (hsp-16.41, hsp-16.2, hsp-70, hsp-16.1 and hsp-16.48). In addition, quantitative proteome analysis showed decreased levels of six proteins involved in protein folding (Table 4), whereby two of them (P11141; HSP-6 and P50140; HSP-60) are known to be induced upon an overload of unfolded proteins in mitochondria. In *pept-1(lg601)* P09446 (HSP-1), a constitutivly expressed chaperone, only accounts for ~ 50% of WT levels. This suggests a decreased activity of the unfolded protein response in general. As the protein synthesis rate in *pept-1(lg601)* appears to be reduced, the folding machineries of the ER, the mitochondria

and the cytosolic compartment encounter lower levels of loading. Nematodes lacking *pept-1* show higher heat tolerance, increased oxidative stress resistance and lower mitochondrial ROS status. Thus, it is likely that ER as well as mitochondrial homeostasis itself are improved[41,42].

4.6. How the interplay of SKN-1, DAF-16 and XBP-1 affects the phenotypic outcome in PEPT-1 deficient worms

Some of the observed characterics of *pept-1(lg601)* are also present in *daf-2* mutants, as for example the elevated fat stores and increased ROS resistance. While *daf-2(e1370)* posses 1.4 times as much total body fat as WT, *pept-1(lg601)* even have twice as much fat[44]. Other phenotypic features of *pept-1(lg601)* are only noticeable in a *daf-2* mutant background. Adult life span of *pept-1(lg601)* was not changed, however knock out of the transporter in *daf-2(e1370)* resulted in a much stronger longevity phenotype as compared to *daf-2(e1370)*[139].

To validate whether reduced PEPT-1 abundance in *daf-2(e1370)* is responsible for the elevation of fat content, we used *wdr-23*(RNAi) to counterregulate PEPT-1 levels. Indeed, indirect over-expression of SKN-1 and subsequently of PEPT-1 using *wdr-23* silencing, did decrease the fat content in *daf-2* mutants. This was independent of PEPT-1 protein function, as the same effect was observed in the *pept-1* knock out strain (Figure 16). Determination of PEPT-1 function after *wdr-23*(RNAi) did decrease β-AlaLys-AMCA uptake (Figure 5). Silencing of *wdr-23* in WT did not influence the fat content. As IIS deficient nematodes already depict increased SKN-1 accumulation in the nucleus, it is rather unlikely that increased SKN-1 function is responsible for the reduction in fat content by *wdr-23*(RNAi). These experiments indicate that not only PEPT-1 function is important for fat metabolism but also protein abundance *per se*. However, literature search did not provide any hints on a possible underlying mechanism. Decrease in PEPT-1 function accompanied by reduced protein levels due to *xbp-1*(RNAi) resulted in an elevated fat content (Figure 14), confirming the proposed model of enhanced fatty acid uptake and altered fatty acid metabolism in *pept-1* deficient nematodes[44]. A conditional knock out of XBP1 in hepatocytes of mice revealed its importance in lipid homeostasis by a decrease in *de novo* synthesis of lipids in the liver[182]. A reduced *de novo* synthesis was also observed in *pept-1(lg601),* although the fat content itself was higher[44]. In *C. elegans* IRE-1 was

associated with fasting induced fatty acid degradation, adding further prove for an interrelationsship of the ER and fat homeostasis. Thus, elevated fat content in *pept-1(lg601)* is most likely due to a diminished PEPT-1 function with a subsequently enhanced fatty acid uptake, while a low level of *de novo* lipid synthesis might be attributed to the low status of the IRE-1/XBP-1 pathway.

SKN-1 is one of the major transcription factors involved in life span regulation as well as thermotolerance. As both are altered in *pept-1* knock, in WT as well as *daf-2* mutant background, and SKN-1 is a regulator of *pept-1* gene expression we assessed its role in life span expansion. Interestingly, silencing of *skn-1* had a greater impact on life span in *pept-1(lg601)* as compared to WT suggesting SKN-1 to be more active orchestrating some of the compensatory mechanisms (Figure 18). In contrast, the effect of *gsk-3*(RNAi) in WT was stronger than in *pept-1(lg601)*. Hence, the GSK-3 activation status in *pept-1(lg601)* seems to be lowered, whereby SKN-1 activity is raised. This enhanced SKN-1 activation might contribute to the life span increasing effect of *pept-1* knock out in a *daf-2(e1370)* background. Thus, *gsk-3*(RNAi) would be expected to extend life span of *daf-2(e1370)*, while silencing of *skn-1* should decrease the life span of *daf-2(e1370) pept-1(lg601)*. Both effects were observed (Figure 17), confirming the proposed involvement of an altered SKN-1 signaling in *pept-1* knock out worms. Impaired GSK-3 activity and subsequently an activated glycogen synthase might also explain the increased glycogen content found in *daf-2(e1370).* GSK-3 activity is inhibited upon insulin signaling, thus it is supposed to be constitutivly active in *daf-2(e1370)* and, therefore, glycogen synthase should be inhibited. Further characteristics of the *daf-2* mutants as well as the *pept-1* knock out cannot be explained by the proposed reduced GSK-3 acitivty or are even contradictory to the expected phenotype. Elevated glycogenesis in cells is associated with augmented senesecence and aging[183], contradicting the longevity phenotype of *daf-2(e1370)*. As GSK-3 is not only regulated by insulin signaling but also in response to WNT signaling, growth factors and the hedgehog pathway, it is central for various cellular processes including cell development, gene transcription, proliferation and protein translation[184]. Thus, it becomes difficult to define its function in an organism and its effects on cellular outcome. Unfortunately, we were not able to assess the phosphorylation status of GSK-3 in *C. elegans* due to the lack of specific antibodies. As GSK-3 also regulates the activity of various transcription factors (e.g.: CREB, HSF-1 and Myc)[184] the indirect estimation of activity by measuring mRNA

levels of “target” genes, is difficult to interpret. The extreme long life span of *daf-2(e1370) pept-1(lg601)* is therefore probably the sum of various alterations.

4.7. The patterning of the proteome of PEPT-1 deficient nematodes reflects the retarded development

The development of multicellular organisms is complex and requires the exact timing of gene expression and subsequently of the abundance of functional protein. Even though ontogenesis of *C. elegans* is probably the best understood in terms of genetic control, dynamic protein patterns are still rarely studied. Analysis of the dynamics of the proteome might therefore add to the understanding of developmental processes. The delayed postembryonic development of *pept-1(lg601)* was also observed in the proteome changes. A decelerated protein metabolism in *pept-1* knock out animals results in a rather static proteome. In WT animals, the majority of proteins showing a genotype*time interaction changed between 20 and 40 hrs after hatching, while in *pept-1(lg601)* this rise occured between 40 and 60 hrs. A large fraction of the protein clusters constitutes ribosomal proteins (Table 5, cluster 2). Besides the delayed rise in ribosomal protein content, three components of the ribosome (Q9N4I4, P49180 and Q9XVF7) were genotype-specifically down-regulated in *pept-1(lg601)* (Table 4). Various mutations affecting ribosomal genes translated into altered development in Drosophila[185]. In various RNAi based screens, silencing of genes implicated in protein synthesis amongst other metabolic processes larval development as well as reproduction have been found negatively influenced[186,187]. Only five of the differentially expressed proteins found here were also found in the study of Kamath et al. 2003[188], whereby only one (P54412) was associated with protein synthesis. Nevertheless, silencing of four (Q18359, Q05036, Q19749 and P54412) of them resulted in phenotypic alterations of growth. Additionally, amongst others, RNAi of *rpl-4* (O02056) and *rps-2* (P51403) resulted in abnormal development as reported by Kerins et al. 2010[186]. Investigations of protein synthesis during the development of insects showed an augmented total protein content per mg tissue followed by a decline reaching adulthood[189]. This overall pattern matches well with the course of individual proteins obtained here during ontogenesis in wild-type worms. The comparison of *pept-1(lg601)* protein courses during development demonstrates that the retarded development is interconnected with the delayed increase in the majority

of proteins (Table 5, cluster 1 and 2). The increase in ribosome biogenesis therefore seems closely associated with the onset of specific developmental processes.

During WT development, the increase of proteins associated with the TCA cycle as well as with oxidative phosphorylation (Table 2) is indicative for an enhanced mitochondrial biogenesis. This is in accordance with data providing evidence for a mitochondrial burst at the end of the L4 stage[190]. Concomitantly, the respiration rates were shown to augment at later stages of development[191]. These developmental steps were not detected in the protein patterns of *pept-1(lg601)* during ontogenesis (Table 3). Nevertheless, three proteins associated with energy assimilation (Q10657, P34575, Q19749) were found to be up-regualted in *pept-1(lg601)* although time-displaced as compared to WT (Table 5).

Five proteins exhibit not only a delayed increase in abundance but a different pattern of expression in *pept-1* deficient nematodes, including vinuculin (P19826, DEB-1) and an ATP synthase subunit (P46561, ATP-2) (Table 5, cluster 1). The expression pattern obtained for P46561 in the present study is similar with data found in literature[192]. Both are important for normal ontogenesis as their down-regulation resulted in phenotypes with impaired development. Interestingly, ATP-2 is required for the L3-to-L4 transition. Lack of *atp-2*, especially in cell lineages that give rise to body muscles, the gonad and the vulva, is followed by larval arrest at the L3 stage[193]. Thus, gain in ATP-2 at 60 hrs in *pept-1(lg601)* might push the transition to the L4 stage. Three proteins (Q10121, P48162, P34382) were found to be regulated in a reverse fashion, with a decline in WT and an increase in *pept-1(lg601)* (Figure 29, Figure 30). Unfortunately, very little is known about these proteins. The function of Q10121 (C23G10.2) is not yet known, but it was found to interact with SGT-1[194], a protein capable of binding to HSP-70 as well as HSP-90 and thereby regulating their activity[195]. The sequence of Q10121 does not contain any predicted domains associated with chaperone activity as retrieved from KEGG, hence not providing any hint on a possible involvement in protein folding. P48162 (RPL-25.1) is part of the ribosome and its down-regulation is associated with various phenotypes depending on the strain, including a reduced brood size and slow growth (retrieved from Wormbase). The elevation of protein abundance might be an attempt to compensate for the reduced levels of the other ribosomal proteins or for the subsequent lower translation rate. The third protein (P34328; FAR-1) is a fatty acid/ retinol binding

protein. Interestingly, a second member of the FAR-family, FAR-2 (P34383), showed a significant regulation as well (Table 5). FAR-2 is located in the body wall and vulva muscle cells and the increase in abundance of this protein during development might be explained by the differentiation of the vulva. This nicely reflects the retardation of *pept-1(lg601)* as increase in abundance was once again only seen at later stages.

4.8. Genotype specific changes in *pept-1(lg601)* animals contribute to shift in proteome dynamics

Genotype-specific protein changes were only found for six proteins in the mucosa of *PEPT-1* deficient mice. A peptidyl-prolyl-cis-transisomerase (P52015, CYN-7) was found with decreased levels in *pept-1(lg601)*, while a protein with the same function was identified in the mucosa of mice lacking *PEPT1* with more than two fold increased levels[196]. Almost 50 % of the strain specific expressed proteins were identified as involved in protein metabolism. Thus, proteostasis is severly altered in *pept-1* mutant worms, as discussed earlier. As most of the quantified ribosomal proteins only show a delayed expression it might be interesting to elucidate the exceptional position of RPL-1 (Q9N4I4), RPL-33 (P49180) and RPL-2 (Q9XVF7) as they remain at a low level throughout ontogenesis (Table 4). However, a literature search did not provide any studies concerning their expression or possible function other than protein synthesis. Besides a muscle protein (P02566) and a probable NADH dehydrogenase alpha subcomplex (Q18359), an uncharacterized protein (Q05036) conatinaing a HSP70 motif depicted lower levels regardless of developmental stage. Silencing of P02566 or Q05036 was shown to cause abnormalities in growth[188]. Thus, decreased abundances might add to the developmental retardation in *pept-1(lg601)*.

The S-adenosylmethionine synthase (O17680; SAMS-1) was found to be differentially regulated on protein as well as mRNA level in *pept-1(lg601)* compared to WT[103]. The down-regulation at each developmental time point is comparable with the reported decrease[103]. Metabotyping of the mutant strain in combination with transciptomics and proteomics suggests the one carbon metabolism to be altered[103]. Shortly after this study was pusblished, Li et al. (2011) established the link between one carbon metabolism and fat storage/ metabolism in *C. elegans*[197], further supporting the idea of these alterations to be causative for some aspects of the *pept-*

1(lg601) phenotype. However, it remains unanswered why expression as well as protein levels of SAMS-1 are decreased in *pept-1(lg601)*. In wild-type yeast S-adenosylmethionine synthetase expression is diminished by application of external methionine[198]. As methionine conencetration were found to be decreased in *pept-1(lg601)* such a regulatory mechanism can be excluded.

Another protein found to be down-regulated according to genotype is P34559 (ECH-6). It is involved in amino acid as well as lipid metabolism. Not only fatty acid uptake was shown to be altered in *pept-1(lg601)* but also fatty acid metabolism. Monounsaturated fatty acids increased in *pept-1(lg601)* while polyunsaturated fatty acids decreased. Although transcriptomic data mainly showed alterations in peroxisomal fatty acid metabolism, mitochondria may as well contribute to the observed alterations. ECH-6 is a mitochondrial enoyl-CoA hydratase, catalyzing fatty acid elongation. However, composition of fatty acids of short and medium chain length were increased in *pept-1(lg601)*[44]. As OP50 feeding bacteria mainly provide short and medium chain fatty acids, the increased absorption rate in *pept-1(lg601)* might cause a compensatory down-regulation of proteins involved in *de novo* fatty acid synthesis.

5. Summary

Deletion of *pept-1* in *C. elegans* causes severe defects in development, growth and reproduction. Thus, expression of *pept-1* is of great importance in the nematode and therefore tightly regulated. To elucidate the regulatory network controlling gene expression, an *in silico* analysis of the promoter region was conducted. The influence of a candidate transcription factor, namely SKN-1, on promoter activity, mRNA, protein and function of PEPT-1 was determined. The results identified SKN-1 as an activator of *pept-1* gene expression in response to stress. To assess the possible conservation between species, human PEPT1 promoter was analyzed for potential binding sites of Nrf2, the mammalian homologue of SKN-1. Four binding sites were predicted for Nrf2, which is the major regulator of various stress responses, including oxidative and xenobiotic stress. Reporter gene assays in Caco2 cell cultures confirmed the involvement of Nrf2 in PEPT1 gene expression. Similar to *C. elegans*, Nrf2 seems to be responsible for stress induced expression of PEPT1 in mammals. Unlike in nematodes, oxidative stress is not causing up-regulation of PEPT1 in Caco2 cells, however, increased autophagy transmitted by Nrf2 increases PEPT1 protein content and to a lesser extent transport function. Thus, we propose more PEPT-1 to reside in lysosomal membranes. In addition, autophagy induces PKC, which mediates PEPT1 retrieval from the apical membrane. Clearance of protein adducts or aggregates is either accomplished by the ubiquitin dependent proteasome or by macroautophagic processes. Damaged proteins or organelles are engulfed and degraded after fusion with late endosomes or lysosomes. Degradation of these proteins results in amino acids and small peptides, which are delivered to the cytosol by various transporters including PEPT1.

Engagement of XBP-1/UPR in the expression of *pept-1* in *C. elegans* further supports this model, although this mechanism seems not to be conserved between nematodes and mammals. Hence, PEPT-1 in *C. elegans* might be of greater importance for proteastasis than in mammals. Lack of an obivious phenotype in the knock mouse may be taken as evidence for this. Quantitative proteome analysis as a function of development of *pept-1(lg601)* in comparison with WT revealed a delayed protein expression pattern as well as lower levels of proteins involved in protein synthesis, folding and degradation. Additionally, a lower protein synthesis rate in *pept-1(lg601)* was found for a heterologously expressed reporter protein. The lack of

PEPT-1 with subsequent amino acid deprivation leads to a decreased protein synthesis and lower ribosome biogenesis. This, in turn, results in a lower protein load for the folding machinery and, hence, a down-regulation of chaperones reflecting a well-balanced proteostasis.

Besides SKN-1/Nrf2 and XBP-1, the FOXO transcription factor DAF-16 was identified as a repressor of *pept-1* gene expression in *C. elegans*. Thus, insulin/IGF-like signaling coupled with DAF-16 provides a negative feedback loop, repressing *pept-1* expression in the prescence of sufficient nutrient supply.

6. Zusammenfassung

Durch den Verlust des Di- und Tripeptidtransporters PEPT-1 werden im Fadenwurm *C. elegans* starke phänotypische Veränderungen hervorgerufen. Hingegen scheint die Deletion dieses Genes in Säugern nur geringfügige Auswirkungen zu haben, wie man an Hand der PEPT1 defizienten Maus gezeigt wurde. Diese Ergebnisse lassen eine zentrale Rolle des Peptidtransporters im Nährstoffhaushalt des Nematoden und somit eine hochspezifische Expressionsregulation vermuten. *In silico* Analyse des *pept-1* Promotors erzielte die Vorhersage von zwei Bindestellen für den Transkriptionsfaktor SKN-1. Mittels RNAi wurde dessen Aktivität erhöht, damit einhergehend die *pept-1* Expression gesteigert und somit seine biologische Relevanz bewiesen. Auch im Promotorbereich des humanen *PEPT1* konnten vier mögliche Bindestellen für Nrf2, dem Säugetierhomolog zu SKN-1, gefunden werden. Durch Reportergenuntersuchungen gelang es den Einfluss von Nrf2 auf die Promotoraktivität zu zeigen. Da sowohl in *C. elegans* als auch in Mäusen keine basale Regulation der Expression vermittelt durch SKN-1/Nrf2 gezeigt werden konnte, wurden verschiedene Stressoren eingesetzt. In allen Fällen wurde bereits eine vermehrte Proteinaggregation und Autophagie beschrieben. Diese führt unteranderem zur Aktivierung von PKC und damit zur Internalisierung von PEPT1 aus der Membran. Da die Induktion des Proteingehalts höher war als die Induktion der PEPT1 spezifischen Aufnahme wird eine zellinterne Lokalisation in lysosomalen Membranen angenommen. Proteinaddukte sowohl als Proteinaggregate werden durch Makroautophagie abgebaut, wodurch kleine Peptide und Aminosäuren frei gesetzt werden. Diese werden durch Aminosäuretransporter als auch PEPT1 aus dem Inneren von Lysosomen der Zelle wieder zur Verfügung gestellt. Damit wird PEPT1 als Antwort auf erhöhte Autophagie zum einen aus der Membran genommen und zum anderen verstärkt exprimiert um Abbauprodukte aus den Lysosomen zurück in das Zytosol zu überführen.

Desweitern wurde XBP-1 als Aktivator der *pept-1* Expression in *C. elegans* identifiziert. Allerdings scheint die durch die Stressantwort nach Anhäufung ungefalteter Proteine im ER vermittelte Regulation in Säugern nicht konserviert zu sein. Dies deutet daraufhin, dass die Proteinhomöostase in *C. elegans* mit der Expression von PEPT-1 verknüpft ist. Dies konnte auch bei der Analyse des Proteoms von *pept-1(lg601)* und WT Würmern während der Entwicklung gezeigt werden. Sowohl der Gehalt von Proteinen, welche in Ribosomen enthalten, als auch

für die Faltung von Polypeptidketten verantwortlich sind war durch den Verlust von PEPT-1 vermindert. Dies wurde auch in einer langsameren Proteinbiosynthese wiedergespiegelt.

Zusätzlich zu SKN-1 und XBP-1 konnte in *C. elegans* ein weiterer Transkriptionfaktor ermittelt werden, welcher in die Regulation der *pept-1* Expression involviert ist. Der FOXO Transkriptionsfaktor DAF-16 reprimiert nach Stimulierung durch die Insulin/IGF Signal Kaskade die Transkription des *pept-1* Gens.

7. Material and Methods

7.1. Material

7.1.1. Instruments and Kits

Table 6: List of instruments used

Instrument	Company
Confocal laser scanning microscope system (DM IRBE; TCS SP2)	Leica Microsystems, Wetzlar, Germany
Stereomicroscope System (Leica MZ7.5; KL 2500)	Leica Microsystems, Wetzlar, Germany
Varioskan	Thermo Elektron Corporation, Munich, Germany
Centrifuge 5417R	Eppendorf AG, Hamburg, Germany
Centrifuge 5424	Eppendorf AG, Hamburg, Germany
Centrifuge Universal 32R	Hettich, Tuttlingen, Germany
FastPrep-24	MP Biomedicals
KL1500 LCD Microscope	Leica Microsystems, Wetzlar, Germany
Odyssey Imager	LI-COR Biosciences, Lincoln, USA
SDS- and Western Blot Equipment	Bio-Rad Laboratories,Munich; Germany
Ultraspec 3100pro Photometer	Amersham Bioscience
Luminoscan Ascent	Labsystem, Finland
Realplex	Eppendorf AG, Hamburg, Germany

Table 7: Commercially available kits used during this work

Kit	Company
QIAGEN Plasmid Mini Kit	Qiagen, Hilden, Germany
QIAGEN Gel Extraction Kit	Qiagen, Hilden, Germany
QIAGEN RNeasy Mini Kit	Qiagen, Hilden, Germany
QuantiTect SYBR Green one step Kit	Qiagen, Hilden, Germany

Table 8: Software tools freely available on the internet

Name	Web-adress	Purpose
Oligo Calculator	http://www.cnr.berkeley.edu/~zimmer/oligoTMcalc.html	Calculation of T_m
TESS	http://www.cbil.upenn.edu/cgi-bin/tess/tess	Prediction of TF binding site
ClutalW2	http://www.ebi.ac.uk/Tools/msa/clustalw2/	Sequence alignment
Gene Regulation	http://www.gene-regulation.com/index.html	Prediction of TF binding site
Wormbase	http://www.wormbase.org/	General information
Wormbook	http://www.wormbook.org/	General information
TRANSFAC	http://www.gene-regulation.com/pub/databases.html	Promoter analysis
Genomatix	http://www.genomatix.de/en/index.html	Promoter analysis
KEGG	http://www.genome.jp/kegg/mapper.html	Pathway analysis

Table 9: Software packages employed during this work

Software	Purpose
Microsoft Excel	Data analysis
Microsoft Word	Generation of text files
Microsoft Power Point	Design of overviews
GraphPad Prism 4	Statistical analysis
Odyssee V3.0	Densitometric analysis
Leica confocal software	Analysis of confocal microscope pictures
Perl Primer	Primer Design
Distiller version 2.4.0.0	Processing of mass spectra and peptide quantification
R	Statistical analysis
Tinn-R	Statistical analysis

7.1.2. *C. elegans* and *E.coli* strains

Table 10: C. elegans strains, genetic alterations and references

Strain	Gene	Reference
N2 var. Bristol	wildtype	
Cl2070	*hsp16.2::GFP*	Link et al., 1999
CF1038	*daf-16(mu68)*	Lin et al., 1997
TJ356	DAF16::GFP	Henderson & Johnson, 2001
BR2875	P*pept-1::GFP; rol-6 (su1006)*	Meissner et al., 2004
CB1370	*daf-2 (e1370) III*	Riddle ,1977
BR2742	*pept-1 (lg601)X*	EleGene, Munich
DR1309	*daf16(m26); daf-2 (e1370) III*	Riddle et al., 1981
DR1564	*daf-2(m41)*	
DR1572	*daf-2(e1368)*	
BR2688	*daf-2(e1370)III; pept-1(lg601)X*	Meissner, 2004
BW1851	*pal-1::GFPpRF4 iintegrated:rd-6(su1006)*	Gift of L. G. Edgar and W. B. Wood,

Table 11: Bacterial strains either used for cloning or as *C. elegans* feeding bacteria

Strain	Gene	Reference
OP50	ura-	Brenner, 1974
Top10F´	F'[lacIq Tn10(tetR)] mcrA Δ(mrr-hsdRMS-mcrBC) φ80lacZΔM15 ΔlacX74 deoR nupG recA1 araD139 Δ(araleu) 7697 galU galK rpsL(StrR) endA1 λ	Invitrogen
HT115	*F-, mcr*A, *mcr*B, IN*(rrnD-rrnE)1, lambda-, rnc14::Tn10(DE3 lysogen:*lacUV5 promoter-T7 polymerase, RNAse III minus	

Cosmid number	Gene
T19E7.2	skn-1
C38D4.6	pal-1
T22C8.5	sptf-2
K04E7.2	pept-1
R13H8.1	daf-16
Y18D10A.5	gsk-3
D2030.9	wdr-23
R74.3	xbp-1
Y55D5A.5	daf-2
F53F8.1	klf-2
Y40B1A.4	sptf-3
C12D8.10	akt-1
R03G5.2	sek-1
F43C1.2	mpk-1

7.1.3. Plasmids, Primer and Antibodies

Table 12: Plasmids used during this work

Plasmid	Backbone	Application	Reference
pPCRscript		Subcloning of blunt-end PCR products	Stratagene
pGL3basic		Reportergen assay	Promega
PEPT1_prom_0bds	pGL3basic	Reportergen assay	
PEPT1_prom_1bds	pGL3basic	Reportergen assay	
PEPT1_prom_2bds	pGL3basic	Reportergen assay	
PEPT1_prom_3bds	pGL3basic	Reportergen assay	
PEPT1_prom_4bds	pGL3basic	Reportergen assay	
pcDNA3		Reportergen assay	Promega
pSV (β-Gal)		Reportergen assay	Promega
pcDNA3-Nrf2	pcDNA3	Reportergen assay	

Table 13: Primer sequences for PCR or qRT-PCR as indicated in table below

Name	T_m [°C]	Sequence 5` → 3´	Enz-yme	Usage	Reference
pept-1_for	59.1	gcaacacactgtacggaac		Verification of *pept-1* deletion	
pept-1_rev	71.1	ccagtgggtgcaccacaagg		Verification of *pept-1* deletion	
pept1_Prom_rv	58	atatAGATCTcatggcggcggctcc cca	BglII	Cloning of human PEPT1 promoter into pGL3basic	
pept1Prom_0bds	58	atatGAGCTCcctgggaatccgcg tttagact	SacI	Cloning of human PEPT1 promoter into pGL3basic	
pept1Prom_1bds	58	atatGAGCTCgatggtagtttcttttg ctgtgcagaag	SacI	Cloning of human PEPT1 promoter into pGL3basic	
pept1Prom_2bds	58	atatGAGCTCcgtgtgtctgttggct gcataaatg	SacI	Cloning of human PEPT1 promoter into	

				pGL3basic	
pept1Prom_3bds	58	atatGAGCTCggtatttctagttctagatccttgagg	SacI	Cloning of human PEPT1 promoter into pGL3basic	
pept1Prom_4bds	58	atatGAGCTCctatcactgatggacatttgagctgg	SacI	Cloning of human PEPT1 promoter into pGL3basic	
pept1Prom_5bds	62.5	ggctgatgtacttcataccatgga		Cloning of human PEPT1 promoter into pGL3basic	
2pept-1_RT_for	55.8	cctcaccaacaaatgcaacag		mRNA expression	
2pept-1_RT_rev	56.9	gaattgcacctgtctctgct		mRNA expression	
gcs-1_for_RT	60.2	gtagtccgttgacgtgg		mRNA expression	
gcs-1_rev_RT	60.0	acctccgtaaggcattc		mRNA expression	
ama-1_for_RT	56.0	gtgccgagacaactcatc		mRNA expression	
ama-1_rev_RT	56.0	gagtctggatgggtactg		mRNA expression	
sod-3_for_RT	58.0	agcatcatgccacctacgtga		mRNA expression	
sod-3_rv_RT	58.0	caccaccattgaatttcagcg			
xbp-1_spliced_for_RT		tgcctttgaatcagcagtgg		mRNA expression	Richardson et al. 2010
xbp-1_ total _for_RT		ccgatccacctccatcaac		mRNA expression	Richardson et al. 2010
xbp-1_ rv_RT		accgtctgctccttcctcaatg		mRNA expression	Richardson et al. 2010
pal-1_for_RT		ctggaacgaataatgtccgtg		mRNA expression	
pal-1_rv_RT		cttgcgatctgatgttatgaatgg		mRNA expression	
klf-2_for_RT		gttaataatcaggtcatcgagca		mRNA expression	
klf-2_rv_RT		tcgaaggttccatgtgattgag		mRNA expression	
sptf-2_for_RT		gctcatcttcatctagcattgg		mRNA expression	
sptf-2_rv_RT		ggtatgcttccttaaatgtgct		mRNA expression	
sptf-3_for_RT		cctcaccaacaaatgcaacag		mRNA expression	
sptf-3_rv_RT		gaattgcacctgtctctgct		mRNA expression	
wdr-23_for_RT		caaaggatgaaaccgaatcacag		mRNA expression	
wdr-23_rv_RT		gatctccaatatgacatcttccac		mRNA expression	
gsk-3_for_RT		aaactgtctacagagttgccc		mRNA expression	
gsk-3_rv_RT		cgggtcaatgagcaaattctg		mRNA expression	
hGAPDH_for		ccacccatggcaaattccatggca		mRNA expression	
hGAPDH_rv		tctagacggcaggtcaggtccacc		mRNA expression	
hPEPT1_for_RT		gtagccctgattgtgtttgtc		mRNA expression	
hPEPT1_rv_RT		cgtatttctctttagcccagtc		mRNA expression	
HO1_for_RT	66,5	gccctgcccttcagcat		mRNA expression	Tang et al. 2011
HO1_rv_RT	65,8	agctgccacattagggtgtctt		mRNA expression	Tang et al. 2011
NQO1_for_RT	62,9	ggagagtttgcttacacttacgc		mRNA expression	Devling et al. 2004
NQO1_rv_RT	71,9	agtggtgatggaaagcactgccttc		mRNA expression	Devling et al. 2004

Table 14: Antibodies used for detection of proteins in Western Blot technique and immunohistochemistry

Raised against	Source	Dilution	Company /Reference
CePEPT-1	rabbit	1: 5000	generated in house
mPEPT-1	rabbit	1: 5000 (WB) 1: 30 000 (IHC)	generated in house
hPEPT1	rabbit	1: 5000	generated in house
ß-Actin	goat	1: 1000	Santa Cruz
Na^+/K^+-ATPase	rabbit	1:1000	Santa Cruz
ERK	rabbit	1:1000	Cell Signaling
P-ERK	rabbit	1:1000	Cell Signaling
Grp78	mouse	1:1000	Transduction Laboratories
anti-rabbit IgG	donkey	1:800	Jackson
anit-rabbit-IRDye 680	donkey	1:10 000	Li-Cor
anit-mouse-IRDye 680	donkey	1:10 000	Li-Cor
anit-goat-IRDye 800	donkey	1:10 000	Li-Cor

7.1.4. Buffer and Solutions

Table 15: List of buffer composition and corresponding concentrations

Bleach Solution			Coomassie staining solution		
NaOCl (12%)	0.24%	Roth	Coomasie BlueR	0.05 %	Merck
KOH	200 mM	Roth	Acetic Acid		
			Isopropanol	10%	Roth
				25%	Roth
Freezing buffer			**Igepal-Lysis-buffer**		
K_2HPO_4	6.45 mM	Roth	Tris	50 mM	Roth
KH_2PO_4	43.55 mM	Roth	NaCl	140 mM	Roth
NaCl	100 mM	Roth	MgSO4	1.5 mM	Roth
Glycerol	30%	Roth	Igepal	0.5 %	Roth
			pH was set to 8.0 using HCl		
Loading dye			**Lysis buffer (protein)**		
EDTA	100 mM	Roth	Tris/HCl pH 7.4	100 mM	Merck
Glycerol	60%	Roth	NaCl	200 mM	Roth
Bromphenolblue	0.25 %	Roth	EDTA	2 µM	Roth
Xylencyanol	0.25 %		Glycerol	8%	Roth
			DTT (to be added fresh)	1.25 mM	Roth

M9 buffer		
KH_2PO_4	22 mM	Roth
Na_2HPO_4	38.5 mM	Roth
NaCl	85.5 mM	Roth
$MgSO_4$ (added after autoclaving)	1 mM	Roth

Mes-Tris buffer		
NaCl	140 mM	Roth
KCl	5.36 mM	Roth
$CaCl_2$	1.76 mM	Roth
$MgSO_4$	0.8 mM	Roth
Glucose	5 mM	Merck
Mes Pufferan	27.5 mM	Roth
pH set to 6.0 using Tris		

Nystatin solution (filter-sterilised)		
Nystatin	1%	Roth
Ethanol	50%	Merck
Ammoniumacetate	3.75 M	Roth

PBS (T) (10x) pH 7.4		
NaCl	1.4 M	Roth
KCl	27 mM	Roth
Na_2PO_4	100 mM	Roth
KH_2PO_4	18 mM	Roth
(Tween 20)	0.1 %	Sigma

SDS-running buffer		
Tris/HCl pH 6.8	25 mM	Merck
SDS	0.1 %	Roth
Glycin	192 mM	Merck

SDS-sample buffer (4x)		
Tris/HCl pH 6.8	250 mM	Merck
Glycerol	8%	Roth
SDS	20%	Roth
ß-Mercaptoethanol	20%	Roth
Bromphenolblue	0.4 %	Roth

Separating gel buffer		
Tris/HCl pH 8.8	1.126 M	Merck
SDS	0.3 %	Roth

Stacking gel buffer		
Tris/HCl pH 6.8	0.139 M	Merck
SDS	0.11 %	Roth

STET buffer		
Sucrose	233 mM	Roth
Triton X-100	5%	Sigma
EDTA	50 mM	Roth
Tris/HCl pH 8.0	50 mM	Merck

Storage buffer		
NaCl	100 mM	Roth
HEPES	10 mM	Roth
EDTA	150 mM	Roth
Glycerol	10%	Roth
DTT (to be added fresh)	1 mM	Roth
HisPic (to be added fresh)	0.2 %	

Taq buffer (10x)		
KCL	500 mM	Roth
Tris/HCl pH 8.3	100 mM	Merck
Tween 20	0.25 %	Roth
Nonidet P40	0.25 %	Roth
BSA	0.25 mg/ml	Applichem
$MgCl_2$	20 mM	Roth

TBE (5x)		
Tris/HCl pH 8.0	445 mM	Merck
Boric acid	445 mM	Roth
EDTA	5 mM	Roth

TB-buffer		
PIPES	10 mM	Roth
$MnCl_2$	55 mM	Roth
$CaCl_2$	15 mM	Roth
KCl	250 mM	Roth

Transfer buffer (2x)		
Tris	40 mM	Merck
Glycin	296 mM	Merck
Methanol	40%	Merck
SDS	0.04 %	Roth

Worm lysis buffer (2x)		
KCL	50 mM	Roth
Tris/HCl pH8.0	50 mM	Merck
$MgCl_2$	2.5 mM	Roth
Tween 20	0.15 %	Roth
Gelatine	0.01 %	Roth
Proteinase K	0.2 mg/ml	Fluka

7.1.5. Media for culture of model organisms

Table 16: Bacterial and nematode media/ plates constituents

Agarose plates		
Agarose	12 g	Roth
NaCl	3 g	Roth
$MgCl_2$	1 mM	Roth
$CaCl_2$	1 mM	Roth
K_2HPO_4/KH_2PO_4 pH 6.0	40mM	Roth
Cholesterol	5 mg/l	Sigma

DYT (1l)		
Peptone	16 g	Roth
Bacto Yeast Extract	10 g	Roth
NaCL	5 g	Roth

LB /amp (1l)		
LB-Broth	20 g	Roth
Agar (high strength)	5 g	Serva
Ampicillin	1 ml	Sigma

MMA		
Na_2HPO_4	42 mM	Roth
KH_2PO_4	22 mM	Roth
NaCl	8.5 mM	Roth
$CaCl_2$	0.01 mM	Roth
$MgSO_4$	0.002 mM	
Glucose	0.1 mM	Roth
Uracil	0.18 mM	Roth
NH_4Cl	19 mM	Sigma

NGM / IPTG (1l)		
Agar (high strength)	17 g	Serva
NaCl	3 g	Roth
Pepton	2.5 g	Roth
MgCl	1 mM	Roth
$CaCl_2$	1 mM	Roth
K_2HPO_4/KH_2PO_4 pH 6.0	40 mM	Roth
Cholesterol	5 mg/l	Sigma
Nystatin	13 ml	Roth
IPTG	1 mM	Sigma
Carbenicellin	1 ml	Sigma

7.1.6. Chemicals and reagents

Table 17: Chemicals/ reagents used are listed alphabetically

Substance	Company
$^{15}NH_4Cl$	Sigma-Aldrich, Steinheim, Germany
Acrylamide (30%)	Roth, Karlsruhe, Germany
Agar-agar (high strength)	Serva, Heidelberg, Germany
Agarose	Roth, Karlsruhe, Germany
Ammonium acetate	Merck, Darmstadt, Germany
Amplex Red	Invitrogen, Darmstadt, Germany
APS (ammonium persulfate)	Serva, Heidelberg, Germany
ATP (Adenosine-5'-triphosphate)	Sigma-Aldrich, Steinheim, Germany
Bacto yeast extract	Roth, Karlsruhe, Germany
Bio-Rad protein assay	Bio-Rad, Munich, Germany
Boric acid	Roth, Karlsruhe, Germany
BSA (bovine serum albumin)	Applichem, Darmstadt, Germany
CaCl2	Roth, Karlsruhe, Germany
Carbenicellin	Sigma-Aldrich, Steinheim, Germany
Cholesterol	Sigma-Aldrich, Steinheim, Germany
Coenzym A	Sigma-Aldrich, Steinheim, Germany
Coomassie blue R	Sigma-Aldrich, Steinheim, Germany
Cycloheximid	Applichem, Darmstadt, Germany
diaminobenzidine	DakoCytomation, Hamburg, Germany
DMEM E15-825	PAA, Cölbe, Germany
DMSO (dimethyl sulfoxide)	Sigma-Aldrich, Steinheim, Germany
DTT	Roth, Karlsruhe, Germany
Ebselen	Sigma-Aldrich, Steinheim, Germany
EDTA (ethylenediaminetetraacetic acid)	Sigma-Aldrich, Steinheim, Germany
EGTA (ethylene glycol tetraacetic acid)	Roth, Karlsruhe, Germany
Ethanol	Merck, Darmstadt, Germany

Substance	Company
Gelatine	Roth, Karlsruhe, Germany
Gene Ruler Ladder Mix	Fermentas, St. Leon-Rot, Germany
Glycerol	Roth, Karlsruhe, Germany
Glycine	Merck, Darmstadt, Germany
HEPES	Roth, Karlsruhe, Germany
HEPES (4-(2-hydroxyethyl)-1-piperazineethanesulfonic acid)	Roth, Karlsruhe, Germany
HisPic	Sigma-Aldrich, Steinheim, Germany
Histofine Simple Stain Mouse Max PO (rabbit)	Nichirei Biosciences, Tokyo, Japan
Igepal	Roth, Karlsruhe, Germany
IPTG	Sigma-Aldrich, Steinheim, Germany
Isol-RNA Lysis Reagent	5Prime, Hamburg, Germany
K2HPO4	Roth, Karlsruhe, Germany
KCl	Roth, Karlsruhe, Germany
KH2PO4	Roth, Karlsruhe, Germany
KOH	Roth, Karlsruhe, Germany
Levamisole	Sigma-Aldrich, Steinheim, Germany
Loading Dye	Fermentas, St. Leon-Rot, Germany
Luciferin	P.J.K., Kleinbittersdorf, Germany
Menadione	Sigma-Aldrich, Steinheim, Germany
Mes Pufferan	Roth, Karlsruhe, Germany
Methanol	Merck, Darmstadt, Germany
MgCl2	Roth, Karlsruhe, Germany
MgSO4	Sigma-Aldrich, Steinheim, Germany
Na2HPO4 dihydrate	Roth, Karlsruhe, Germany
NaCl	Roth, Karlsruhe, Germany
NaOCl (12%)	Roth, Karlsruhe, Germany
Naringenin	Sigma-Aldrich, Steinheim, Germany
NH_4Cl	Roth, Karlsruhe, Germany
Nonidet P40	Roth, Karlsruhe, Germany
Nystatin dihydrate	Roth, Karlsruhe, Germany
Peptone	Roth, Karlsruhe, Germany
PhosphoSTOP	Roche, Penzberg, Germany
Phusion	Thermo Scientific, Vanataa, Finland
PIPES	Roth, Karlsruhe, Germany
PMSF	Roth, Karlsruhe, Germany
Proteinase K	Sigma-Aldrich, Steinheim, Germany
Restriction Enzymes	Fermentas, St. Leon-Rot, Germany
Resveratrol	Sigma-Aldrich, Steinheim, Germany
SB-415286	Sigma-Aldrich, Steinheim, Germany
SDS (sodium dodecyl sulfate)	Roth, Karlsruhe, Germany
ß-Ala-Lys-AMCA	BioTrend, Cologne, Germany
Sucrose	Roth, Karlsruhe, Germany
Sudan Black	Roth, Karlsruhe, Germany
Sulforaphane	Sigma-Aldrich, Steinheim, Germany

Substance	Company
TEMED (Tetramethylethylenediamine)	Sigma-Aldrich, Steinheim, Germany
TfxTM20	Promega, Madison, USA
Tris (2-Amino-2-hydroxymethyl-propane-1,3-diol)	Roth, Karlsruhe, Germany
Triton X-100	Roth, Karlsruhe, Germany
Tunicamycin	Applichem, Darmstadt, Germany
TWEEN 20	Sigma-Aldrich, Steinheim, Germany
TWEEN 80	Sigma-Aldrich, Steinheim, Germany
Uracil	Roth, Karlsruhe, Germany
Xylencyanol	Roth, Karlsruhe, Germany

7.2. Methods

7.2.1. Cultivation of model organisms

7.2.1.1. Cultivation of Bacteria

Top10F´ were grown on/in LB or LBamp plates/media depending on eventually contained plasmids. OP50 were grown over night in DYT media except for ^{15}N labeling purposes at 37°C. HT115 RNAi bacteria were cultured in LBamp media. After an over night culture in 2 ml media, bacteria were diluted 1:50 with fresh media and further shaked at 37°C for another 4 hrs until spread on IPTG containing plates.

In case of heavy isotope labeling OP50 were grown in MMA containing $^{15}NH_4Cl$. Over night culture was inoculated into a large culture flask and allowed to grow for 8 hrs until bacteria were concentrated by centrifugation. Labeled cells were placed onto nitrogen-free agarose plates.

7.2.1.2. Cultivation of C. elegans

Worms were kept on NGM agar plates seeded with OP50 bacteria at 20°C as mixed cultures. In some cases NGM agar plates were supplied with additional substances (e.g.: glucose), exact concentrations are noted with the according results. In case of RNAi treated C. elegans RNAi bacteria were spread on IPTG containing plates (induction of dsRNA transcription) one day before worms were transferred onto the plates.

7.2.1.3. Labeling of C. elegans

Worms were grown on agarose plates seeded with ^{15}N labeled OP50 for several generations starting with 5 L4 Larvae. Population was allowed to reproduce for approximately 10 days, before worms were placed on fresh plates. Food supply was ensured to be adequate at all times. Plates of worms were again separated on new paltes and allowed to overgrow until synchronization of worms.

7.2.1.4. Syncronization of C. elegans population

Mixed staged worms were washed of cultivation plates using M9 buffer. Treatment with hypochlorid solution for 3 min while strong shaking resulted in release of the eggs. Hatching of the eggs occurred during incubation in M9 buffer at 20°C over night. L1 larvae were washed once with fresh M9 buffer and subsequently placed onto new plates.

7.2.1.5. Cell Culture

Caco2 cell line was kept in DMEM containing 10 % FCS if not otherwise noted. Cells were seeded into 6 well plates or petri dishes. Media was refreshed 3 days after seeding. Experiments were conducted 6 days post confluent.

HepG2 cells were cultured in RPMI1640 containing 10 % FCS, only in case of transfection RPMI1640 without FCS was used.

7.2.2. Molecular biological methods

Molecular biology standard methods (agarose-gel electrophoresis, DNA-digestion, DNA-ligation) were performed as described in Ringlstetter S. (2011)[199]. DNA purification and extraction was done using either a kit from QUIAGEN or Stratagene. DNA sequencing was accomplished by GATC.

7.2.2.1. Preparation of chemically competent E. coli

A single colony of bacteria was inoculated into 10 ml LB media containing selective antibiotics. Over-night culture was diluted into SOB media with SOC to OD_{600} ~ 0.1. Cells were shaken in a water bath to keep temperature stable at 18°C. When bacterial suspension reached OD_{600} of 0.6, cells were cooled to 4°C by shaking in an ice bath and harvested by centrifugation (10 min, 2500 g, 4°C). Pellet was resuspended in 10 ml TB-buffer. After incubation for 10 min at 4°C cells were pelleted again and suspended in 20 ml TB-buffer, 20% Glycerole was added and 400 µl cell-suspension was transferred into 1.5 ml reaction tubes. Chemically competent bacteria were frozen in liquid nitrogen and stored at –80°C.

7.2.2.2. E.coli Transformation

Competent cells were thawed on ice. DNA was mixed with competent cells, which were kept on ice for another 10 min until heat pulse for 45 sec at 42°C. Bacteria were quickly cooled on ice followed by the addition of 1 ml LB media and incubation at 37°C for 45 min. By centrifugation at 6000 rpm for 30 sec cells were pelleted and resuspended in 100 µl LB media before plating onto selective plates.

7.2.2.3. Plasmid Isolation from bacteria

Over-night culture of bacteria was pelleted and resuspended in 500 µl STET buffer. Addition of 100 µl Lysozyme (10 mg / ml in STET buffer) was followed by incubation at 95°C for 2 min. Centrifugation at 13 200 rpm for 2 min resulted in cloudy pellets, which were removed by a sterile tooth pick. DNA was precipitated by addition of 400 µl Isopropanol to the supernatant. DNA was spun down (13 200 rpm, 5 min) and washed with 200 µl 70 % ethanol. Ethanol evaporated completely using a Speedvac. Pellet was treated with 100 µl RNaseA (100 µg / ml) in TE-buffer for 5 min at 65 °C. After centrifugation for 3 min at 13 200 rpm supernatant contained plasmid DNA.

QIAprep Spin Miniprep Kits were used regarding manufacturers advice to isolate pure plasmid for sequence analysis.

7.2.2.4. Polymerase Chain Reaction (PCR)

DNA amplification using Taq-Polymerase was done in 25 µl reactions containing ~ 50 ng template, 1x ThermoPol reaction buffer, dNTPs (0.25 mM, each), primer (100 pmol, each) and 0.5 µl polymerase.

PCR-assays with Phusion High-Fidelity kit were done according to the manufacturers instructions.

7.2.2.5. Colony-PCR

Single colonies were picked into PCR-reaction tubes and transferred to 2 ml LB_{amp} media. Master-Mix for PCR-reaction contained 1x ThermoPol buffer, 0.25 mM dNTPs (each), 30 pmol primer (each) and 1U Taq polymerase in a final volume of 25 µl. After addition of 24.5 µl to each PCR-tube, reaction was repeated 20 times.

7.2.2.6. Protein extraction from C. elegans

200 µl worm pellet in 400 µl Worm Lysis Buffer was disrupted using glass beats in combination with mechanical force (Ribolyser, 3 x 30 sec, level 5). Using a hot pin wholes were drilled into the lid and the bottom of the reaction tube placed on top of a 15 ml tube. Centrifugation by 2000 rpm for 2 min separated lysate from the glass beats, which were washed again using 100 µl Worm Lysis buffer. Whole worm lysate was transferred to 1.5 ml reaction tube and cell debris was spun down at 10 000 rpm for 1 min. Supernatant was declared as total protein extract. Total protein extract was either further processed by centrifugation for 45 min at 14 000 rpm at 4°C or used for analysis. After centrifugation pellet contained membrane protein fraction, while supernatant was seen as cytosolic fraction. Membrane proteins were dissolved in storage buffer (volume according to the size of the pellet) by vortexing every 5 – 10 min.

7.2.2.7. Protein extraction from Caco 2

Cells were washed twice using ice-cold PBS containing 1 mM PMSF. After addition of appropriate volume of PBS + 1mM PMSF, cells were scraped of the plates and transferred into 15 ml tube. Before lysis, cells were washed again (2500 rpm, 2 min, 4°C). Cell lysis was done in 300 µl PBS + 1 mM PMSF using a 24´G syringe. Protein solution was cleared from cell debris (3 min, 2000 rpm, 4°C) and supernatant was centrifuged for 45 min at 20 000 rpm at 4°C. Cytosolic fraction was collected, and pellet containing membrane protein fraction was resuspended in appropriate volume of PBS + 1 mM PMSF using 24´G syringe.

7.2.2.8. Protein extraction from tissue

Tissue was homogenized in PBS + 1 mM PMSF using Ultrathurrax. Raw extract was centrifuged (5min, 3600 rcf. 4°C) and membrane protein fraction was separated by 60 min of centrifugation (32 500 rcf, 4°C). Pellet was resuspended in 200 – 300 µl PBS + 1 mM PMSF using 27´G syringe.

7.2.2.9. Deglycosylation of membrane protein fraction

PNGaseF was used to cleave oligosaccharide structures of glycoproteins. Therefore 10 µg of protein fraction were treated as manufacturer redommended, except denaturing step, which was eliminated. .

7.2.2.10. Bradford-Assay

800 µl of water were predeposited in a 1.5 ml reaction tube. After addition of 200 µl of BioRad Bradford reagent protein sample or water (blank) was added. Formation of coomassie complex was allowed to occur during 10 min incubation at room temperature. Absorbtion was measured at 595 nm using a photometer. Protein concentration was calculated using a standard curve done with BSA at known concentrations.

7.2.2.11. SDS-PAGE

SDS-Polyacrylamide gels were prepared as follows:

		10 % dissolving gel	Stacking gel
30 % Polyacrylamide	Roth	3 ml	0.6 ml
buffer		3 ml	3.4 ml
H_2O		3 ml	
10 % APS	Roth	100 µl	24 µl
TEMED	Roth	5 µl	3 µl

Determined amount of protein was denatured using 4x SDS-sample buffer. Using a Hamilton syringe protein solution was loaded into gel pockets. Until proteins reached the dissolving gel 140 V were used for electrophoresis. For further separation of proteins voltage was increased to 200 V.

7.2.2.12. Western Blot analysis

Transfer of proteins from the gel to the nitrocellulose membrane was accomplished by wet blot technique as described in Benner (2011)[42]

Incubation with the primary antibody was conducted at 4 °C during constant shaking. After 3 x 10 min of washing with blocking solution the secondary antibody was diluted in blocking solution following 2 hrs of incubation at room temperature. Detection of antibody binding was done either using ECL in combination with x-ray films for horseradish-conjugated antibodys or by fluorometric measurement using Odessey scanner for fluorophor-conjugated antibodys. For quantitative analysis densitometric analysis was accomplished by Odysse software. Intensity of target protein was normalized by adjusting it to intensities of corresponding actin bands. For further analysis resulting fluorometric intensities were set into relation with experimental control sample.

7.2.2.13. RNA isolation

C. elegans were disrupted in 1 ml Isol-RNA Lysis Reagent using glass beads and mechanical force (Ribolyser, 3 x 20 sec, level 5). Using a hot pin wholes were drilled into the lid and the bottom of the reaction tube placed on top of a 15 ml tube. Centrifugation by 2000 rpm for 2 min separated lysate from the glass beats, which were washed again using 250 µl Isol-RNA Lysis Reagent. Supernatant was transferred to 2 ml tubes.

Caco2 cells were scraped off 6-wel plates in 500 µl Isol-RNA Lysis Reagent and transferred to 2 ml tubes. In both cases 1/5 vol. of chloroform was added, mixed and incubated at room temperature for 2-5 min. After 15 min of centrifugation (4°C, 13 000 rpm) the clear supernatant was added to one vol. of cold ethanol, inverted and the mixture was subjected to Qiagen RNeasy isolation kit. RNA was eluted in 30 µl of RNase-free water according to manufacturer´s protocol.

7.2.2.14. qRT-PCR

RNA was diluted to 10 ng/µl and primers were used in a concentration of 20 µM. After all reagents were thawed MasterMix was prepared in relation to sample number.

Table 18: Master Mix for one-step qRT-PCR

Reagent	MM: Single Reaction (µl)
H_2O	7.8
QuantiTect	10
RT Mix (added last)	0.2
Aliquot to plate	18
Add template/H_2O	1
Add primer/H_2O	1

After aliquoting MM into 96 well plate template and primer were added and plate subsequently sealed. After centrifugation for 2 min at 300 g plate is placed into realplex machine. qRT-PCR is conducted as one step RT-PCR with 30 min at 50°C, 15 min 95°C followed 40 cycles of 15 sec at 95°C, 30 sec at T_m of 58°C, 30 sec elongation at 72°.

7.2.2.15. ^{14}C-GlySar Uptake

Cells were grown in a six well plate. Before uptake studies, cells of one well were washed with 1 ml PBS and after addition of 500 µl PBS scraped of the plate to be transferred into 1.5 ml reaction tube. To avoid loss of cells, each well was washed using 500 µl PBS. Disruption of cells was accomplished using ultrasonification (20 strokes at an amplitude of 35). Cell debris was pelleted during 1 min of centrifugation at 10 000 rpm. Bradford assay was used to determine the protein concentration.

Remaining wells were washed with 1 ml MES-Tris buffer. Uptake was initiated by adding 500 µl of 20 µmol/l ^{14}C-GlySar in Mes-Tris buffer and plates were incubated for 10 min at 37°C. One well contained additionally 10 Mm GlyGly to determine saturable transport. Removal of substrate terminated uptake. Cells were washed twice using 1 ml cold MES-Tris buffer before disruption using 1 ml RIPA buffer. Solubilised cells were transferred into scintillation vials, containing 3 ml scintillation cocktail. Background radioactivity of RIPA buffer was determined using 1 ml of buffer was mixed with 3 ml scintillation cocktail. Furthermore one vial contained 3 ml scintillation cocktail, 1 ml RIPA buffer and 25 µl of 20 µmol/l ^{14}C-GlySar in Mes-Tris buffer. Radioactivity was measured using liquid scintillation spectrometry in a TriCarbCounter from Perkin Elmer.

CPMA of RIPA buffer on its own was substracted of CPMA of samples and controls. To calculate specific uptake non-carrier mediated transport was substracted from total transport. Transport rate was expressed as nmol / g protein min.

7.2.2.16. ß-AlaLys-AMCA uptake

C. elegans was washed of culturing plates and twice washed with M9 buffer. Worms were incubated with 0.25 mM ß-Ala-Lys-AMCA in 3 ml of M9 buffer under continuous rotation. After 3 h 500 µl OP50 suspension was added and allowed to rotate one more hour. To remove residual fluorescent dipeptide worms were washed 5 times with M9 before being placed on empty NGM agar plates. After photographs to measure worm length were taken, 20 worms were placed into each well. 384 well plate contained 100 µl of M9 buffer per well. Each sample was at least measured in technical triplicate.

Measurement of fluorescence was accomplished using Varioscan with an excitation wavelength of 345 nm and emission at 445 nm.

7.2.2.17. Measurement of promoter activity

C. elegans strain expressing GFP under the control of the pept-1 promoter were grown for 7 days on RNAi plates. 100 µl of M9 buffer were pre-deposited in each well of a 384 well plate. 50 worms were picked per well and each sample was measured at least in technical triplicate. Fluorescence was measured using Variscan with a excitation wavelength of 395 nm and an emission of 513 nm. Fluorescence signal was related to body size, therefore pictures of worm cultures were taken and individuals measured using Motic Images Plus software.

7.2.2.18. Life Span Analysis

Worms were grown on NGM plates for four days before being synchronized. L1 larvae were allowed to grow either on VC or RNAi plates until they reached L4 stage. At day 0 L4 larvae were transferred to 3 cm RNAi plates. Each plate was habituated by 28 – 35 animals. Each construct was done in triplicate. Every day worms were checked for viability, if they did not respond to mechanical stimulus they were regarded as dead. During reproductive phase worms were placed onto new plates every two days, for the rest of the time being plates were renewed every four to six days.

7.2.2.19. Determination of protein biosynthesis rate

To identify the maximum of the GFP expression in hsp16.2::GFP worms after one hour of heat shock at 34 °C fluorescence was measured using confocal microscope and varioscan every two to four hours for 32 hours after heat shock. As experimental control hsp16.2::GFP worms were treated the same way only heat shock was replaced by further incubation at 20 °C. Analysis using varioscan occurred in a black 384 well plate. 50 µl of M9 buffer were predeposited in each well. At each time point 2 x 50 worms (technical duplicates) were transferred into separate wells. In addition 50 worms per sample were frozen in liquid nitrogen for analysis at the confocal microscope. After collecting all the samples, worms were thawed on ice and placed onto agarpads. Laser intensity was set to a fixed percentage of 30 throughout the whole processing of all samples to be able to compare resulting fluorescence intensities. As both methods achieved comparable results, while varioscan analysis was more practical further experiments were done using only this method. Maximum of GFP synthesis was detected between two to four hours after heat shock, taken this into account time points 0, 2 hrs and 4 hrs after heat shock were chosen for analysis of fluorescence.

For experiments hsp16.2::GFP were grown either on VC or RNAi plates for four days. Worms were synchronized by egg-prep and L1 larva were placed on either VC or RNAi plates for approximately 60 hrs (L4 stage). For each construct one plate was incubated at 34 °C in a preheated incubator for one hour while one plate was retained at 20 °C. At time points 0 hrs, 2 hrs and 4 hrs after heat shock 50 worms of each sample were transferred into 50 µl of M9 buffer per well of a black 384 well plate. Each sample was conducted in technical duplicate. GFP expression was measured using varioscan. Increase of fluorescence was depicted against time and the slope of a linear regression was calculated. The slope of samples without heat pulse was substracted as background from the slope of the sample with heat pulse. For further analysis slopes were set into relation of experimental control.

7.2.2.20. Induction of stress in C. elegans

Oxidative stress was initiated by incubating worms for 20 min at 20°C in 7 ml M9 buffer containing either no-stimulant, H2O2, NaN3 or Juglone. After worms were washed using M9 buffer they were placed on plates seeded with fresh OP50 bacteria. During a four hour period at 20°C worm were allowed to recover. After stress induction was finished worms were washed of plates and either subjected to protein extraction and western blot analysis or to confocal microscopy.

7.2.2.21. Analysis of GFP expressing strains using confocal microscopy

Worms were washed of plates using M9 buffer, incubated with Levamisole for 10 min and subsequently placed on agarose-pads. To visualize GFP expression Leica TCS SP2 confocal microscope was used. To analyze expression laser intensity and pinhole size were kept constant during analysis of all samples. Per sample approximately 50 animals were analyzed. Of each determined using Leica confocal software.

To test for transcription factor localization 100 worms per sample were grouped according to fluorescence intensity in cytosolic, intermediate and nuclear.

7.2.2.22. Sudan Black B staining of fat droplets

Worms were washed of culture plates rinsed four times using M9 buffer. Fixation was conducted using 700 µl of 1 % paraformaldehyde in combination with four freezing/thawing cycles in liquid nitrogen. Before staining worms were dehydrated using 25 %, 50 % and 70 % ethonal respectively.Staining occurred over night by incubation with 800 ml of a 50 % saturated Sudan Black B solution. At the next day residual dye was cleared using 70 % ethanol. Worms were subsequently placed on agar pads and pictures were taken using Leica CTR4000.

7.2.2.23. Luciferase activity assay (carried out by A. Kipp, Dife; Potsdam-Rehbrücke)

HepG2 cells were seeded in 24 well plates one day prior to transfection with TfxTM20-Reagent following the protocol of manufacturer. Cells were transfected with either empty pGL3 vector or *PEPT-1* promoter reporter constructs. In all cases pSV(β-gal) was co-transfected for normalization of transfection efficiency. Overexpression of Nrf2 was accomplished by co transfection with pcDNA3-Nrf2^{112}. Cells were harvested after 48 h and lysed in 150 µl/well RLB-Puffer under shaking for 15 min. 20 µl of lysate were placed into a white 96-well plate. 6,2 mg Coenzym A (Sigma), 4,3 mg Luciferin (P.J.K., Kleinbittersdorf), 8,84 mg ATP (Sigma) were dissolved in 5 ml of 100 mM Tris (pH 7,8), 500 µl aliquots were subsequently lyophilized. One aliquot was resuspended in 3 ml reaction buffer resulting luciferin-mix. 100 µl of the luciferin-mix were added and measurement of bioluminescence was conducted immediately using a Luminoscan Ascent. To normalize for transfection efficiency ß-galactosidase activity as determined by photometric measurement of conversion of O-Nitrophenyl-β-D-Galactopyranosid (ONPG) (4 mg/ml ONPG in 60 mM Na_2HPO_4, pH 7.5) to O-Nitrophenol. 50 µl lysate, 70 µl ß-gal-buffer were placed into a 96 well plate. 30 µl ONPG were added to start reaction. Absorbance was measured at a wavelength of 405 nm after 30, 60, 90, 120 and 180 min at 37 °C.

7.2.2.24. Immunohistochemical staining

Paraffin of micortome sections (2 µm) was removed using toluol. Subsequently graded ethanols were used to dehydrate tissue, before antigens were unmasked by heat treatment (microwave, 2x 4 min, 850 W) in combination with citrate buffer. Slides were incubated in 3 % hydrogen peroxide for 10 min to block endogenous peroxidase activity. Primary antibody rabbit anti-mouse PEPT1 was diluted 1: 30 000 in antibody diluent. After over night incubation at 4°C secondary antibody conjugated with biotin was incubated with the sections for 30 min at room temperature. Visualization of antibody binding was accomplished using N-Histofine Simple Stain Mouse Max PO and diaminobenzidine.

7.2.3. Proteomics

7.2.3.1. Protein Precipitation

Cytosolic proteins were diluted with 1 vol bidest water. Using 4 vol ice-cold acetone proteins were precipitated. For higher efficiency protein/acetone solution was incubated for at least 6 hrs at -20°C. Proteins were pelleted by centrifugation (13 000- 15 000 g, 30 min, 4°C) and the supernatant was carefully discarded. By inversion of the tube the pellet was dried to eliminate acetone residues. Proteins were resuspended in a minimal volume of lysis-buffer. To increase protein recovery solution was ultrasonificated. Remaining protein aggregates were removed by centrifugation (8 000 rpm, 10 min, 4°C).

7.2.3.2. Passive Rehydration

260µg of recovered protein were mixed with 2 % Pharmalyte pH 3-10 and 15µl 30 % DTT. Rehydration buffer was added to a total volume of 370 µl. 350 µl were spread per lane of the reswelling tray. A 24 cm IPG-Strip was placed gel side towards the protein solution in each lane. After covering the strip using silicon oil, the strip was allowed to reswell over night (min 8 hrs) at room temperature.

7.2.3.3. Isoelectric focussing (1st Dimension)

Manifold was filled with 108 ml of silicon oil. After IPG-strips were quickly dried on a tissue, they were placed with the gel facing up into the manifold. At the anode a paper wig soaked with water and at the cathode soaked with 3,5 % DTT made contact with the gel. After 1h the run was paused and the paper wigs were replaced.

Program:
Current: 50 µA per IPG-Strip
0,3 min 500 V
1,5 h Grad. 4000 V
Grad. 8000 V until total volt of 25 000 Vhrs reached
Step-n-hold at 500 V to avoid diffusion
Strips were stored at -80°C until 2nd Dimension was done.

7.2.3.4. SDS-PAGE (2nd Dimension)

Under gentle agitation strips were incubated with 1 % DTT for 15 min at room temperature, followed by incubation with 4 % IAA. Before placing the strips onto the gels, they were first washed in water and followed by running buffer. Air bubbles between the strip and the gel were removed by pressing the strip with a spatula towards the gel. To avoid new air bubbles and to increase the contact between gel and strip, it was covered by 0,5 % agarose. Gel cassettes were then placed into the electrophoresis apparatus, already filled with cooled running buffer. The electrophoresis was done using the following program:

Constant Ampere

Pump Auto

For 12 Gels:

1. 44 mA für 1 h (min. 30 mA)
2. 144 mA für 15 h
3. 144 mA für 6 h

The run was terminated when the blue front reached the bottom of the gel. After gels were taken out of the glas cassettes, they were incubated at least 2 hrs in fixing solution. 2D-Gels were stained using Coomassie Brilliant Blue. Staining was done at room temperature under gentle agitation. After 4 days gels were shaken in water to remove excess Coomassie.

7.2.3.5. In-Gel-Digest

Protein spots are excised using a biopsy punch and transferred to 0,2 ml tubes. For removal of coomassie spots were treated 15 min with 50 mM Ammoniumbicarbonat, followed by 15 min incubation with 1: 1 ACN / Ammonibicarbonat solution. These steps were repeated until no blue staining was visible anymore. Treating the spots for 15 min with ACN dehydration was achieved. Residual ACN evaporated leaving the tubes open under the fume hood. Spots were rehydrated for 2 hrs at 4°C using 5 µl of trypsin containing solution. Excess solution was removed and spots incubated over night at 37°C. By incubating the gel slice with 4µl of TA30 while sonificating in liquid bath, peptides were extracted. After a short spin supernatant was transferred to a fresh tube.

7.2.3.6. MALDI-target spotting

1 µl of sample or peptide calibration standard was placed on an 384 anchor chip steel target and allowed to co-crystallize with HCCA in TA30, before remaining slats were washed off using 1 µl of 10 mM ammonium hydrogen phosphate in 0.1 % TFA. Mass spectrometry was conducted using Bruker Ultraflex3 in the positive ion reflection mode. Obtained mass spectra were processed using FlexAnalysis software and protein identification conducted using Biotools in combination with MASCOT search engine (Database: Swissprot with species constraint on C. elegans, peptide mass tolerance: ±150 ppm, max. missed cleavage of 1, fixed modifications: carbamidomethyl (C), variable modifications:oxidation (M))

7.2.3.7. Short gel electrophoresis and tryptic digestion of proteins (carried out by K. Kuhlmann; MPC; Bochum)

For sample clean-up, 10 µg of total protein per sample were shortly subjected to one-dimensional SDS-polyacrylamide gel electrophoresis (1-D SDS-PAGE) using 4-12% NuPageTM Bis-Tris gradient gels (Invitrogen, Karlsruhe, Germany) according to the manufacturer's instructions and visualized by colloidal Coomassie Brilliant Blue G-250. One slice per lane was cut out. Destaining, trypsin digestion, peptide extraction and preparation for LC-MS/MS analysis were performed as described in [Wiese et al. 2007]. Peptide concentration after extraction was determined by amino acid analysis, and 300 ng total peptide per sample were used for LC-MS/MS analysis.

7.2.3.8. NanoHPLC/ESI-MS/MS analysis (carried out by K. Kuhlmann; MPC Bochum)

Peptide mixtures were analyzed by nanoHPLC/ESI-MS/MS using the UltiMateTM 3000 RSLCnano system (Dionex, now Thermo Fisher Scientific, Bremen, Germany) online coupled to an LTQ Orbitrap Velos instrument (Thermo Fisher Scientific, Bremen, Germany). Peptide mixtures were loaded onto a C18 RP precolumn (75µm inner diameter x 20 mm; PepMap, Dionex) equilibrated with 0.1% (v/v) TFA, washed and preconcentrated for 7 min at a flow rate of 7 µl/min. The precolumn was then switched in line with a C18 RP nano LC column (75 µm inner diameter x 500 mm, 2 µm particle size; PepMap, Dionex). Peptides were separated with a binary solvent system consisting of 0.1% (v/v) FA (solvent A) and 0.1% (v/v) FA in 84% (v/v) ACN (solvent B) using the following gradient: 7-25% solvent B in 128 min, 25-40% B in 20 min and 40-95% solvent B in 2 min. The flow rate was 400 nl/min and the column was heated to 40 °C. The LTQ-Orbitrap velos was equipped with a nanoelectrospray ion source (Thermo Fisher Scientific) and distal coated SilicaTips (New Objective, Woburn, USA). To provide high mass accuracy, lock masses (derived from a set of distinctive air contaminants) were routinely used for internal calibration of each MS spectrum acquired. The general mass spectrometric parameters were as follows: spray voltage, 1.3–1.5 kV, capillary temperature, 300°C. For data-dependent MS/MS analyses, the software XCalibur 2.1 (Thermo Fisher Scientific) was used. Full scan MS spectra ranging from m/z 300 to 2,000 were acquired in the Orbitrap with a resolution of 30,000 at m/z 400. Automatic gain control (AGC) was set to 1 x 106 ions and a maximum fill time of 500 ms. The 20 most intense multiply charged ions were selected for fragmentation by low energy collision-induced dissociation (CID) in the linear ion trap. The AGC of the LTQ was set to 5000 ions and a maximum fill time of 120 ms. Fragmentation was carried out at a normalized collision energy of 35% with an activation q = 0.25 and an activation time of 10 ms. The ion selection threshold was set to 500. Fragmentation of previously selected precursor ions was dynamically excluded for the following 30 sec.

7.2.3.9. Mass spectrometric data Analysis

Generation of peaklists from mass spectrometric data and peptide and protein quantitation were done using Mascot Distiller version 2.4.0.0. Parameters for peak picking were set according to recommendations of software supplier; briefly correlation threshold was set 0.7 with a S/N of 2. Peak lists were correlated to the Uniprot/Swissprot database (Uniprot/Swissprot release 2011_06) with taxonomy restricted to C. elegans (3332 sequences) using the Mascot (version 2.3) search engine

(www.matrixscience.com)[200]. A decoy version of the database was used that was complemented with a duplicate of itself in which the amino acid sequence of each protein entry was randomly shuffled in order to enable the calculation of a false discovery rate. Search parameters were as follows: Tryptic specificity, maximum one missed cleavage site, oxidation of methionine as variable modification, precursor mass tolerance: 4 ppm, fragment mass tolerance: 0.5 Da. Protein identifications from Mascot were ranked by Mascot score and the lists were truncated at a false discovery rate of 1%. A minimum of 1 peptide per protein was required. For peptide and protein quantitation, the ^{15}N Metabolic method in the Mascot Distiller Quantitation toolbox was used .Impurity of labeling was set to 92%. Protein ratio was calculated based on the average of quantified peptides with at least two peptides meeting the selection criteria of a correlation threshold above 0.9 and a standard deviation below 0.2 whereby at least one peptide had to be unique to the protein[201].

Lists of identified proteins were first merged for the two biological replicates and three time points, to give one combined list of identified proteins. Proteins that were not quantified in all the samples and in each replicate were eliminated from this list, as progression of protein abundances during the time course was the major focus (lists of proteins specific for time points can be extracted from the supplementary). Statistical analysis of obtained dataset was conducted using the free available R software package applying an one-way ANOVA following a Tukey Posthoc test for comparison of changes in wild type or pept-1 knock out. Analysis of the complete data set was done using a two-way ANOVA.

Reference List

1. McGhee, J. D. The C. elegans intestine. *WormBook.* **2007**, 1-36.

2. Holmes, R.;Lobley, R. W. Intestinal brush border revisited. *Gut* **1989**, *30* (12), 1667-1678.

3. Ferraris, R. P.;Diamond, J. Regulation of intestinal sugar transport. *Physiol Rev.* **1997**, *77* (1), 257-302.

4. Yoshikawa, T.; Inoue, R.; Matsumoto, M.; Yajima, T.; Ushida, K.;Iwanaga, T. Comparative expression of hexose transporters (SGLT1, GLUT1, GLUT2 and GLUT5) throughout the mouse gastrointestinal tract. *Histochem.Cell Biol.* **2011**, *135* (2), 183-194.

5. Iqbal, J.;Hussain, M. M. Intestinal lipid absorption. *Am.J Physiol Endocrinol.Metab* **2009**, *296* (6), E1183-E1194.

6. Goodman, B. E. Insights into digestion and absorption of major nutrients in humans. *Adv.Physiol Educ.* **2010**, *34* (2), 44-53.

7. Kunzelmann, K.;Mall, M. Electrolyte transport in the mammalian colon: mechanisms and implications for disease. *Physiol Rev.* **2002**, *82* (1), 245-289.

8. Doring, F.; Will, J.; Amasheh, S.; Clauss, W.; Ahlbrecht, H.;Daniel, H. Minimal molecular determinants of substrates for recognition by the intestinal peptide transporter. *J Biol.Chem.* **1998**, *273* (36), 23211-23218.

9. Amasheh, S.; Wenzel, U.; Boll, M.; Dorn, D.; Weber, W. M.; Clauss, W.;Daniel, H. Transport of charged dipeptides by the intestinal H+/peptide symporter PepT1 expressed in Xenopus laevis oocytes. *Journal of Membrane Biology* **1997**, *155* (3), 247-256.

10. Mackenzie, B.; Loo, D. D.; Fei, Y.; Liu, W. J.; Ganapathy, V.; Leibach, F. H.;Wright, E. M. Mechanisms of the human intestinal H+-coupled oligopeptide transporter hPEPT1. *J Biol.Chem.* **1996**, *271* (10), 5430-5437.

11. Anderson, C. M.; Mendoza, M. E.; Kennedy, D. J.; Raldua, D.;Thwaites, D. T. Inhibition of intestinal dipeptide transport by the neuropeptide VIP is an anti-absorptive effect via the VPAC1 receptor in a human enterocyte-like cell line (Caco-2). *Br.J Pharmacol.* **2003**, *138* (4), 564-573.

12. Boll, M.; Markovich, D.; Weber, W. M.; Korte, H.; Daniel, H.;Murer, H. Expression cloning of a cDNA from rabbit small intestine related to proton-coupled transport of peptides, beta-lactam antibiotics and ACE-inhibitors. *Pflugers Arch.* **1994**, *429* (1), 146-149.

13. Fei, Y. J.; Kanai, Y.; Nussberger, S.; Ganapathy, V.; Leibach, F. H.; Romero, M. F.; Singh, S. K.; Boron, W. F.;Hediger, M. A. Expression cloning of a

mammalian proton-coupled oligopeptide transporter. *Nature* **1994**, *368* (6471), 563-566.

14. Liang, R.; Fei, Y. J.; Prasad, P. D.; Ramamoorthy, S.; Han, H.; Yang-Feng, T. L.; Hediger, M. A.; Ganapathy, V.;Leibach, F. H. Human intestinal H+/peptide cotransporter. Cloning, functional expression, and chromosomal localization. *J Biol.Chem.* **1995**, *270* (12), 6456-6463.

15. Saito, H.; Masuda, S.;Inui, K. Cloning and functional characterization of a novel rat organic anion transporter mediating basolateral uptake of methotrexate in the kidney. *J Biol.Chem.* **1996**, *271* (34), 20719-20725.

16. Fei, Y. J.; Sugawara, M.; Liu, J. C.; Li, H. W.; Ganapathy, V.; Ganapathy, M. E.;Leibach, F. H. cDNA structure, genomic organization, and promoter analysis of the mouse intestinal peptide transporter PEPT1. *Biochimica et Biophysica Acta (BBA)-Gene Structure and Expression* **2000**, *1492* (1), 145-154.

17. Klang, J. E.; Burnworth, L. A.; Pan, Y. X.; Webb, K. E., Jr.;Wong, E. A. Functional characterization of a cloned pig intestinal peptide transporter (pPepT1). *J Anim Sci.* **2005**, *83* (1), 172-181.

18. Ronnestad, I.; Gavaia, P. J.; Viegas, C. S.; Verri, T.; Romano, A.; Nilsen, T. O.; Jordal, A. E.; Kamisaka, Y.;Cancela, M. L. Oligopeptide transporter PepT1 in Atlantic cod (Gadus morhua L.): cloning, tissue expression and comparative aspects. *J Exp.Biol.* **2007**, *210* (Pt 22), 3883-3896.

19. Verri, T.; Kottra, G.; Romano, A.; Tiso, N.; Peric, M.; Maffia, M.; Boll, M.; Argenton, F.; Daniel, H.;Storelli, C. Molecular and functional characterisation of the zebrafish (Danio rerio) PEPT1-type peptide transporter. *FEBS Lett.* **2003**, *549* (1-3), 115-122.

20. Covitz, K. M.; Amidon, G. L.;Sadee, W. Membrane topology of the human dipeptide transporter, hPEPT1, determined by epitope insertions. *Biochemistry* **1998**, *37* (43), 15214-15221.

21. Hu, Y.; Smith, D. E.; Ma, K.; Jappar, D.; Thomas, W.;Hillgren, K. M. Targeted disruption of peptide transporter Pept1 gene in mice significantly reduces dipeptide absorption in intestine. *Mol.Pharm.* **2008**, *5* (6), 1122-1130.

22. Shiraga, T.; Miyamoto, K. I.; Tanaka, H.; Yamamoto, H.; Taketani, Y.; Morita, K.; Tamai, I.; Tsuji, A.;Takeda, E. Cellular and molecular mechanisms of dietary regulation on rat intestinal H< sup>+</sup>/peptide transporter PepT1. *Gastroenterology* **1999**, *116* (2), 354-362.

23. Erickson, R. H.; Gum, J. R., Jr.; Lindstrom, M. M.; McKean, D.;Kim, Y. S. Regional expression and dietary regulation of rat small intestinal peptide and amino acid transporter mRNAs. *Biochem.Biophys.Res Commun.* **1995**, *216* (1), 249-257.

24. Hui, L.; Ling, W.; Zhi-jun, C.;Sheng-li, L. L. W. Responses of mRNA expression of PepT1 in small intestine to graded duodenal soybean small peptides infusion in lactating goats. *African Journal of Biotechnology* **2009**, *8*1973-1978.

25. Nduati, V.; Yan, Y.; Dalmasso, G.; Driss, A.; Sitaraman, S.;Merlin, D. Leptin Transcriptionally Enhances Peptide Transporter (hPepT1) Expression and Activity via the cAMP-response Element-binding Protein and Cdx2 Transcription Factors. *Journal of Biological Chemistry* **2006**, *282* (2), 1359-1373.

26. Buyse, M.; Berlioz, F.; Guilmeau, S.; Tsocas, A.; Voisin, T.; PÃ©ranzi, G.; Merlin, D.; Laburthe, M.; Lewin, M. J. M.; RozÃ©, C.;others PepT1-mediated epithelial transport of dipeptides and cephalexin is enhanced by luminal leptin in the small intestine. *Journal of Clinical Investigation* **2001**, *108* (10), 1483-1483.

27. Hindlet, P.; Bado, A.; Kamenicky, P.; Delomenie, C.; Bourasset, F.; Nazaret, C.; Farinotti, R.;Buyse, M. Reduced intestinal absorption of dipeptides via PepT1 in mice with diet-induced obesity is associated with leptin receptor down-regulation. *J Biol.Chem.* **2009**, *284* (11), 6801-6808.

28. Shimakura, J.; Terada, T.; Saito, H.; Katsura, T.;Inui, K. Induction of intestinal peptide transporter 1 expression during fasting is mediated via peroxisome proliferator-activated receptor ${$alpha$}$. *American Journal of Physiology- Gastrointestinal and Liver Physiology* **2006**, *291* (5), G851-

29. Hirai, T.; Fukui, Y.;Motojima, K. PPARα agonists positively and negatively regulate the expression of several nutrient/drug transporters in mouse small intestine. *Biological & pharmaceutical bulletin* **2007**, *30* (11), 2185-2190.

30. Rubio-Aliaga, I.;Daniel, H. Peptide transporters and their roles in physiological processes and drug disposition. *Xenobiotica* **2008**, *38* (7-8), 1022-1042.

31. Nozawa, T.; Toyobuku, H.; Kobayashi, D.; Kuruma, K.; Tsuji, A.;Tamai, I. Enhanced intestinal absorption of drugs by activation of peptide transporter PEPT1 using proton-releasing polymer. *Journal of pharmaceutical sciences* **2003**, *92* (11), 2208-2216.

32. Shimakura, J.; Terada, T.; Katsura, T.;Inui, K. I. Characterization of the human peptide transporter PEPT1 promoter: Sp1 functions as a basal transcriptional regulator of human PEPT1. *American Journal of Physiology- Gastrointestinal and Liver Physiology* **2005**, 00025-2005.

33. McGhee, J. D.; Fukushige, T.; Krause, M. W.; Minnema, S. E.; Goszczynski, B.; Gaudet, J.; Kohara, Y.; Bossinger, O.; Zhao, Y.; Khattra, J.;others ELT-2 is the predominant transcription factor controlling differentiation and function of the C. elegans intestine, from embryo to adult. *Developmental biology* **2009**, *327* (2), 551-565.

34. Miyamoto, K.; Shiraga, T.; Morita, K.; Yamamoto, H.; Haga, H.; Taketani, Y.; Tamai, I.; Sai, Y.; Tsuji, A.;Takeda, E. Sequence, tissue distribution and developmental changes in rat intestinal oligopeptide transporter. *Biochim.Biophys.Acta* **1996**, *1305* (1-2), 34-38.

35. Shen, H.; Smith, D. E.;Brosius, F. C., III Developmental expression of PEPT1 and PEPT2 in rat small intestine, colon, and kidney. *Pediatr.Res* **2001**, *49* (6), 789-795.

36. Hussain, I.; Kellett, L.; Affleck, J.; Shepherd, J.;Boyd, R. Expression and cellular distribution during development of the peptide transporter (PepT1) in the small intestinal epithelium of the rat. *Cell Tissue Res* **2002**, *307* (1), 139-142.

37. Van, L.; Pan, Y. X.; Bloomquist, J. R.; Webb Jr, K. E.; Wong, E. A.;others Developmental regulation of a turkey intestinal peptide transporter (PepT1). *Poultry science* **2005**, *84* (1), 75-82.

38. McCarroll, S. A.; Murphy, C. T.; Zou, S.; Pletcher, S. D.; Chin, C. S.; Jan, Y. N.; Kenyon, C.; Bargmann, C. I.;Li, H. Comparing genomic expression patterns across species identifies shared transcriptional profile in aging. *nature genetics* **2004**, *36* (2), 197-204.

39. Nassl, A. M.; Rubio-Aliaga, I.; Fenselau, H.; Marth, M. K.; Kottra, G.;Daniel, H. Amino acid absorption and homeostasis in mice lacking the intestinal peptide transporter PEPT1. *Am.J Physiol Gastrointest.Liver Physiol* **2011**, *301* (1), G128-G137.

40. Nassl, A. M.; Rubio-Aliaga, I.; Sailer, M.;Daniel, H. The intestinal peptide transporter PEPT1 is involved in food intake regulation in mice fed a high-protein diet. *PLoS ONE* **2011**, *6* (10), e26407-

41. Meissner, B. Phenotype analysis of Caenorhabditis elegans lacking the intestinal peptide transporter Technische Universität München, 2004

42. Benner, J. Amino acid homeostasis in *Caenorhabditis elegans*: Role of peptide and heteromeric amino acid transporters Technische Universität München, 2011

43. Spanier, B.; Lasch, K.; Marsch, S.; Benner, J.; Liao, W.; Hu, H.; Kienberger, H.; Eisenreich, W.;Daniel, H. How the intestinal peptide transporter PEPT-1 contributes to an obesity phenotype in Caenorhabditits elegans. *PLoS One* **2009**, *4* (7), e6279-

44. Spanier, B.; Lasch, K.; Marsch, S.; Benner, J.; Liao, W.; Hu, H.; Kienberger, H.; Eisenreich, W.;Daniel, H. How the intestinal peptide transporter PEPT-1 contributes to an obesity phenotype in Caenorhabditits elegans. *PLoS One* **2009**, *4* (7), e6279-

45. Bailyes, E. M.; Nave, B. T.; Soos, M. A.; Orr, S. R.; Hayward, A. C.;Siddle, K. Insulin receptor/IGF-I receptor hybrids are widely distributed in mammalian tissues: quantification of individual receptor species by

selective immunoprecipitation and immunoblotting. *Biochem.J* **1997**, *327 (Pt 1)*209-215.

46. Skolnik, E. Y.; Batzer, A.; Li, N.; Lee, C. H.; Lowenstein, E.; Mohammadi, M.; Margolis, B.;Schlessinger, J. The function of GRB2 in linking the insulin receptor to Ras signaling pathways. *Science* **1993**, *260* (5116), 1953-1955.

47. Khoo, S. Regulation of Insulin Gene Transcription by ERK1 and ERK2 in Pancreatic Â Cells. *Journal of Biological Chemistry* **2003**, *278* (35), 32969-32977.

48. Anderson, K. E.; Coadwell, J.; Stephens, L. R.;Hawkins, P. T. Translocation of PDK-1 to the plasma membrane is important in allowing PDK-1 to activate protein kinase B. *Current Biology* **1998**, *8* (12), 684-691-

49. Manning, B. D.;Cantley, L. C. AKT/PKB Signaling: Navigating Downstream. *Cell* **2006**, *129* (7), 1261-1274.

50. Alessi, D. R.; Kozlowski, M. T.; Weng, Q. P.; Morrice, N.;Avruch, J. 3-Phosphoinositide-dependent protein kinase 1 (PDK1) phosphorylates and activates the p70 S6 kinase in vivo and in vitro. *Current Biology* **1998**, *8* (2), 69-81.

51. Kimura, K. D. daf-2, an Insulin Receptor-Like Gene That Regulates Longevity and Diapause in Caenorhabditis elegans. *Science* **1997**, *277* (5328), 942-946.

52. Paradis, S.;Ruvkun, G. Caenorhabditis elegans Akt/PKB transduces insulin receptor-like signals from AGE-1 PI3 kinase to the DAF-16 transcription factor. *Genes & Development* **1998**, *12* (16), 2488-2498.

53. Gems, D.; Sutton, A. J.; Sundermeyer, M. L.; Albert, P. S.; King, K. V.; Edgley, M. L.; Larsen, P. L.;Riddle, D. L. Two pleiotropic classes of daf-2 mutation affect larval arrest, adult behavior, reproduction and longevity in Caenorhabditis elegans. *Genetics* **1998**, *150* (1), 129-155.

54. Murphy, C. T.; McCarroll, S. A.; Bargmann, C. I.; Fraser, A.; Kamath, R. S.; Ahringer, J.; Li, H.;Kenyon, C. Genes that act downstream of DAF-16 to influence the lifespan of Caenorhabditis elegans. *Nature* **2003**, *424* (6946), 277-283.

55. Henderson, S. T.;Johnson, T. E. daf-16 integrates developmental and environmental inputs to mediate aging in the nematode Caenorhabditis elegans. *Current Biology* **2001**, *11* (24), 1975-1980.

56. Sies, H. Oxidative stress: oxidants and antioxidants. *Exp.Physiol* **1997**, *82* (2), 291-295.

57. Reth, M. Hydrogen peroxide as second messenger in lymphocyte activation. *Nat.Immunol.* **2002**, *3* (12), 1129-1134.

58. Forman, H. J.; Maiorino, M.;Ursini, F. Signaling functions of reactive oxygen species. *Biochemistry* **2010**, *49* (5), 835-842.

59. Berlett, B. S.;Stadtman, E. R. Protein oxidation in aging, disease, and oxidative stress. *Journal of Biological Chemistry* **1997**, *272* (33), 20313-

60. Aruoma, O. I.; Halliwell, B.; Gajewski, E.;Dizdaroglu, M. Copper-ion-dependent damage to the bases in DNA in the presence of hydrogen peroxide. *Biochem.J* **1991**, *273 (Pt 3)*601-604.

61. Henchcliffe, C.;Beal, M. F. Mitochondrial biology and oxidative stress in Parkinson disease pathogenesis. *Nat.Clin.Pract.Neurol.* **2008**, *4* (11), 600-609.

62. Kawada, T. Oxidative stress markers and cardiovascular disease: Advantage of using these factors in combination with lifestyle factors for cardiovascular risk assessment. *Int.J Cardiol.* **2012**,

63. Selvaraju, V.; Joshi, M.; Suresh, S.; Sanchez, J. A.; Maulik, N.;Maulik, G. Diabetes, oxidative stress, molecular mechanism, and cardiovascular disease - an overview. *Toxicol.Mech.Methods* **2012**,

64. Hybertson, B. M.; Gao, B.; Bose, S. K.;McCord, J. M. Oxidative stress in health and disease: the therapeutic potential of Nrf2 activation. *Mol.Aspects Med.* **2011**, *32* (4-6), 234-246.

65. Martindale, J. L.;Holbrook, N. J. Cellular response to oxidative stress: Signaling for suicide and survival*. *Journal of cellular physiology* **2002**, *192* (1), 1-15.

66. Li, N.;Karin, M. Is NF-kappaB the sensor of oxidative stress? *FASEB J* **1999**, *13* (10), 1137-1143.

67. Thimmulappa, R. K.; Mai, K. H.; Srisuma, S.; Kensler, T. W.; Yamamoto, M.;Biswal, S. Identification of Nrf2-regulated genes induced by the chemopreventive agent sulforaphane by oligonucleotide microarray. *Cancer Res* **2002**, *62* (18), 5196-5203.

68. Huang, H. C.; Nguyen, T.;Pickett, C. B. Regulation of the antioxidant response element by protein kinase C-mediated phosphorylation of NF-E2-related factor 2. *Proc.Natl.Acad.Sci.U.S.A* **2000**, *97* (23), 12475-12480.

69. Huang, H. C.; Nguyen, T.;Pickett, C. B. Phosphorylation of Nrf2 at Ser-40 by protein kinase C regulates antioxidant response element-mediated transcription. *J Biol.Chem.* **2002**, *277* (45), 42769-42774.

70. Sun, Z.; Huang, Z.;Zhang, D. D. Phosphorylation of Nrf2 at multiple sites by MAP kinases has a limited contribution in modulating the Nrf2-dependent antioxidant response. *PLoS One* **2009**, *4* (8), e6588-

71. Sun, Z.; Chin, Y. E.;Zhang, D. D. Acetylation of Nrf2 by p300/CBP augments promoter-specific DNA binding of Nrf2 during the antioxidant response. *Mol.Cell Biol.* **2009**, *29* (10), 2658-2672.

72. He, C. H.; Gong, P.; Hu, B.; Stewart, D.; Choi, M. E.; Choi, A. M.;Alam, J. Identification of activating transcription factor 4 (ATF4) as an Nrf2-interacting protein. Implication for heme oxygenase-1 gene regulation. *J Biol.Chem.* **2001**, *276* (24), 20858-20865.

73. Blank, V. Small Maf proteins in mammalian gene control: mere dimerization partners or dynamic transcriptional regulators? *J Mol.Biol.* **2008**, *376* (4), 913-925.

74. Brown, S. L.; Sekhar, K. R.; Rachakonda, G.; Sasi, S.;Freeman, M. L. Activating transcription factor 3 is a novel repressor of the nuclear factor erythroid-derived 2-related factor 2 (Nrf2)-regulated stress pathway. *Cancer Res* **2008**, *68* (2), 364-368.

75. An, J. H.;Blackwell, T. K. SKN-1 links C. elegans mesendodermal specification to a conserved oxidative stress response. *Genes & Development* **2003**, *17* (15), 1882-

76. Blackwell, T. K.; Bowerman, B.; Priess, J. R.;Weintraub, H. Formation of a monomeric DNA binding domain by Skn-1 bZIP and homeodomain elements *Science* **1994** 266 (5185): 621-629.

77. Carroll, A. S.; Gilbert, D. E.; Liu, X.; Cheung, J. W.; Michnowicz, J. E.; Wagner, G.; Ellenberger, T. E.;Blackwell, T. K. SKN-1 domain folding and basic region monomer stabilization upon DNA binding. *Genes & Development* **1997**, *11* (17), 2227-

78. Choe, K. P.; Przybysz, A. J.;Strange, K. The WD40 Repeat Protein WDR-23 Functions with the CUL4/DDB1 Ubiquitin Ligase To Regulate Nuclear Abundance and Activity of SKN-1 in Caenorhabditis elegans. *Molecular and Cellular Biology* **2009**, *29* (10), 2704-2715.

79. An, J. H.; Vranas, K.; Lucke, M.; Inoue, H.; Hisamoto, N.; Matsumoto, K.;Blackwell, T. K. Regulation of the Caenorhabditis elegans oxidative stress defense protein SKN-1 by glycogen synthase kinase-3. *Proceedings of the National Academy of Sciences* **2005**, *102* (45), 16275-

80. Tullet, J.; Hertweck, M.; An, J. H.; Baker, J.; Hwang, J. Y.; Liu, S.; Oliveira, R. P.; Baumeister, R.;Blackwell, T. K. Direct inhibition of the longevity-promoting factor SKN-1 by insulin-like signaling in C. elegans. *Cell* **2008**, *132* (6), 1025-1038.

81. Okuyama, T.; Inoue, H.; Ookuma, S.; Satoh, T.; Kano, K.; Honjoh, S.; Hisamoto, N.; Matsumoto, K.;Nishida, E. The ERK-MAPK pathway regulates longevity through SKN-1 and insulin-like signaling in Caenorhabditis elegans. *J Biol.Chem.* **2010**, *285* (39), 30274-30281.

82. Kell, A.; Ventura, N.; Kahn, N.;Johnson, T. E. Activation of SKN-1 by novel kinases in Caenorhabditis elegans. *Free Radical Biology and Medicine* **2007**, *43* (11), 1560-1566-

83. Kahn, N.; Rea, S.; Moyle, S.; Kell, A.;Johnson, T. Proteasomal dysfunction activates the transcription factor SKN-1 and produces a selective oxidative-stress response in Caenorhabditis elegans. *Biochem.J* **2008**, *409*205-213.

84. Wang, J.; Robida-Stubbs, S.; Tullet, J. M. A.; Rual, J. F. o.; Vidal, M.;Blackwell, T. K. RNAi Screening Implicates a SKN-1-Dependent Transcriptional Response in Stress Resistance and Longevity Deriving from Translation Inhibition. *PLoS genetics* **2008**, *6* (8), e1001048-

85. Schroder, M.;Kaufman, R. J. The mammalian unfolded protein response. *Annu.Rev.Biochem.* **2005**, *74*739-789.

86. Liu, C. Y.; Wong, H. N.; Schauerte, J. A.;Kaufman, R. J. The protein kinase/endoribonuclease IRE1alpha that signals the unfolded protein response has a luminal N-terminal ligand-independent dimerization domain. *J Biol.Chem.* **2002**, *277* (21), 18346-18356.

87. Cui, W.; Li, J.; Ron, D.;Sha, B. The structure of the PERK kinase domain suggests the mechanism for its activation. *Acta Crystallogr.D.Biol.Crystallogr.* **2011**, *67* (Pt 5), 423-428.

88. Cullinan, S. B.; Zhang, D.; Hannink, M.; Arvisais, E.; Kaufman, R. J.;Diehl, J. A. Nrf2 is a direct PERK substrate and effector of PERK-dependent cell survival. *Mol.Cell Biol.* **2003**, *23* (20), 7198-7209.

89. Yan, W.; Frank, C. L.; Korth, M. J.; Sopher, B. L.; Novoa, I.; Ron, D.;Katze, M. G. Control of PERK eIF2alpha kinase activity by the endoplasmic reticulum stress-induced molecular chaperone P58IPK. *Proc.Natl.Acad.Sci.U.S.A* **2002**, *99* (25), 15920-15925.

90. Vattem, K. M.;Wek, R. C. Reinitiation involving upstream ORFs regulates ATF4 mRNA translation in mammalian cells. *Proc.Natl.Acad.Sci.U.S.A* **2004**, *101* (31), 11269-11274.

91. Fujita, E.; Kouroku, Y.; Isoai, A.; Kumagai, H.; Misutani, A.; Matsuda, C.; Hayashi, Y. K.;Momoi, T. Two endoplasmic reticulum-associated degradation (ERAD) systems for the novel variant of the mutant dysferlin: ubiquitin/proteasome ERAD(I) and autophagy/lysosome ERAD(II). *Hum.Mol.Genet.* **2007**, *16* (6), 618-629.

92. Merksamer, P. I.;Papa, F. R. The UPR and cell fate at a glance. *J Cell Sci.* **2010**, *123* (Pt 7), 1003-1006.

93. Shore, G. C.; Papa, F. R.;Oakes, S. A. Signaling cell death from the endoplasmic reticulum stress response. *Curr.Opin.Cell Biol.* **2011**, *23* (2), 143-149.

94. Li, J.; Lee, B.;Lee, A. S. Endoplasmic reticulum stress-induced apoptosis: multiple pathways and activation of p53-up-regulated modulator of apoptosis (PUMA) and NOXA by p53. *J Biol.Chem.* **2006**, *281* (11), 7260-7270.

95. Shen, X.; Ellis, R. E.; Sakaki, K.;Kaufman, R. J. Genetic interactions due to constitutive and inducible gene regulation mediated by the unfolded protein response in C. elegans. *PLoS genetics* **2005**, *1* (3), e37-

96. Calfon, M.; Zeng, H.; Urano, F.; Till, J. H.; Hubbard, S. R.; Harding, H. P.; Clark, S. G.;Ron, D. IRE1 couples endoplasmic reticulum load to secretory capacity by processing the XBP-1 mRNA. *Nature* **2002**, *415* (6867), 92-96.

97. Ma, Y.;Hendershot, L. M. The unfolding tale of the unfolded protein response. *Cell* **2001**, *107* (7), 827-830.

98. Sood, R.; Porter, A. C.; Ma, K.; Quilliam, L. A.;Wek, R. C. Pancreatic eukaryotic initiation factor-2alpha kinase (PEK) homologues in humans, Drosophila melanogaster and Caenorhabditis elegans that mediate translational control in response to endoplasmic reticulum stress. *Biochem.J* **2000**, *346 Pt 2*281-293.

99. Mori, K. Signalling pathways in the unfolded protein response: development from yeast to mammals. *J Biochem.* **2009**, *146* (6), 743-750.

100. Shen, X.; Ellis, R. E.; Lee, K.; Liu, C. Y.; Yang, K.; Solomon, A.; Yoshida, H.; Morimoto, R.; Kurnit, D. M.; Mori, K.;Kaufman, R. J. Complementary signaling pathways regulate the unfolded protein response and are required for C. elegans development. *Cell* **2001**, *107* (7), 893-903.

101. Tittel, J. N.;Steller, H. A comparison of programmed cell death between species. *Genome Biol.* **2000**, *1* (3), REVIEWS 0003-

102. Adibi, S. A. The oligopeptide transporter (Pept-1) in human intestine: biology and function. *Gastroenterology* **1997**, *113* (1), 332-340.

103. Martin, F. P. J.; Spanier, B.; Collino, S.; Montoliu, I.; Kolmeder, C.; Giesbertz, P.; Affolter, M.; Kussmann, M.; Daniel, H.; Kochhar, S.;others Metabotyping of Caenorhabditis elegans and their culture media revealed unique metabolic phenotypes associated to amino acid deficiency and insulin-like signaling. *Journal of Proteome Research* **2011**,

104. Inoue, H.; Hisamoto, N.; An, J. H.; Oliveira, R. P.; Nishida, E.; Blackwell, T. K.;Matsumoto, K. The C. elegans p38 MAPK pathway regulates nuclear localization of the transcription factor SKN-1 in oxidative stress response. *Genes Dev.* **2005**, *19* (19), 2278-2283.

105. McElwee, J. J. Shared Transcriptional Signature in Caenorhabditis elegans Dauer Larvae and Long-lived daf-2 Mutants Implicates Detoxification

System in Longevity Assurance. *Journal of Biological Chemistry* **2004**, *279* (43), 44533-44543.

106. Zhang, K.;Kaufman, R. J. From endoplasmic-reticulum stress to the inflammatory response. *Nature* **2008**, *454* (7203), 455-462.

107. Henis-Korenblit, S.; Zhang, P.; Hansen, M.; McCormick, M.; Lee, S. J.; Cary, M.;Kenyon, C. Insulin/IGF-1 signaling mutants reprogram ER stress response regulators to promote longevity. *Proceedings of the National Academy of Sciences* **2010**, *107* (21), 9730-

108. Yen, K.; Le, T. T.; Bansal, A.; Narasimhan, S. D.; Cheng, J. X.;Tissenbaum, H. A. A comparative study of fat storage quantitation in nematode Caenorhabditis elegans using label and label-free methods. *PLoS ONE* **2010**, *5* (9),

109. Krijgsveld, J.; Ketting, R. F.; Mahmoudi, T.; Johansen, J.; rtal-Sanz, M.; Verrijzer, C. P.; Plasterk, R. H. A.;Heck, A. J. R. Metabolic labeling of C.elegans and D.melanogaster for quantitaive proteomics. *Nature biotechnology* **2003**, *21* (8), 927-931.

110. Haegler, K.; Mueller, N. S.; Maccarrone, G.; Hunyadi-Gulyas, E.; Webhofer, C.; Filiou, M. D.; Zhang, Y.;Turck, C. W. QuantiSpecâ€”Quantitative mass spectrometry data analysis of 15N-metabolically labeled proteins. *Journal of Proteomics* **2009**, *71* (6), 601-608.

111. Urttiac, A.; SadÃ©e, W.;Johns, S. J. Genomic structure of proton-coupled oligopeptide transporter hPEPT1 and pH-sensing regulatory splice variant. *The AAPS Journal* **2001**, *3* (1), 66-79.

112. Banning, A.; Deubel, S.; Kluth, D.; Zhou, Z.;Brigelius-Flohe, R. The GI-GPx gene is a target for Nrf2. *Mol.Cell Biol.* **2005**, *25* (12), 4914-4923.

113. Rojo, A. I.; Medina-Campos, O. N.; Rada, P.; Zuniga-Toala, A.; Lopez-Gazcon, A.; Espada, S.; Pedraza-Chaverri, J.;Cuadrado, A. Signaling pathways activated by the phytochemical nordihydroguaiaretic acid contribute to a Keap1-independent regulation of Nrf2 stability: Role of glycogen synthase kinase-3. *Free Radic.Biol.Med.* **2012**, *52* (2), 473-487.

114. Salazar, M.; Rojo, A. I.; Velasco, D.; de Sagarra, R. M.;Cuadrado, A. Glycogen synthase kinase-3beta inhibits the xenobiotic and antioxidant cell response by direct phosphorylation and nuclear exclusion of the transcription factor Nrf2. *J Biol.Chem.* **2006**, *281* (21), 14841-14851.

115. Wang, Q.; Zhou, Y.; Wang, X.;Evers, B. M. Glycogen synthase kinase-3 is a negative regulator of extracellular signal-regulated kinase. *Oncogene* **2006**, *25* (1), 43-50.

116. Kode, A.; Rajendrasozhan, S.; Caito, S.; Yang, S. R.; Megson, I. L.;Rahman, I. Resveratrol induces glutathione synthesis by activation of Nrf2 and protects against cigarette smoke-mediated oxidative stress in human

lung epithelial cells. *American Journal of Physiology-Lung Cellular and Molecular Physiology* **2008**, *294* (3), L478-L488.

117. Ungvari, Z.; Bagi, Z.; Feher, A.; Recchia, F. A.; Sonntag, W. E.; Pearson, K.; de, C. R.;Csiszar, A. Resveratrol confers endothelial protection via activation of the antioxidant transcription factor Nrf2. *Am.J Physiol Heart Circ.Physiol* **2010**, *299* (1), H18-H24.

118. Schneider, Y.; Vincent, F.; Duranton, B.; Badolo, L.; Gosse, F.; Bergmann, C.; Seiler, N.;Raul, F. Anti-proliferative effect of resveratrol, a natural component of grapes and wine, on human colonic cancer cells. *Cancer Lett.* **2000**, *158* (1), 85-91.

119. Itoh, K.; Wakabayashi, N.; Katoh, Y.; Ishii, T.; O'Connor, T.;Yamamoto, M. Keap1 regulates both cytoplasmic-nuclear shuttling and degradation of Nrf2 in response to electrophiles. *Genes to Cells* **2003**, *8* (4), 379-391.

120. BriedÃ©, J. J.; Van Delft, J. M. H.; De Kok, T. M. C. M.; Van Herwijnen, M. H. M.; Maas, L. M.; Gottschalk, R. W. H.;Kleinjans, J. C. S. Global Gene Expression Analysis Reveals Differences in Cellular Responses to Hydroxyl-and Superoxide Anion Radical-Induced Oxidative Stress in Caco-2 Cells. *Toxicological Sciences* **2010**, *114* (2), 193-203.

121. Malorni, W.; Iosi, F.; Santini, M. T.;Testa, U. Menadione-induced oxidative stress leads to a rapid down-modulation of transferrin receptor recycling. *Journal of cell science* **1993**, *106* (1), 309-318.

122. Karczewski, J. M.;Noordhoek, J. Toxicity of menadione in the differentiating human colon carcinoma cell line Caco-2. *Toxicol.In Vitro* **1999**, *13* (1), 35-43.

123. Bellomo, G.; Mirabelli, F.; Vairetti, M.; Iosi, F.;Malorni, W. Cytoskeleton as a target in menadione-induced oxidative stress in cultured mammalian cells. I. Biochemical and immunocytochemical features. *Journal of cellular physiology* **1990**, *143* (1), 118-128.

124. Harris, K. E.;Jeffery, E. H. Sulforaphane and erucin increase MRP1 and MRP2 in human carcinoma cell lines. *J Nutr.Biochem.* **2008**, *19* (4), 246-254.

125. Kim, S. J.; Park, C.; Han, A. L.; Youn, M. J.; Lee, J. H.; Kim, Y.; Kim, E. S.; Kim, H. J.; Kim, J. K.; Lee, H. K.;others Ebselen attenuates cisplatin-induced ROS generation through Nrf2 activation in auditory cells. *Hearing research* **2009**, *251* (1-2), 70-82.

126. Sakurai, T.; Kanayama, M.; Shibata, T.; Itoh, K.; Kobayashi, A.; Yamamoto, M.;Uchida, K. Ebselen, a seleno-organic antioxidant, as an electrophile. *Chem.Res Toxicol.* **2006**, *19* (9), 1196-1204.

127. Tamasi, V.; Jeffries, J. M.; Arteel, G. E.;Falkner, K. C. Ebselen augments its peroxidase activity by inducing nrf-2-dependent transcription. *Arch.Biochem.Biophys.* **2004**, *431* (2), 161-168.

128. Benner, J.; Daniel, H.;Spanier, B. A glutathione peroxidase, intracellular peptidases and the TOR complexes regulate peptide transporter PEPT-1 in C. elegans. *PLoS ONE* **2011**, *6* (9), e25624-

129. Muller, M.; Banning, A.; Brigelius-Flohe, R.;Kipp, A. Nrf2 target genes are induced under marginal selenium-deficiency. *Genes Nutr.* **2010**, *5* (4), 297-307.

130. Wooden, S. K.; Li, L. J.; Navarro, D.; Qadri, I.; Pereira, L.;Lee, A. S. Transactivation of the grp78 promoter by malfolded proteins, glycosylation block, and calcium ionophore is mediated through a proximal region containing a CCAAT motif which interacts with CTF/NF-I. *Mol.Cell Biol.* **1991**, *11* (11), 5612-5623.

131. Delmas, D.; Solary, E.;Latruffe, N. Resveratrol, a phytochemical inducer of multiple cell death pathways: apoptosis, autophagy and mitotic catastrophe. *Curr.Med.Chem.* **2011**, *18* (8), 1100-1121.

132. Wang, Y.; Singh, R.; Xiang, Y.;Czaja, M. J. Macroautophagy and chaperone-mediated autophagy are required for hepatocyte resistance to oxidant stress. *Hepatology* **2010**, *52* (1), 266-277.

133. Herman-Antosiewicz, A.; Johnson, D. E.;Singh, S. V. Sulforaphane causes autophagy to inhibit release of cytochrome C and apoptosis in human prostate cancer cells. *Cancer Res* **2006**, *66* (11), 5828-5835.

134. Janen, S. B.; Chaachouay, H.;Richter-Landsberg, C. Autophagy is activated by proteasomal inhibition and involved in aggresome clearance in cultured astrocytes. *Glia* **2010**, *58* (14), 1766-1774.

135. Baudouin-Cornu, P.; Lagniel, G.; Kumar, C.; Huang, M. E.;Labarre, J. Glutathione degradation is a key determinant of glutathione homeostasis. *J Biol.Chem.* **2012**, *287* (7), 4552-4561.

136. Meister, A. On the antioxidant effects of ascorbic acid and glutathione. *Biochem.Pharmacol.* **1992**, *44* (10), 1905-1915.

137. Griffith, O. W. Biologic and pharmacologic regulation of mammalian glutathione synthesis. *Free Radic.Biol.Med.* **1999**, *27* (9-10), 922-935.

138. Meissner, B. Deletion of the Intestinal Peptide Transporter Affects Insulin and TOR Signaling in Caenorhabditis elegans. *Journal of Biological Chemistry* **2004**, *279* (35), 36739-36745.

139. Spanier, B.; Rubio-Aliaga, I.; Hu, H.;Daniel, H. Altered signalling from germline to intestine pushes daf-2;pept-1 Caenorhabditis elegans into extreme longevity. *Aging Cell* **2010**, *9* (4), 636-646.

140. Lieberman, M. W.; Barrios, R.; Carter, B. Z.; Habib, G. M.; Lebovitz, R. M.; Rajagopalan, S.; Sepulveda, A. R.; Shi, Z. Z.;Wan, D. F. gamma-Glutamyl transpeptidase. What does the organization and expression of

a multipromoter gene tell us about its functions? *Am.J Pathol.* **1995**, *147* (5), 1175-1185.

141. Lieberman, M. W.; Wiseman, A. L.; Shi, Z. Z.; Carter, B. Z.; Barrios, R.; Ou, C. N.; Chevez-Barrios, P.; Wang, Y.; Habib, G. M.; Goodman, J. C.; Huang, S. L.; Lebovitz, R. M.;Matzuk, M. M. Growth retardation and cysteine deficiency in gamma-glutamyl transpeptidase-deficient mice. *Proc.Natl.Acad.Sci.U.S.A* **1996**, *93* (15), 7923-7926.

142. Katoh, Y.; Itoh, K.; Yoshida, E.; Miyagishi, M.; Fukamizu, A.;Yamamoto, M. Two domains of Nrf2 cooperatively bind CBP, a CREB binding protein, and synergistically activate transcription. *Genes Cells* **2001**, *6* (10), 857-868.

143. Song, C. Z.; Keller, K.; Chen, Y.; Murata, K.;Stamatoyannopoulos, G. Transcription coactivator CBP has direct DNA binding activity and stimulates transcription factor DNA binding through small domains. *Biochem.Biophys.Res Commun.* **2002**, *296* (1), 118-124.

144. Alteheld, B.; Evans, M. E.; Gu, L. H.; Ganapathy, V.; Leibach, F. H.; Jones, D. P.;Ziegler, T. R. Alanylglutamine dipeptide and growth hormone maintain PepT1-mediated transport in oxidatively stressed Caco-2 cells. *The Journal of nutrition* **2005**, *135* (1), 19-

145. Mizushima, N.;Klionsky, D. J. Protein turnover via autophagy: implications for metabolism. *Annu.Rev.Nutr.* **2007**, *27*19-40.

146. Thamotharan, M.; Lombardo, Y. B.; Bawani, S. Z.;Adibi, S. A. An active mechanism for completion of the final stage of protein degradation in the liver, lysosomal transport of dipeptides. *J Biol.Chem.* **1997**, *272* (18), 11786-11790.

147. Bockman, D. E.; Ganapathy, V.; Oblak, T. G.;Leibach, F. H. Localization of peptide transporter in nuclei and lysosomes of the pancreas. *Int.J Pancreatol.* **1997**, *22* (3), 221-225.

148. Zhou, X.; Thamotharan, M.; Gangopadhyay, A.; Serdikoff, C.;Adibi, S. A. Characterization of an oligopeptide transporter in renal lysosomes. *Biochim.Biophys.Acta* **2000**, *1466* (1-2), 372-378.

149. Lewis, K. N.; Mele, J.; Hayes, J. D.;Buffenstein, R. Nrf2, a Guardian of Healthspan and Gatekeeper of Species Longevity. *Integrative and comparative biology* **2010**, *50* (5), 829-

150. Chen, J.; Xavier, S.; Moskowitz-Kassai, E.; Chen, R.; Lu, C. Y.; Sanduski, K.; Spes, A.; Turk, B.;Goligorsky, M. S. Cathepsin cleavage of sirtuin 1 in endothelial progenitor cells mediates stress-induced premature senescence. *Am.J Pathol.* **2012**, *180* (3), 973-983.

151. Ihara, T.; Tsujikawa, T.; Fujiyama, Y.;Bamba, T. Regulation of PepT1 peptide transporter expression in the rat small intestine under malnourished conditions. *Digestion* **2000**, *61* (1), 59-67.

152. Ma, K.; Hu, Y.;Smith, D. E. Influence of Fed-Fasted State on Intestinal PEPT1 Expression and In Vivo Pharmacokinetics of Glycylsarcosine in Wild-Type and Pept1 Knockout Mice. *Pharmaceutical research* **2011**, *29* (2), 535-545.

153. Thamotharan, M.; Bawani, S. Z.; Zhou, X.;Adibi, S. A. Functional and molecular expression of intestinal oligopeptide transporter (Pept-1) after a brief fast. *Metabolism* **1999**, *48* (6), 681-684.

154. Mertl, M.; Daniel, H.;Kottra, G. Substrate-induced changes in the density of peptide transporter PEPT1 expressed in Xenopus oocytes. *Am.J Physiol Cell Physiol* **2008**, *295* (5), C1332-C1343.

155. Zhang, H.; Liu, H.; Davies, K. J.; Sioutas, C.; Finch, C. E.; Morgan, T. E.;Forman, H. J. Nrf2-regulated phase II enzymes are induced by chronic ambient nanoparticle exposure in young mice with age-related impairments. *Free Radic.Biol.Med.* **2012**, *52* (9), 2038-2046.

156. Maiorino, M.; Thomas, J. P.; Girotti, A. W.;Ursini, F. Reactivity of phospholipid hydroperoxide glutathione peroxidase with membrane and lipoprotein lipid hydroperoxides. *Free Radic.Res Commun.* **1991**, *12-13 Pt 1*131-135.

157. Yoo, M. H.; Gu, X.; Xu, X. M.; Kim, J. Y.; Carlson, B. A.; Patterson, A. D.; Cai, H.; Gladyshev, V. N.;Hatfield, D. L. Delineating the role of glutathione peroxidase 4 in protecting cells against lipid hydroperoxide damage and in Alzheimer's disease. *Antioxid.Redox.Signal.* **2010**, *12* (7), 819-827.

158. Ferrington, D. A.;Kapphahn, R. J. Catalytic site-specific inhibition of the 20S proteasome by 4-hydroxynonenal. *FEBS Lett.* **2004**, *578* (3), 217-223.

159. Friguet, B.;Szweda, L. I. Inhibition of the multicatalytic proteinase (proteasome) by 4-hydroxy-2-nonenal cross-linked protein. *FEBS Lett.* **1997**, *405* (1), 21-25.

160. Hill, B. G.; Haberzettl, P.; Ahmed, Y.; Srivastava, S.;Bhatnagar, A. Unsaturated lipid peroxidation-derived aldehydes activate autophagy in vascular smooth-muscle cells. *Biochem.J* **2008**, *410* (3), 525-534.

161. Marques, C.; Pereira, P.; Taylor, A.; Liang, J. N.; Reddy, V. N.; Szweda, L. I.;Shang, F. Ubiquitin-dependent lysosomal degradation of the HNE-modified proteins in lens epithelial cells. *FASEB J* **2004**, *18* (12), 1424-1426.

162. Burk, R. F.; Hill, K. E.; Nakayama, A.; Mostert, V.; Levander, X. A.; Motley, A. K.; Johnson, D. A.; Johnson, J. A.; Freeman, M. L.;Austin, L. M. Selenium deficiency activates mouse liver Nrf2-ARE but vitamin E deficiency does not. *Free Radic.Biol.Med.* **2008**, *44* (8), 1617-1623.

163. Senn, E.; Scharrer, E.;Wolffram, S. Effects of glutathione and of cysteine on intestinal absorption of selenium from selenite. *Biol.Trace Elem.Res* **1992**, *33*103-108.

164. Gangopadhyay, A.; Thamotharan, M.;Adibi, S. A. Regulation of oligopeptide transporter (Pept-1) in experimental diabetes. *American Journal of Physiology-Gastrointestinal and Liver Physiology* **2002**, *283* (1), G133-

165. Thamotharan, M.; Bawani, S. Z.; Zhou, X.;Adibi, S. A. Hormonal regulation of oligopeptide transporter pept-1 in a human intestinal cell line. *Am.J Physiol* **1999**, *276* (4 Pt 1), C821-C826.

166. Nielsen, C. U.; Amstrup, J.; Nielsen, R.; Steffansen, B.; Frokjaer, S.;Brodin, B. Epidermal growth factor and insulin short-term increase hPepT1-mediated glycylsarcosine uptake in Caco-2 cells. *Acta physiologica scandinavica* **2003**, *178* (2), 139-148.

167. Watanabe, K.; Terada, K.;Sato, J. Intestinal absorption of cephalexin in diabetes mellitus model rats. *Eur.J Pharm.Sci.* **2003**, *19* (2-3), 91-98.

168. Watanabe, K.; Terada, K.; Jinriki, T.;Sato, J. Effect of insulin on cephalexin uptake and transepithelial transport in the human intestinal cell line Caco-2. *Eur.J Pharm.Sci.* **2004**, *21* (1), 87-95.

169. Bikhazi, A. B.; Skoury, M. M.; Zwainy, D. S.; Jurjus, A. R.; Kreydiyyeh, S. I.; Smith, D. E.; Audette, K.;Jacques, D. Effect of diabetes mellitus and insulin on the regulation of the PepT 1 symporter in rat jejunum. *Molecular Pharmaceutics* **2004**, *1* (4), 300-308.

170. Murphy, C. T.; McCarroll, S. A.; Bargmann, C. I.; Fraser, A.; Kamath, R. S.; Ahringer, J.; Li, H.;Kenyon, C. Genes that act downstream of DAF-16 to influence the lifespan of Caenorhabditis elegans. *Nature* **2003**, *424* (6946), 277-283.

171. Beloto-Silva, O.; Machado, U. F.;Oliveira-Souza, M. Glucose-induced regulation of NHEs activity and SGLTs expression involves the PKA signaling pathway. *J Membr.Biol.* **2011**, *239* (3), 157-165.

172. Kim, D. I.; Lim, S. K.; Park, M. J.; Han, H. J.; Kim, G. Y.;Park, S. H. The involvement of phosphatidylinositol 3-kinase /Akt signaling in high glucose-induced downregulation of GLUT-1 expression in ARPE cells. *Life Sci.* **2007**, *80* (7), 626-632.

173. Ha, H.; Yoon, S. J.;Kim, K. H. High glucose can induce lipid peroxidation in the isolated rat glomeruli. *Kidney Int.* **1994**, *46* (6), 1620-1626.

174. Lee, H. B.; Yu, M. R.; Song, J. S.;Ha, H. Reactive oxygen species amplify protein kinase C signaling in high glucose-induced fibronectin expression by human peritoneal mesothelial cells. *Kidney Int.* **2004**, *65* (4), 1170-1179.

175. Ahren, B.; Mansson, S.; Gingerich, R. L.;Havel, P. J. Regulation of plasma leptin in mice: influence of age, high-fat diet, and fasting. *Am.J Physiol* **1997**, *273* (1 Pt 2), R113-R120.

176. Naruhashi, K.; Sai, Y.; Tamai, I.; Suzuki, N.;Tsuji, A. PepT1 mRNA expression is induced by starvation and its level correlates with absorptive transport of cefadroxil longitudinally in the rat intestine. *Pharmaceutical research* **2002**, *19* (10), 1417-1423.

177. Zhou, Y.; Lee, J.; Reno, C. M.; Sun, C.; Park, S. W.; Chung, J.; Lee, J.; Fisher, S. J.; White, M. F.; Biddinger, S. B.;Ozcan, U. Regulation of glucose homeostasis through a XBP-1-FoxO1 interaction. *Nat.Med.* **2011**, *17* (3), 356-365.

178. Richardson, C. E.; Kinkel, S.;Kim, D. H. Physiological IRE-1-XBP-1 and PEK-1 signaling in Caenorhabditis elegans larval development and immunity. *PLoS Genet.* **2011**, *7* (11), e1002391-

179. Iadevaia, V.; Huo, Y.; Zhang, Z.; Foster, L. J.;Proud, C. G. Roles of the mammalian target of rapamycin, mTOR, in controlling ribosome biogenesis and protein synthesis. *Biochem.Soc.Trans.* **2012**, *40* (1), 168-172.

180. Lee, J.; Moir, R. D.; McIntosh, K. B.;Willis, I. M. TOR signaling regulates ribosome and tRNA synthesis via LAMMER/Clk and GSK-3 family kinases. *Mol.Cell* **2012**, *45* (6), 836-843.

181. Conde, R. D.;Scornik, O. A. Faster synthesis and slower degradation of liver protein during developmental growth. *Biochem.J* **1977**, *166* (1), 115-121.

182. Glimcher, L. H.;Lee, A. H. From sugar to fat: How the transcription factor XBP1 regulates hepatic lipogenesis. *Ann.N.Y.Acad.Sci.* **2009**, *1173 Suppl 1*E2-E9.

183. Seo, Y. H.; Jung, H. J.; Shin, H. T.; Kim, Y. M.; Yim, H.; Chung, H. Y.; Lim, I. K.;Yoon, G. Enhanced glycogenesis is involved in cellular senescence via GSK3/GS modulation. *Aging Cell* **2008**, *7* (6), 894-907.

184. Frame, S.;Cohen, P. GSK3 takes centre stage more than 20 years after its discovery. *Biochem.J* **2001**, *359* (Pt 1), 1-16.

185. Kay, M. A.;Jacobs-Lorena, M. Developmental genetics of ribosome synthesis in Drosophila. *Trends in Genetics* **1987**, *3*347-351.

186. Kerins, J. A.; Hanazawa, M.; Dorsett, M.;Schedl, T. PRP-17 and the pre-mRNA splicing pathway are preferentially required for the proliferation versus meiotic development decision and germline sex determination in Caenorhabditis elegans. *Developmental Dynamics* **2010**, *239* (5), 1555-1572.

187. Kamath, R. S.; Fraser, A. G.; Dong, Y.; Poulin, G.; Durbin, R.; Gotta, M.; Kanapin, A.; Le Bot, N.; Moreno, S.; Sohrmann, M.;others Systematic functional analysis of the Caenorhabditis elegans genome using RNAi. *Nature* **2003**, *421* (6920), 231-237.

188. Kamath, R. S.; Fraser, A. G.; Dong, Y.; Poulin, G.; Durbin, R.; Gotta, M.; Kanapin, A.; Le Bot, N.; Moreno, S.; Sohrmann, M.;others Systematic functional analysis of the Caenorhabditis elegans genome using RNAi. *Nature* **2003**, *421* (6920), 231-237.

189. Patel N.G. Protein Synthesis During Insect Development. *Insect Biochem.* **1971**, *1*391-427.

190. Tsang, W. Y.;Lemire, B. D. Mitochondrial genome content is regulated during nematode development. *Biochem.Biophys.Res Commun.* **2002**, *291* (1), 8-16.

191. De Cuyper, C.;Vanfleteren, J. R. Oxygen consumption during development and aging of the nematode Caenorhabditis elegans. *Comparative Biochemistry and Physiology Part A: Physiology* **1982**, *73* (2), 283-289.

192. Tabuse, Y.; Nabetani, T.;Tsugita, A. Proteomic analysis of protein expression profiles during Caenorhabditis elegans development using two-dimensional difference gel electrophoresis. *Proteomics* **2005**, *5* (11), 2876-2891.

193. Tsang, W. Y.;Lemire, B. D. Mitochondrial ATP synthase controls larval development cell nonautonomously in Caenorhabditis elegans. *Dev.Dyn.* **2003**, *226* (4), 719-726.

194. Simonis, N.; Rual, J. F.; Carvunis, A. R.; Tasan, M.; Lemmens, I.; Hirozane-Kishikawa, T.; Hao, T.; Sahalie, J. M.; Venkatesan, K.; Gebreab, F.; Cevik, S.; Klitgord, N.; Fan, C.; Braun, P.; Li, N.; yivi-Guedehoussou, N.; Dann, E.; Bertin, N.; Szeto, D.; Dricot, A.; Yildirim, M. A.; Lin, C.; de Smet, A. S.; Kao, H. L.; Simon, C.; Smolyar, A.; Ahn, J. S.; Tewari, M.; Boxem, M.; Milstein, S.; Yu, H.; Dreze, M.; Vandenhaute, J.; Gunsalus, K. C.; Cusick, M. E.; Hill, D. E.; Tavernier, J.; Roth, F. P.;Vidal, M. Empirically controlled mapping of the Caenorhabditis elegans protein-protein interactome network. *Nat.Methods* **2009**, *6* (1), 47-54.

195. Worrall, L. J.; Wear, M. A.; Page, A. P.;Walkinshaw, M. D. Cloning, purification and characterization of the Caenorhabditis elegans small glutamine-rich tetratricopeptide repeat-containing protein. *Biochim.Biophys.Acta* **2008**, *1784* (3), 496-503.

196. Nassl, A. M. Amino acid absorption and homeostasis in mice lacking the intestinal peptide transporter PEPT1, Universität München, 2012

197. Li, Y.; Na, K.; Lee, H. J.; Lee, E. Y.;Paik, Y. K. Contribution of sams-1 and pmt-1 to lipid homoeostasis in adult Caenorhabditis elegans. *J Biochem.* **2011**, *149* (5), 529-538.

198. Thomas, D.; Rothstein, R.; Rosenberg, N.;Surdin-Kerjan, Y. SAM2 encodes the second methionine S-adenosyl transferase in Saccharomyces cerevisiae: physiology and regulation of both enzymes. *Mol.Cell Biol.* **1988**, *8* (12), 5132-5139.

199. Ringlstetter Stefan Identification of the biotin transporter in Escherichia coli, biotinylation of histones in Saccharomyces cerevisiae and analysis of biotin sensing in Saccharomyces cerevisiae. Universität Regensburg, 2011

200. Perkins, D. N.; Pappin, D. J. C.; Creasy, D. M.;Cottrell, J. S. Probability-based protein identification by searching sequence databases using mass spectrometry data. *Electrophoresis* **1999**, *20*3551-3567.

201. Bindschedler, L. V.;Cramer, R. Fully automated software solution for protein quantitation by global metabolic labeling with stable isotopes. *Rapid Communications in Mass Spectrometry* **2011**, *25* (11), 1461-1471.

List of Figures

List of Tables

Abbreviations

2D-PAGE	two dimensional polyacrylamide gel electrophoresis
4-HNE	4-hydroxynonenal
AC	agglomerative coefficient
ANOVA	analysis of variance
ARE	antioxidant response element
ATP	Adenosintriphosphate
BBM	Brush border membrane
bds	binding sites
bp	base pair
Caco2	colorectal adenocarcinoma cell line
cDNA	complementary DNA
Col	colon
CyX	cycloheximide
DNA	Deoxyribonucleic acid
Duo	duodenum
ER	endoplasmatic reticulum
ERAD	ER associated degradation
ERK	extracellular regulated signaling kinases
FC	Fold change
FCS	fetal calf serum
GC-MS	gas chromatography-mass spectrometry
GFP	green fluorescent protein
GGT	γ- glutamyl transpeptidase
Glc	glucose
GLUT	Glucose Transporter
GlySar	Glycyl-sarcosine
GPx4	glutathione peroxidase
GS	GSH Synthetase
GSH	Glutathione (reduced)
GSK-3	Glycogen synthase kinase-3
H2O2	hydrogen peroxide
HepG2	liver hepatocellular carcinoma cell line
HO-1	heme oxygenase 1
IIS	Insulin/IGF-1 like signaling
kb	kilo base
kDa	kilo dalton
mRNA	messenger RNA
mTOR	mammalian target of rapamycin
NaN3	sodium azide
NGM	nematode growth medium
NQO1	NAD(P)H dehydrogenase [quinone] 1
Nrf2	nuclear factor erythoid 2-related factor 2
OSR	oxidative stress response
PEPT1	peptide transporter 1

PEPT2	peptide transporter 2
P*pept-1*	Promoter of *pept-1*
qRT-PCR	quantitative real time polymerase chain reaction
RLS	Reactive lipid species
RNA	ribonucleic acid
ROS	reactive oxygen species
SGLT-1	Sodium coupled glucose transporter 1
TCA	tricarboxylic acid
TF	transcription factor
UPR	unfolded protein response
WT	wild-type
γGCS	glutamate-cysteine ligase

Supplement

Overview of literature on factors regulating PEPT1

Table 19: Summary of literature reporting on regulation of PEPT1 either on transcriptional, translational or functional level in various experimental models.

Organism	Intervention	Effect	Reference	Diverse
Caco-2		SP1 basal transcription	Shimkura et al. 2005	Reporter constructs
Caco2	Butyrate	Increased promoter activity & uptake, CREB &Cdx2	Dalmasso et al. 2008	Reporter constructs, EMSA
Caco2	Leptin	Upregulation via Cdx2 Binding	Nduati et al. 2007	Identification of CREB element and Cdx2 bds
Caco2, mouse	0.2 nM Leptin	Upregulation of mRNA, protein & transport	Hindelt et al. 2009	Mediated via MAPK and S6K
Caco2, rat	1-100 nM Leptin 0-30 min	Increased Vmax, steady Km, increased apical PM appearance	Buyse et al. 2001	Only apical applied leptin showed effect, no change in mRNA
Caco2	EGF 26-28days	mRNA downregulation	Nielsen et al. 2003	No mechanism shown
Caco2	EGF and Insulin 60 min	Increased Vmax	Nielsen et al. 2003	No increase in PM abundance
Caco2	5 nM Insulin 2 hrs	Increased uptake	Watanabe et al. 2004	Translocation of PEPT1 upon insulin stimulus
Caco2	Insulin 60 min	Increase in Vmax	Thamotharan et al. 1999	Increased apical population, no mRNA change
Rat	STZ for 96 h or 1 month ± Insulin	Decrease due to STZ, rescue by insulin treatment	Bikhazi et al. 2004	Insulin treated rats still showed hyperglycemia
Rat	STZ	Increased apical protein & mRNA, also in kidney	Gangopadhyay et al. 2002	Increased mRNA stability, not transcription
Rat	STZ, Zucker-fa/fa and GK Jcl rats	STZ: reduction of PEPT1 uptake, Zucker/GK: increase in uptake & BBM abundance	Watanabe et al. 2003	mRNA did not change, effects only in duodenal uptake
Caco2, mouse	HFD, rosiglitazone, metformin	HFD: reduction of PEPT1 uptake, rosiglitazone: increase in protein &	Hindlet et al. 2012	Rosiglitazone mediates effect via

		uptake, metformin: decrease in mRNA, protein & uptake		mTOR, metformin inhibits transcription via AMPK
Caco2	Gly-Gln 14days	Increase in mRNA, protein & activity	Walker et al. 1998	both increased transcription and mRNA stability
Rat	High protein diet 14 days	Increase in mRNA	Erickson et al. 1995	
Goat	Infusion of soybean small peptides	Increase in mRNA	Hui et al. 2009	
Rat	AA and dipeptides	Increased in mRNA	Shiraga et al. 1999	No factor itself identified
Mouse	16 h fasting	Increase in protein	Ma et al. 2011	No change in mRNA
Rat	Fasting 4 days and refeeding, restricted food intake	Increase in mRNA & protein by starvation, reduction by refeeding	Ihara et al. 2000	Peak after 2 days of starvation followed by decrease
Rat	24 h fasting	Incresed mRNA & function	Thamotharan et al. 1999	No mechanism shown
Rat	48 h starvation	Increased mRNA	Naruhashi et al. 2002	No mechanism shown
Caco2, mouse, rat	48 fasting, PPARα ligand WY-14643	Increase in expression, directed by PPARα	Shimakura et al. 2006	Compared WT and PPARα -/-
Mouse	PPARα ligand WY-14643 and GW7647	No change in mRNA	Hirai et al. 2007	Compared WT and PPARα -/-
Zebrafish	*klf4a* morphants,	Decreased mRNA	Chen-Li et al. 2011	No direct interaction of Klf4a and promoter shown
Rat	$1,25(OH)_2D_3$ injected intraperitoneally for 4 days	Increased protein in intestine, decreased PepT1 in kidney	Chow et al. 2009	No mechanism shown
Caco2	100 nM $1,25(OH)2D_3$ 6 days	Decrease in mRNA	Fan et al. 2009	no change in protein
Rat	Circadian rhythm	mRNA changes over time	Saito et al. 2008	DBP shown to bind promoter
Rat	L-thyroxine	Decrease in mRNA, protein & uptake	Ashida et al. 2004	No mechanism shown
Mouse, rat	T_3 and T_4 supplement	Decrease in mRNA	Lu et al. 2006	No mechanism shown
Caco2	H_2O_2	Decreased uptake & protein	Altheld et al. 2004	Not shown on mRNA level

Role of transcription factor homologues in *C. elegans pept-1* gene expression

Literature was searched for already known TFs influencing *PEPT1* expression regardless of species. Subsequently a BLAST search was carried out to detect homologues in *C. elegans* (Table 20). This resulted in total in eight candidates of which five were further investigated.

Table 20: Transcription factors found in literature with potential or confirmed regulatory function on pept1 expression as well as their homologues in *C. elegans* found by BLAST search.

TF	Species	Reference	*C. elegans* homolog
ELT-2	*C. elegans*	McGhee et al. 2009	
DBP1	*mus musculus*	Saito et al. 2008	------
Cdx2	human	Nduati et al. 2007	PAL-1
SP1	human	Shimkura et al. 2005	SPTF-1
			SPTF-2
			SPTF-3
Klf4a	zebrafish	Chen-Li et al. 2011	KLF-1
			KLF-2
Nrf2	human		SKN-1

Although eight candidate TFs are listed, only the results of investigation of five are shown. RNAi construct of *klf-1* is not part of the RNAi library of Julie Ahringer, therefore only influence of KLF-2 was investigated. ELT-2 was shown to be a major regulator of intestinal gene expression during development and was even proposed to influence the expression of *pept-1* during development[33]. Unfortunately we had problems to down regulate this transcription factor due to its important role during ontogenesis. Therefore, we tried to over express ELT-2 in adult animals using a *C. elegans* strain expressing *elt-2* under the heat shock promoter *hsp16.2*, which was kindly provided by Prof. Dr. McGhee. So far up-regulation was only achieved by Prof. Dr. McGhee during embryogenesis, thus it was not surprising that we could not show elevation of ELT-2 in adult animals. Therefor we focused on the potential regulatory function of the remaining candidates.

KLF-2, SPTF-2 and SPTF-3

Genome of *C. elegans* encodes three kruppel-like transcription factors, of which KLF-2 is homologues to human WT1. However, its function in nematodes is hardly investigated. *C. elegans* also harbors three specificity protein related transcription factors (SPTF1 to 3). Using GFP fusion constructs expression of all three was shown throughout development and in adulthood. Nevertheless, their regulation and potential target genes are not known yet. TF of interest was down regulated using RNAi and subsequently promoter activity was measured using worms expressing

GFP under the control of 2,4 kb of the *pept-1* promoter, while change of protein

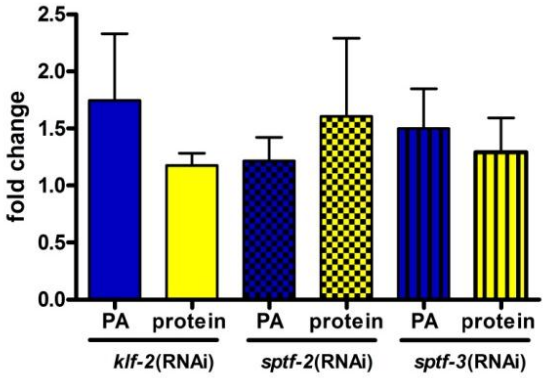

Figure 49: Influence of *klf-2, sptf-2* and *sptf-3*(RNAi) on pept-1 expression: Promoter activity of P*pept*-1:GFP and PEPT-1 protein levels after RNAi treatment depicted as fold change in relation to vector control treated animals. Each bar represents at least two independent experiments ± SEM

abundance was detected using western blot analysis of crude membrane protein extracts. Each experiment was at least conducted twice. Although RNAi of *klf-2* seemed to increase GFP signal, large variations between experiments in combination with no change in PEPT-1 protein abundance let to the conclusion of no direct influence of KLF-2 on *pept-1* expression. RNAi of *sptf-2* did not change promoter activity nor PEPT-1 protein levels consistently. The same was true for the third Sp-related transcription factor (SPTF-3) (Figure 49).

PAL-1

Expression and function of the homeobox protein PAL-1 was mainly investigated during embryogenesis of *C. elegans* PAL-1 is involved in specification of mesectodermal development. Therefore, we first examined its expression using a P*pal-1*::GFP fusion construct during larval development and adulthood. As a distinct GFP signal was detectable throughout larval development as well as in adult worms (Figure 50) its influence on *pept-1* expression was analyzed. While protein levels

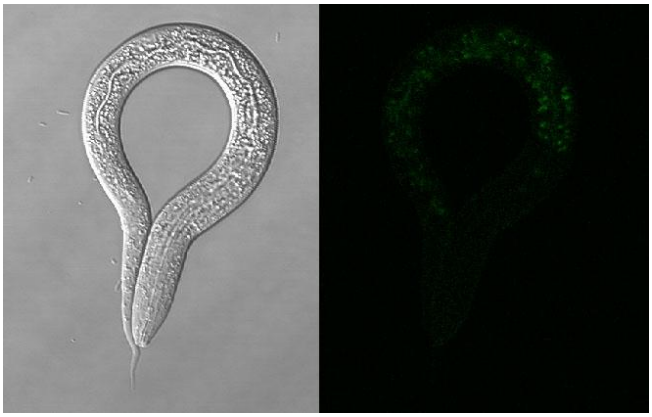

Figure 50: Adult nematode express *pal-1*: synchronized BW1851 were used to visualize pal-1:GFP using a confocal microscope at various time points during development. Bright field image of young adult nematode expressing GFP under the control of *pal-1* promoter, as seen in green on the right.

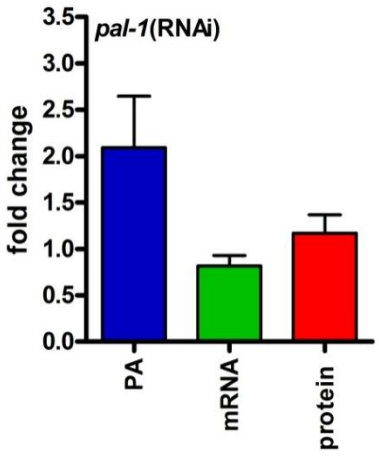

Figure 51: Influence of *pal-1*(RNAi) on *pept-1* expression: Promoter activity of *pept-1*, mRNA levels and protein abundance measured after *pal-1*(RNAi) in relation to vector control treated animals. Values depict at least three independent experiments ± SEM.

were slightly increased, mRNA abundance was rather reduced (Figure 51). Efficiency of RNAi was assessed by detecting *pal-1* mRNA levels, which showed a reduction of about 50 %. An even stronger decrease (~ 70 %) was observed for *sod-3* expression, while *gcs-1* and *xbp-1* total and spliced stayed unchanged. To check whether this decrease was due to increased DAF-16 activity, its localization was determined using a *C. elegans* strain expressing DAF-16::GFP fusion protein. Down regulation of *pal-1* did not alter DAF-16 distribution significantly (). Unfortunately literature did not give any hints on how *pal-1*(RNAi) could affect *sod-3* expression.

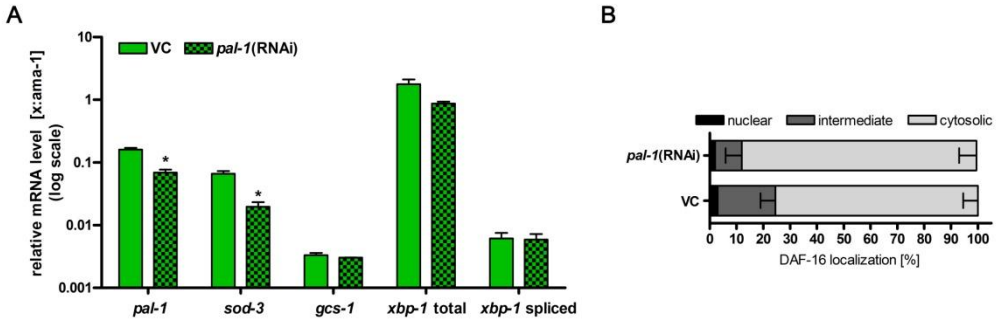

Figure 52: *pal-1*(RNAi) reduces *sod-3* mRNA independent on DAF-16 nuclear localization: (A) mRNA levels of Genes as noted on the x-axes, while log scale on the y-axes depicts values in relation to housekeeping gene ama-1. (B) TJ356 was grown for 7 days on *pal-1*(RNAi). DAF16::GFP was observed in at least hundred animals of two independent replicates scored under the confocal microscope

Inhibition of GSK3 in Caco2

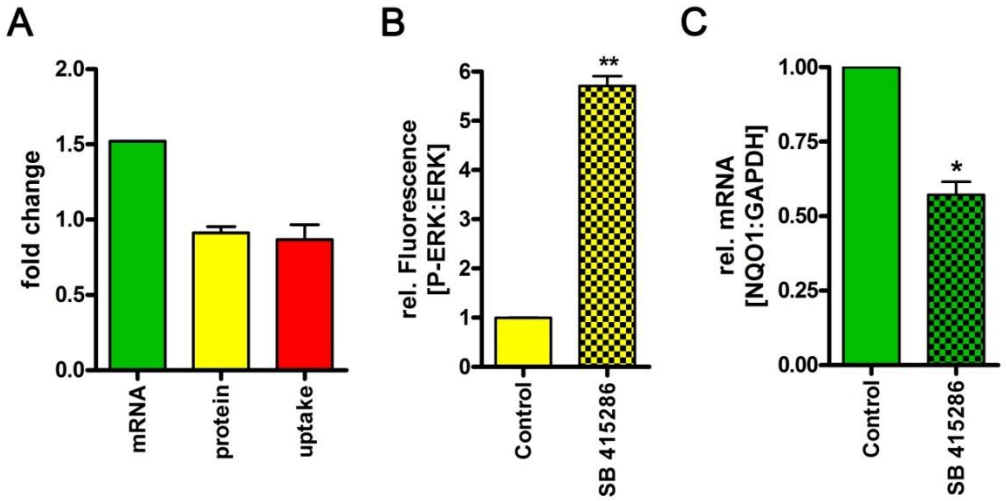

Figure 53: Inhibition of GSK3 shows controverse effects: (A) Effect of SB 415286 on *PEPT1* expression: PEPT1 mRNA, protein and uptake values after treatment with SB 415285 for 4 hrs in relation to DMSO control. (B) SB 415286 induces ERK phosphorylation: Protein levels of phosphorylated fraction of ERK in relation to total ERK after treatment with SB 415285. Two independent experiments ± SEM (C) Effect of SB 415286 on *NQO1* mRNA levels: Caco2 cells treated with SB 415285 for 4 hrs, before RNA was isolated and *NQO1* mRNA detected by qRT-PCR. Two independent experiments ± SEM

Life span

Table 21: Overview of Life span results

N2

RNAi	Median (days)	Subjects	log-rank test p-value
VC	14	144	
gsk-3	11	137	<0.0001
skn-1	12	144	<0.0001

pept-1(lg601)

RNAi	Median (days)	Subjects	log-rank test p-value
VC	12	83	
gsk-3	10	72	<0.0001
skn-1	7	100	<0.0001
gsk-3 skn-1	10	79	<0.0001

daf-2(e1370)

RNAi	Median (days)	Subjects	log-rank test p-value
VC	18	67	
gsk-3	21	80	0.0037
skn-1	13	57	<0.0001
gsk-3 skn-1	21	77	0.2144

daf-2(e1370) pept-1(lg601)

RNAi	Median (days)	Subjects	log-rank test p-value
VC	20	89	
gsk-3	20	106	0.04371
skn-1	16	156	0.0121
daf-16	14	151	<0.0001

Proteomics

Table 22: Proteins regulated during ontogenesis in WT: Proteins with p-values <0.05 in one-way ANOVA are listed with corresponding p-values of tukey posthoc test and fold changes of protein abundances between times

	p-Values			Fold change			
Accesion #	**20-40**	**20-60**	**60-40**	**FC4020**	**FC4060**	**FC2060**	**Cosmid Number**
Q18688	0,053755	0,053795	0,999999	3,095632	0,999799	3,095011	C47E8.5
Q9XXK1	0,022755	0,020383	0,972104	3,258664	1,028145	3,350380	H28O16.1
P53014	0,028606	0,030948	0,988110	0,568885	1,021693	0,581226	F09F7.2
P34697	0,004732	0,005118	0,963974	0,359547	1,047501	0,376626	C15F1.7
Q93572	0,038177	0,024048	0,696078	2,235609	1,102994	2,465863	F25H2.10
Q10454	0,012124	0,008296	0,627467	3,775721	1,104421	4,169984	F46H5.3
O02056	0,044387	0,060148	0,882706	2,770391	0,929004	2,573704	B0041.4
Q9N3X2	0,048549	0,077663	0,771681	2,846622	0,889966	2,533397	Y43B11AR.4
P34382	0,022345	0,022345	0,022345	0,460305	0,835544	0,384606	F02A9.2
O01802	0,030564	0,078473	0,392781	3,378172	0,784964	2,651743	F53G12.10
Q22866	0,001625	0,002267	0,390835	0,393069	1,169126	0,459547	Y105E8B.1
Q21215	0,037095	0,045184	0,940529	3,009844	0,951934	2,865172	K04D7.1
Q966C6	0,106230	0,045160	0,499661	2,259809	1,229484	2,778399	Y24D9A.4
O01530	0,003561	0,007217	0,195627	0,431838	1,284446	0,554672	F21F8.7
Q22037	0,040940	0,046793	0,972989	0,389905	1,077670	0,420189	F42A6.7
Q06561	0,030415	0,030415	0,030415	0,742889	0,989908	0,735391	ZC101.2
P34575	0,013898	0,013762	0,999700	3,564216	1,002508	3,573157	T20G5.2
P54412	0,181035	0,042202	0,248246	2,808090	1,546501	4,342713	F17C11.9
P55955	0,015173	0,031040	0,413392	0,368277	1,391644	0,512511	Y5F2A.1
Q21752	0,057280	0,021548	0,322833	5,122684	1,356096	6,946849	R05G6.7
P48150	0,019518	0,295080	0,053466	3,221808	0,526107	1,695015	F37C12.9
P91917	0,055446	0,046847	0,960993	4,535313	1,052519	4,773504	W08E3.3
P34500	0,004277	0,098952	0,012694	0,246985	3,089000	0,762936	K03H1.4
P52013	0,021179	0,029055	0,817101	0,422348	1,148968	0,485264	F31C3.1
Q9N358	0,053441	0,042145	0,922103	3,223010	1,065862	3,435285	Y55F3AR.3
Q10121	0,019563	0,019563	0,019563	0,506455	0,972059	0,492304	C23G10.2
Q9U1Q4	0,021864	0,009587	0,274482	4,567158	1,265618	5,780280	Y87G2A.5
Q10657	0,113877	0,044101	0,445029	1,986607	1,232444	2,448382	Y17G7B.7
P18948	0,999946	0,049016	0,049316	3,535594	306,145	1082,41	K07H8.6
Q03577	0,012523	0,014333	0,944996	3,763735	0,965773	3,634915	B0464.1
Q94300	0,041273	0,039190	0,995663	2,695172	1,012429	2,728670	T22F3.4
Q23500	0,032703	0,114614	0,275862	3,174269	0,730799	2,319752	ZK455.1
Q18785	0,030987	0,036220	0,957538	0,277718	1,146822	0,318493	C52E4.2
P34383	0,077565	0,001006	0,001950	3,141032	3,564456	11,1961	F02A9.3
O01805	0,004838	0,010328	0,210544	0,562660	1,179845	0,663852	C44E4.6
P34334	0,034125	0,053551	0,749092	3,979083	0,882069	3,509825	C14B9.7
Q23680	0,027967	0,033833	0,934825	0,490643	1,070620	0,525292	ZK970.4

	p-Values			Fold change			
Accesion #	**20-40**	**20-60**	**60-40**	**FC4020**	**FC4060**	**FC2060**	**Cosmid Number**
O44480	0,018901	0,022900	0,917465	3,392388	0,952805	3,232283	E04A4.8
O76840	0,000113	0,000291	0,035938	0,380335	1,260653	0,479471	C37C3.6
Q22633	0,019695	0,016520	0,923949	3,238323	1,044932	3,383828	T21C12.2
Q21276	0,001242	0,001695	0,364218	7,282535	0,909775	6,625467	K07C5.4
Q95008	0,053572	0,010857	0,095018	2,304396	1,449110	3,339324	F25H2.9
Q95Y04	0,001510	0,001510	0,001510	0,514277	0,917955	0,472083	Y41D4B.5
Q19749	0,025738	0,007454	0,116287	2,239949	1,305681	2,924660	F23B12.5
P49180	0,026270	0,037714	0,796817	3,071379	0,915395	2,811523	F10E7.7
Q9TZH6	0,030375	0,047934	0,730868	0,338429	1,308535	0,442846	T10B11.1
Q965S8	0,078494	0,037449	0,543258	1,435358	1,101597	1,581186	Y74C10AR.1
Q09665	0,009567	0,009567	0,009567	0,281066	0,821700	0,230952	ZK673.7
O18650	0,035704	0,019580	0,543802	2,080662	1,127882	2,346742	T05F1.3
Q10663	0,049522	0,032879	0,778774	2,969574	1,111168	3,299696	C05E4.9
Q9N3B0	0,000178	0,000375	0,047771	0,534897	1,134225	0,606693	Y54G2A.23
P49181	0,005374	0,003665	0,480205	5,174485	1,113639	5,762508	F37C12.4
P45971	0,019692	0,004662	0,060539	4,951559	1,524032	7,546335	T09A5.11
Q09610	0,010669	0,025318	0,270804	0,374296	1,443860	0,540432	R07B1.10
Q9TYK1	0,063197	0,059619	0,995662	1,675750	1,009399	1,691500	Y66H1A.4
P55954	0,023036	0,029805	0,875623	1,514867	0,969421	1,468545	Y37D8A.14
Q95YF3	0,700133	0,043334	0,075030	3,020861	3,784136	11,4313	C07H6.5
Q23445	0,067138	0,019946	0,225400	4,686246	1,455816	6,822311	ZK180.4
Q21217	0,064006	0,047464	0,889705	6,670892	1,105248	7,372989	K04D7.3
Q18787	0,012550	0,003540	0,062787	5,733807	1,455174	8,343685	C52E4.4
O17919	0,078713	0,031058	0,401888	3,335381	1,303227	4,346758	K01G5.5

Table 23: Overrepresented gene ontologies in data set of regulated proteins during development of WT

Category	Term	Count	%	P-Value	Benjamini
GOTERM_BP_FAT	translation	16	26,2	2,6E-11	6,8E-09
GOTERM_BP_FAT	nematode larval development	28	45,9	1,9E-06	0,00025
GOTERM_BP_FAT	larval development	28	45,9	1,9E-06	0,00017
GOTERM_BP_FAT	post-embryonic development	28	45,9	2,4E-06	0,00016
GOTERM_BP_FAT	growth	23	37,7	1,5E-05	0,00079
GOTERM_BP_FAT	embryonic development ending in birth or egg hatching	32	52,5	5,9E-05	0,0026
GOTERM_BP_FAT	generation of precursor metabolites and energy	7	11,5	0,00023	0,0087
GOTERM_BP_FAT	positive regulation of growth rate	23	37,7	0,00057	0,019

Category	Term	Count	%	P-Value	Benjamini
GOTERM_BP_FAT	regulation of growth rate	23	37,7	0,00058	0,017
GOTERM_BP_FAT	molting cycle, collagen and cuticulin-based cuticle	8	13,1	0,001	0,027
GOTERM_BP_FAT	molting cycle, protein-based cuticle	8	13,1	0,001	0,027
GOTERM_BP_FAT	molting cycle	8	13,1	0,0011	0,025
GOTERM_BP_FAT	regulation of growth	24	39,3	0,0014	0,031
GOTERM_BP_FAT	positive regulation of growth	23	37,7	0,0023	0,046
GOTERM_BP_FAT	ribosome biogenesis	4	6,6	0,0041	0,075
GOTERM_BP_FAT	aging	7	11,5	0,0047	0,079
GOTERM_BP_FAT	multicellular organismal aging	7	11,5	0,0047	0,079
GOTERM_BP_FAT	determination of adult life span	7	11,5	0,0047	0,079
GOTERM_BP_FAT	ribonucleoprotein complex biogenesis	4	6,6	0,0048	0,077
GOTERM_BP_FAT	tricarboxylic acid cycle	3	4,9	0,0081	0,12
GOTERM_BP_FAT	acetyl-CoA catabolic process	3	4,9	0,0081	0,12
GOTERM_BP_FAT	aerobic respiration	3	4,9	0,0088	0,12
GOTERM_BP_FAT	coenzyme catabolic process	3	4,9	0,0088	0,12
GOTERM_BP_FAT	cofactor catabolic process	3	4,9	0,0088	0,12
GOTERM_BP_FAT	acetyl-CoA metabolic process	3	4,9	0,0096	0,13
GOTERM_BP_FAT	coenzyme metabolic process	4	6,6	0,019	0,23
GOTERM_BP_FAT	cellular respiration	3	4,9	0,032	0,33
GOTERM_BP_FAT	ncRNA metabolic process	4	6,6	0,041	0,4
GOTERM_BP_FAT	energy derivation by oxidation of organic compounds	3	4,9	0,043	0,4
GOTERM_BP_FAT	pyruvate metabolic process	2	3,3	0,045	0,4
GOTERM_BP_FAT	cofactor metabolic process	4	6,6	0,052	0,43
GOTERM_BP_FAT	translational elongation	2	3,3	0,075	0,55
GOTERM_BP_FAT	protein folding	3	4,9	0,087	0,59

Table 24: Functional annotation clustering of regulated proteins during development of WT

Annotation Cluster 1	**Enrichment Score: 11.01**	**Count**	**P_Value**	**Benjamini**
SP_PIR_KEYWORDS	ribonucleoprotein	16	1.2E-20	1.3E-18
SP_PIR_KEYWORDS	ribosomal protein	13	1.7E-16	1.3E-14
GOTERM_CC_FAT	ribonucleoprotein complex	16	1.2E-14	7.4E-13
GOTERM_CC_FAT	ribosome	13	5.6E-12	1.7E-10
GOTERM_BP_FAT	translation	16	2.6E-11	6.8E-9
GOTERM_CC_FAT	intracellular non-membrane-bounded organelle	18	1.3E-10	2.6E-9
GOTERM_CC_FAT	non-membrane-bounded organelle	18	1.3E-10	2.6E-9
GOTERM_MF_FAT	structural constituent of ribosome	12	1.0E-8	1.4E-6
KEGG_PATHWAY	Ribosome	13	1.7E-8	4.4E-7
GOTERM_MF_FAT	structural molecule activity	12	7.7E-4	5.2E-2
Annotation Cluster 2	**Enrichment Score: 5.22**	**Count**	**P_Value**	**Benjamini**
GOTERM_BP_FAT	nematode larval development	28	1.9E-6	2.5E-4
GOTERM_BP_FAT	larval development	28	1.9E-6	1.7E-4
GOTERM_BP_FAT	post-embryonic development	28	2.4E-6	1.6E-4
GOTERM_BP_FAT	growth	23	1.5E-5	7.9E-4
GOTERM_BP_FAT	embryonic development ending in birth or egg hatching	32	5.9E-5	2.6E-3
Annotation Cluster 3	**Enrichment Score: 2.99**	**Count**	**P_Value**	**Benjamini**
GOTERM_BP_FAT	positive regulation of growth rate	23	5.7E-4	1.9E-2
GOTERM_BP_FAT	regulation of growth rate	23	5.8E-4	1.7E-2
GOTERM_BP_FAT	regulation of growth	24	1.4E-3	3.1E-2
GOTERM_BP_FAT	positive regulation of growth	23	2.3E-3	4.6E-2
Annotation Cluster 4	**Enrichment Score: 2.98**	**Count**	**P_Value**	**Benjamini**
GOTERM_BP_FAT	molting cycle, protein-based cuticle	8	1.0E-3	2.7E-2
GOTERM_BP_FAT	molting cycle, collagen and cuticulin-based cuticle	8	1.0E-3	2.7E-2
GOTERM_BP_FAT	molting cycle	8	1.1E-3	2.5E-2
Annotation Cluster 5	**Enrichment Score: 2.96**	**Count**	**P_Value**	**Benjamini**
SP_PIR_KEYWORDS	Secreted	9	4.4E-8	1.7E-6
SP_PIR_KEYWORDS	signal	12	5.4E-8	1.5E-6
GOTERM_CC_FAT	extracellular region	9	1.1E-4	1.7E-3

Annotation Cluster 5	**Enrichment Score: 2.96**	**Count**	**P_Value**	**Benjamini**
SP_PIR_KEYWORDS	glycoprotein	7	2.1E-3	1.8E-2
SP_PIR_KEYWORDS	disulfide bond	4	4.0E-2	2.1E-1
UP_SEQ_FEATURE	signal peptide	12	1.5E-1	1.0E0
UP_SEQ_FEATURE	disulfide bond	4	7.7E-1	1.0E0
UP_SEQ_FEATURE	glycosylation site:N-linked (GlcNAc...)	7	8.2E-1	1.0E0
Annotation Cluster 6	**Enrichment Score: 2.33**	**Count**	**P_Value**	**Benjamini**
GOTERM_BP_FAT	multicellular organismal aging	7	4.7E-3	7.9E-2
GOTERM_BP_FAT	aging	7	4.7E-3	7.9E-2
GOTERM_BP_FAT	determination of adult life span	7	4.7E-3	7.9E-2
Annotation Cluster 7	**Enrichment Score: 2.21**	**Count**	**P_Value**	**Benjamini**
SP_PIR_KEYWORDS	rna-binding	6	2.1E-5	3.0E-4
GOTERM_MF_FAT	RNA binding	6	3.5E-2	8.1E-1
SP_PIR_KEYWORDS	nucleus	5	3.1E-1	8.2E-1
Annotation Cluster 8	**Enrichment Score: 2.07**	**Count**	**P_Value**	**Benjamini**
GOTERM_BP_FAT	generation of precursor metabolites and energy	7	2.3E-4	8.7E-3
SP_PIR_KEYWORDS	tricarboxylic acid cycle	3	1.2E-3	1.1E-2
GOTERM_BP_FAT	tricarboxylic acid cycle	3	8.1E-3	1.2E-1
GOTERM_BP_FAT	acetyl-CoA catabolic process	3	8.1E-3	1.2E-1
GOTERM_BP_FAT	coenzyme catabolic process	3	8.8E-3	1.2E-1
GOTERM_BP_FAT	cofactor catabolic process	3	8.8E-3	1.2E-1
GOTERM_BP_FAT	aerobic respiration	3	8.8E-3	1.2E-1
GOTERM_BP_FAT	acetyl-CoA metabolic process	3	9.6E-3	1.3E-1
GOTERM_BP_FAT	coenzyme metabolic process	4	1.9E-2	2.3E-1
GOTERM_BP_FAT	cellular respiration	3	3.2E-2	3.3E-1
GOTERM_BP_FAT	energy derivation by oxidation of organic compounds	3	4.3E-2	4.0E-1
GOTERM_BP_FAT	cofactor metabolic process	4	5.2E-2	4.5E-1
Annotation Cluster 9	**Enrichment Score: 1.84**	**Count**	**P_Value**	**Benjamini**
SP_PIR_KEYWORDS	mitochondrion	6	1.6E-4	2.0E-3
SP_PIR_KEYWORDS	transit peptide	5	1.6E-4	1.9E-3
GOTERM_CC_FAT	mitochondrial part	6	6.3E-4	7.8E-3
GOTERM_CC_FAT	mitochondrion	6	4.2E-3	4.3E-2
GOTERM_CC_FAT	organelle lumen	5	5.0E-3	4.4E-2
GOTERM_CC_FAT	intracellular organelle lumen	5	5.0E-3	4.4E-2

Annotation Cluster 9	**Enrichment Score: 1.84**	**Count**	**P_Value**	**Benjamini**
GOTERM_CC_FAT	membrane-enclosed lumen	5	5.8E-3	4.4E-2
GOTERM_CC_FAT	mitochondrial matrix	3	1.6E-2	1.0E-1
GOTERM_CC_FAT	mitochondrial lumen	3	1.6E-2	1.0E-1
SP_PIR_KEYWORDS	transferase	6	2.5E-2	1.5E-1
GOTERM_CC_FAT	organelle membrane	4	7.3E-2	3.8E-1
UP_SEQ_FEATURE	transit peptide:Mitochondrion	5	8.0E-2	1.0E0
GOTERM_CC_FAT	mitochondrial membrane	3	9.0E-2	4.1E-1
GOTERM_CC_FAT	mitochondrial envelope	3	9.4E-2	4.0E-1
GOTERM_CC_FAT	organelle envelope	3	1.3E-1	4.9E-1
GOTERM_CC_FAT	envelope	3	1.6E-1	5.1E-1
SP_PIR_KEYWORDS	membrane	4	6.9E-1	9.9E-1
Annotation Cluster 10	**Enrichment Score: 0.82**	**Count**	**P_Value**	**Benjamini**
GOTERM_BP_FAT	negative regulation of multicellular organism growth	3	1.2E-1	7.3E-1
GOTERM_BP_FAT	negative regulation of multicellular organismal process	3	1.2E-1	7.3E-1
GOTERM_BP_FAT	negative regulation of growth	3	1.2E-1	7.3E-1
GOTERM_BP_FAT	regulation of multicellular organism growth	5	2.8E-1	9.2E-1
Annotation Cluster 11	**Enrichment Score: 0.76**	**Count**	**P_Value**	**Benjamini**
GOTERM_MF_FAT	hydrogen ion transmembrane transporter activity	3	9.1E-2	9.6E-1
GOTERM_MF_FAT	monovalent inorganic cation transmembrane transporter activity	3	9.5E-2	9.4E-1
GOTERM_MF_FAT	inorganic cation transmembrane transporter activity	3	1.6E-1	9.8E-1
KEGG_PATHWAY	Oxidative phosphorylation	3	6.4E-1	1.0E0
Annotation Cluster 12	**Enrichment Score: 0.75**	**Count**	**P_Value**	**Benjamini**
GOTERM_BP_FAT	hermaphrodite genitalia development	8	1.6E-1	8.0E-1
GOTERM_BP_FAT	genitalia development	8	1.6E-1	8.0E-1
GOTERM_BP_FAT	reproductive developmental process	9	1.7E-1	8.0E-1
GOTERM_BP_FAT	reproductive process in a multicellular organism	6	1.7E-1	8.0E-1

Annotation Cluster 12	**Enrichment Score: 0.75**	**Count**	**P_Value**	**Benjamini**
GOTERM_BP_FAT	multicellular organism reproduction	6	1.7E-1	7.9E-1
GOTERM_BP_FAT	sex differentiation	8	2.3E-1	8.8E-1
Annotation Cluster 13	**Enrichment Score: 0.63**	**Count**	**P_Value**	**Benjamini**
SP_PIR_KEYWORDS	nucleotide-binding	10	8.2E-4	8.5E-3
SP_PIR_KEYWORDS	atp-binding	8	3.5E-3	2.8E-2
GOTERM_MF_FAT	purine ribonucleotide binding	10	5.1E-1	1.0E0
GOTERM_MF_FAT	ribonucleotide binding	10	5.1E-1	1.0E0
GOTERM_MF_FAT	purine nucleotide binding	10	5.9E-1	1.0E0
GOTERM_MF_FAT	ATP binding	8	6.1E-1	1.0E0
GOTERM_MF_FAT	adenyl ribonucleotide binding	8	6.2E-1	1.0E0
GOTERM_MF_FAT	nucleotide binding	11	6.4E-1	1.0E0
GOTERM_MF_FAT	adenyl nucleotide binding	8	6.9E-1	1.0E0
GOTERM_MF_FAT	purine nucleoside binding	8	6.9E-1	1.0E0
GOTERM_MF_FAT	nucleoside binding	8	7.0E-1	1.0E0
UP_SEQ_FEATURE	nucleotide phosphate-binding region:ATP	4	7.3E-1	1.0E0
Annotation Cluster 14	**Enrichment Score: 0.59**	**Count**	**P_Value**	**Benjamini**
SP_PIR_KEYWORDS	transport	5	1.0E-1	4.4E-1
SP_PIR_KEYWORDS	ion transport	3	2.1E-1	6.7E-1
GOTERM_BP_FAT	ion transport	3	8.3E-1	1.0E0
Annotation Cluster 15	**Enrichment Score: 0.4**	**Count**	**P_Value**	**Benjamini**
GOTERM_BP_FAT	reproductive process in a multicellular organism	6	1.7E-1	8.0E-1
GOTERM_BP_FAT	multicellular organism reproduction	6	1.7E-1	7.9E-1
GOTERM_BP_FAT	oviposition	3	5.6E-1	1.0E0
GOTERM_BP_FAT	reproductive behavior in a multicellular organism	3	5.7E-1	1.0E0
GOTERM_BP_FAT	reproductive behavior	3	5.8E-1	1.0E0
GOTERM_BP_FAT	behavior	3	7.5E-1	1.0E0
Annotation Cluster 16	**Enrichment Score: 0.28**	**Count**	**P_Value**	**Benjamini**
GOTERM_MF_FAT	endopeptidase activity	4	3.2E-1	1.0E0
GOTERM_MF_FAT	peptidase activity, acting on L-amino acid peptides	4	5.8E-1	1.0E0
GOTERM_MF_FAT	peptidase activity	4	6.3E-1	1.0E0
GOTERM_BP_FAT	proteolysis	4	6.7E-1	1.0E0
Annotation Cluster 17	**Enrichment Score: 0.21**	**Count**	**P_Value**	**Benjamini**
SP_PIR_KEYWORDS	iron	3	1.2E-1	4.8E-1
GOTERM_MF_FAT	calcium ion binding	3	4.9E-1	1.0E0
GOTERM_MF_FAT	iron ion binding	3	6.1E-1	1.0E0

Annotation Cluster 17	Enrichment Score: 0.21	Count	P_Value	Benjamini
SP_PIR_KEYWORDS	metal-binding	4	6.2E-1	9.8E-1
GOTERM_MF_FAT	metal ion binding	8	1.0E0	1.0E0
GOTERM_MF_FAT	cation binding	8	1.0E0	1.0E0
GOTERM_MF_FAT	ion binding	8	1.0E0	1.0E0
GOTERM_MF_FAT	transition metal ion binding	5	1.0E0	1.0E0

Table 25: Proteins showing time dependent regulation in *pept-1(lg601):* Listed are proteins with p-values <0.05 in one-way_ANOVA, depicted are corresponding p-values of Tukey posthoc test, and fold changes of protein abundance between time points.

	p-Values			Fold change			
Accesion #	**20-40**	**40-60**	**60-80**	**FC2040**	**FC4060**	**FC6080**	**Cosmid Number**
P02566	0,99817	**0,00188**	**0,00466**	0,92704	8,46527	0,32811	F11C3.3
P27604	0,42172	**0,01466**	**0,02334**	0,60268	3,77836	0,38961	K02F2.2
P52275	**0,04625**	**0,02241**	**0,01766**	0,47056	2,46660	0,36485	C36E8.5
P34575	0,06367	0,28205	0,07833	0,50392	1,50937	0,43131	T20G5.2
P52015	0,10213	0,99993	0,51143	0,54504	0,98752	0,67817	Y75B12B.2
P37806	0,26599	0,66049	0,76046	0,64225	0,71227	0,75729	F08B6.4
P34690	0,09626	0,05261	**0,03982**	0,48066	2,36972	0,38804	C47B2.3
Q966C6	0,26858	0,12126	0,08433	0,56888	2,09999	0,35273	Y24D9A.4
Q10657	0,07047	0,41807	0,21276	0,42676	1,57072	0,52513	Y17G7B.7
Q94300	0,06438	**0,04944**	**0,03661**	0,44752	2,36560	0,39174	T22F3.4
O02639	**0,03975**	0,12603	0,05020	0,43046	1,83965	0,41583	C09D4.5
P45971	0,99899	0,13949	0,20852	0,53560	21,89791	0,04183	T09A5.11
P47209	0,33771	**0,03579**	0,06038	0,27480	8,01555	0,17118	C07G2.3
O62327	**0,00639**	0,13896	0,06770	0,38189	1,51546	0,67279	R05H10.5
O45499	**0,03069**	0,64082	0,09353	0,48077	1,23446	0,45348	F39B2.6
Q9N4G9	0,09122	0,15400	0,09847	0,56908	1,60659	0,53199	Y71F9B.4

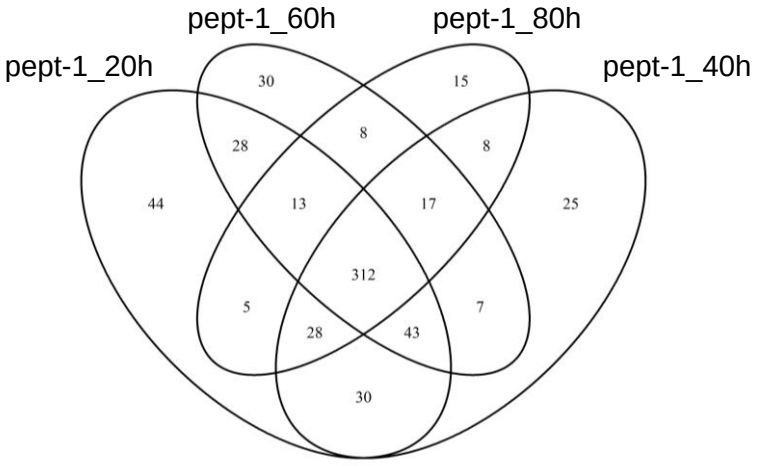

Figure 54 Venn diagram: Proteins identified in each replicate of each timepoint during development of *pept-1(lg601)*

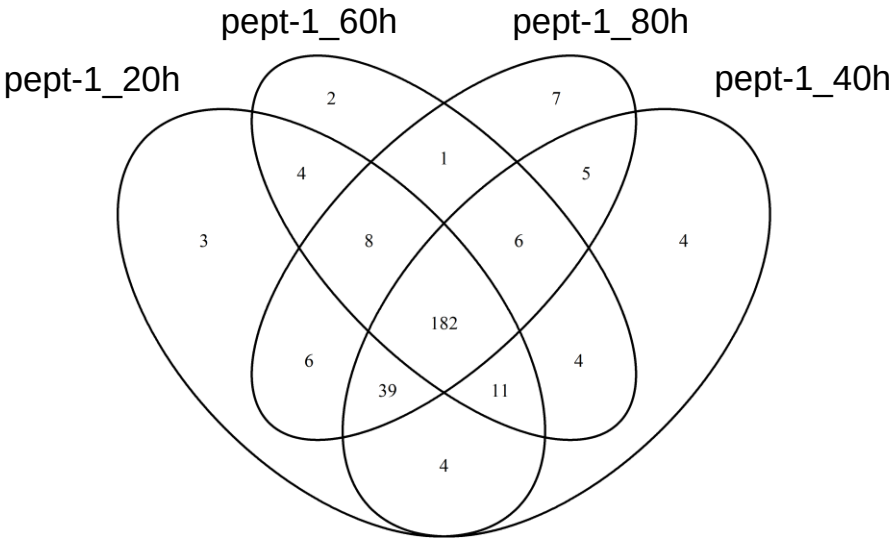

Figure 55: Venn diagram: Proteins identified and quantified in both replicates of each time point during development *pept-1(lg601)*

Table 26: Gene ontology by DAVID: Input: 15 proteins which were down-regulated between *pept-1(g601)* and WT after two-way ANOVA;

Category	Term	Count	%	P-Value	Benjamini
GOTERM_BP_FAT	nematode larval development	11	68,8	3,10E-04	4,30E-02
GOTERM_BP_FAT	larval development	11	68,8	3,10E-04	2,20E-02
GOTERM_BP_FAT	post-embryonic development	11	68,8	3,40E-04	1,60E-02
GOTERM_BP_FAT	protein folding	4	25	3,70E-04	1,30E-02
GOTERM_BP_FAT	growth	9	56,2	1,70E-03	4,70E-02
GOTERM_BP_FAT	embryonic development ending in birth or egg hatching	11	68,8	8,90E-03	1,90E-01
GOTERM_BP_FAT	positive regulation of growth rate	8	50	3,00E-02	4,60E-01
GOTERM_BP_FAT	regulation of growth rate	8	50	3,00E-02	4,20E-01
GOTERM_BP_FAT	positive regulation of growth	8	50	4,90E-02	5,50E-01
GOTERM_BP_FAT	regulation of growth	8	50	5,80E-02	5,70E-01
GOTERM_BP_FAT	translation	3	18,8	8,00E-02	6,60E-01
GOTERM_BP_FAT	body morphogenesis	4	25	9,50E-02	7,00E-01

Table 27: Functional annotation clustering by DAVID: Input: 15 proteins which were down-regulated between pept-1(g601) and WT after two-way ANOVA;

Annotation Cluster 1	**Enrichment Score: 4.31**	**Count**	**P_Value**	**Benjamini**
INTERPRO	Heat shock protein Hsp70	3	4.6E-5	1.9E-3
INTERPRO	Heat shock protein 70	3	4.6E-5	1.9E-3
INTERPRO	Heat shock protein 70, conserved site	3	5.5E-5	1.1E-3
Annotation Cluster 2	**Enrichment Score: 3.02**	**Count**	**P_Value**	**Benjamini**
GOTERM_BP_FAT	growth	9	9.2E-4	5.7E-2
GOTERM_BP_FAT	nematode larval development	10	9.4E-4	3.9E-2
GOTERM_BP_FAT	larval development	10	9.4E-4	2.9E-2
GOTERM_BP_FAT	post-embryonic development	10	1.0E-3	2.6E-2
Annotation Cluster 3	**Enrichment Score: 2.54**	**Count**	**P_Value**	**Benjamini**
SP_PIR_KEYWORDS	atp-binding	6	4.0E-5	1.9E-3
SP_PIR_KEYWORDS	nucleotide-binding	6	1.2E-4	2.9E-3
GOTERM_MF_FAT	adenyl nucleotide binding	8	2.3E-3	1.0E-1
GOTERM_MF_FAT	purine nucleoside binding	8	2.3E-3	5.2E-2
GOTERM_MF_FAT	nucleoside binding	8	2.4E-3	3.7E-2
GOTERM_MF_FAT	purine nucleotide binding	8	5.9E-3	6.7E-2
GOTERM_MF_FAT	ATP binding	7	8.4E-3	7.6E-2
GOTERM_MF_FAT	adenyl ribonucleotide binding	7	8.5E-3	6.5E-2
GOTERM_MF_FAT	nucleotide binding	8	1.3E-2	8.5E-2
GOTERM_MF_FAT	ribonucleotide binding	7	1.9E-2	1.1E-1
GOTERM_MF_FAT	purine ribonucleotide binding	7	1.9E-2	1.1E-1
Annotation Cluster 4	**Enrichment Score: 2.07**	**Count**	**P_Value**	**Benjamini**
GOTERM_CC_FAT	organelle lumen	3	8.3E-3	1.0E-1
GOTERM_CC_FAT	intracellular organelle lumen	3	8.3E-3	1.0E-1
GOTERM_CC_FAT	membrane-enclosed lumen	3	9.0E-3	5.7E-2
Annotation Cluster 5	**Enrichment Score: 1.66**	**Count**	**P_Value**	**Benjamini**
SP_PIR_KEYWORDS	ribosomal protein	3	1.9E-3	2.2E-2
SP_PIR_KEYWORDS	ribonucleoprotein	3	2.8E-3	2.6E-2
GOTERM_CC_FAT	ribosome	3	1.0E-2	5.1E-2
GOTERM_CC_FAT	ribonucleoprotein complex	3	1.7E-2	6.0E-2
GOTERM_MF_FAT	structural constituent of ribosome	3	3.6E-2	1.8E-1
GOTERM_BP_FAT	translation	3	7.1E-2	5.7E-1
KEGG_PATHWAY	Ribosome	3	8.1E-2	8.2E-1
GOTERM_MF_FAT	structural molecule activity	3	2.6E-1	7.5E-1
Annotation Cluster 6	**Enrichment Score: 1.58**	**Count**	**P_Value**	**Benjamini**
GOTERM_BP_FAT	positive regulation of growth rate	8	1.9E-2	3.0E-1
GOTERM_BP_FAT	regulation of growth rate	8	1.9E-2	2.7E-1
GOTERM_BP_FAT	positive regulation of growth	8	3.3E-2	3.8E-1
GOTERM_BP_FAT	regulation of growth	8	3.9E-2	4.0E-1

Table 28: Gene ontology by DAVID: Input: 30 proteins which showed time*strain interaction between *pept-1(g601)* and WT after two-way ANOVA and grouped in cluster 2 of hierarchical cluster.

Category	Term	Count	%	P-Value	Benjamini
GOTERM_BP_FAT	translation	15	50	5,1E-15	6,6E-13
GOTERM_BP_FAT	embryonic development ending in birth or egg hatching	23	76,7	1,1E-07	0,0000072
GOTERM_BP_FAT	nematode larval development	18	60	3,3E-06	0,00014
GOTERM_BP_FAT	larval development	18	60	3,3E-06	0,00011
GOTERM_BP_FAT	post-embryonic development	18	60	3,9E-06	0,0001
GOTERM_BP_FAT	growth	16	53,3	4,3E-06	0,000092
GOTERM_BP_FAT	multicellular organismal aging	5	16,7	0,0079	0,14
GOTERM_BP_FAT	determination of adult life span	5	16,7	0,0079	0,14
GOTERM_BP_FAT	aging	5	16,7	0,0079	0,14
GOTERM_BP_FAT	pyruvate metabolic process	2	6,7	0,023	0,31
GOTERM_BP_FAT	translational elongation	2	6,7	0,039	0,44
GOTERM_BP_FAT	protein polymerization	2	6,7	0,058	0,54
GOTERM_BP_FAT	generation of precursor metabolites and energy	3	10	0,074	0,59
GOTERM_BP_FAT	glycolysis	2	6,7	0,083	0,61

Table 29: Functional annotation clustering by DAVID: Input30 proteins which showed time*strain interaction between *pept-1(g601)* and WT after two-way ANOVA and grouped in cluster 2 of hierarchical cluster.

Annotation Cluster 1	Enrichment Score 16.22	Count	P_Value	Benjamini
SP_PIR_KEYWORDS	ribosomalprotein	15	2.2E-25	1.2E-23
SP_PIR_KEYWORDS	ribonucleoprotein	15	3.6E-24	9.8E-23
GOTERM_CC_FAT	ribosome	15	5.2E-19	1.7E-17
GOTERM_CC_FAT	ribonucleoprotei complex	15	2.3E-17	3.7E-16
GOTERM_MF_FAT	structral constituent of ribosome	14	2.3E-15	1.5E-13
GOTERM_BP_FAT	translation	15	5.1E-15	6.6E-13
GOTERM_CC_FAT	intracellulr non-membran-bounded organelle	17	2.4E-14	2.7E-13
GOTERM_CC_FAT	non-membrane-boundedorganelle	17	2.4E-14	2.7E-13
KEGG_PATHWAY	Ribosome	15	3.4E-13	4.4E-12
GOTERM_MF_FAT	structuralmolecule activity	16	3.0E-11	1.0E-9
Annotation Cluster 2	**Enrichment Score 5.43**	**Count**	**P_Value**	**Benjamini**
GOTERM_BP_FAT	nematod elarval development	18	3.3E-6	1.4E-4
GOTERM_BP_FAT	larvaldevelopment	18	3.3E-6	1.1E-4
GOTERM_BP_FAT	post-embryonicdevelopment	18	3.9E-6	1.0E-4

Annotation Cluster 2	**Enrichment Score 5.43**	**Count**	**P_Value**	**Benjamini**
GOTERM_BP_FAT	growth	16	4.3E-6	9.2E-5
Annotation Cluster 3	**Enrichment Score 2.15**	**Count**	**P_Value**	**Benjamini**
SP_PIR_KEYWORDS	mitochondrion	4	1.9E-3	3.3E-2
GOTERM_CC_FAT	mitochondrialpart	4	7.9E-3	5.1E-2
GOTERM_CC_FAT	mitochondrion	4	2.5E-2	1.3E-1
Annotation Cluster 4	**Enrichment Score 2.10**	**Count**	**P_Value**	**Benjamini**
GOTERM_BP_FAT	aging	5	7.9E-3	1.4E-1
GOTERM_BP_FAT	determinationof adult life span	5	7.9E-3	1.4E-1
GOTERM_BP_FAT	multicelllar organismal aging	5	7.9E-3	1.4E-1
Annotation Cluster 5	**Enrichment Score 1.56**	**Count**	**P_Value**	**Benjamini**
GOTERM_CC_FAT	mitochondrialmatrix	3	5.6E-3	4.5E-2
GOTERM_CC_FAT	mitochondriallumen	3	5.6E-3	4.5E-2
SP_PIR_KEYWORDS	transitpeptide	3	7.8E-3	1.0E-1
GOTERM_CC_FAT	intracellularorganelle lumen	3	6.3E-2	2.7E-1
GOTERM_CC_FAT	organellelumen	3	6.3E-2	2.7E-1
GOTERM_CC_FAT	membrane-enclosedlumen	3	6.8E-2	2.5E-1
UP_SEQ_FEATURE	transitpeptide:mitochondrion	3	1.9E-1	9.8E-1
Annotation Cluster 6	**Enrichment Score 0.97**	**Count**	**P_Value**	**Benjamini**
SP_PIR_KEYWORDS	gtp-binding	3	2.4E-2	2.3E-1
UP_SEQ_FEATURE	nucleotidephosphate-bindingregion:GTP	3	1.0E-1	9.5E-1
GOTERM_MF_FAT	GT Pbinding	3	1.8E-1	9.9E-1
GOTERM_MF_FAT	guan ylribonucleotide binding	3	1.8E-1	9.7E-1
GOTERM_MF_FAT	guanylnucleotide bidnding	3	1.8E-1	9.4E-1
Annotation Clusgter 7	**Enrichment Score 0.7**	**Count**	**P_Value**	**Benjamini**
GOTERM_BP_FAT	moltingcycle protein-based cuticle	3	2.0E-1	9.6E-1
GOTERM_BP_FAT	moltin cycle, collagen, cuticle cuticulin based	3	2.0E-1	9.6E-1
GOTERM_BP_FAT	molng cycle	3	2.0E-1	9.4E-1
Annotation Cluster 8	**Enrichment Score 0.44**	**Count**	**P_Value**	**Benjamini**
GOTERM_BP_FAT	regulationof growth	9	3.2E-1	9.9E-1
GOTERM_BP_FAT	positiv regulation of growth rate	8	3.4E-1	9.9E-1
GOTERM_BP_FAT	regulation of growth rate	8	3.4E-1	9.8E-1
GOTERM_BP_FAT	positiveregulation of growth rate	8	4.5E-1	9.9E-1

Annotation Cluster 9	**Enrichment Score 0.34**	**Count**	**P_Value**	**Benjamini**
GOTERM_BP_FAT	hermaphrodite genitalia development	4	4.0E-1	9.9E-1
GOTERM_BP_FAT	genitalia development	4	4.1E-1	9.9E-1
GOTERM_BP_FAT	sex differentiation	4	4.8E-1	9.9E-1
GOTERM_BP_FAT	reproductive developmental process	4	5.3E-1	1.0E0
Annotation Cluster 10	**Enrichment Score 0.23**	**Count**	**P_Value**	**Benjamini**
SP_PIR_KEYWORDS	nucleotide-binding	4	1.2E-1	6.3E-1
GOTERM_MF_FAT	ribonucleotide binding	4	8.5E-1	1.0E0
GOTERM_MF_FAT	purineribonucleotide binding	4	8.5E-1	1.0E0
GOTERM_MF_FAT	purine nucleotide binding	4	8.8E-1	1.0E0
GOTERM_MF_FAT	nucleotide binding	4	9.4E-1	1.0E0

Acknowledgments

Es ist unmöglich all die Leute aufzuzählen die Spuren in mir und meiner Arbeit hinterlassen haben. Deshalb hoffe ich dass mir die Unvollständigkeit der Liste nicht übel genommen wird, denn sie ist nur meinem unzulänglichem Gedächtnis zu zuschreiben:

Marc Smales for getting me addicted to science

Ingolf Krause für die Faszination der Massenspektrometrie

Irmgard Sperrer für die Beständigkeit bei der Hilfe mit den zahlreichen Western Blots

Katrin Lasch (die Pipettiergöttin) für die unermüdliche Hege und Pflege von Zellen und Würmern

Margot Siebler und **Beate Rauscher** für die vielen Ermunterungen zur richtigen Zeit

Barbara Gelhaus für mehr als nur für die Gespräche, für Verständnis und Vertrauen

Christine Schulze für die Freundschaft, für das Ohr, die Ruhe, das Lachen und die offenen Arme

Dem **Littel** und **Sperrer Cla**n für ein Stückchen Heimat

Jaquceline Benner für Kaffee, die Zeit, die Worte und das Ohr dazu

Gregor Grünz für die bezaubernden Komplimente die mir sooft den Tag gerettet haben

Melina Claussnitzer für die Offenheit und den Austausch

Verena Hirschberg, Laure Fourchaud and **Ramona Menezes for the friendship that does not care about countries**

Mena Marth und **Manuela Sailer** für den Spass und die Arbeit an R

Jürgen Stolz und **Stefan Ringlstetter** für die Methodenvielfalt

Den Bachelors und Masterpraktikanten: Anja Hermann, Stafanie Maurer, Isabel Schulien, Teresa Kellerer, Fabian Tetzlaff und Katharina Wozny für ihre tolle Arbeit

Anna Kipp für die Kooperation und den Austausch von Wissenschaft und Leben

Katja Kuhlmann für die Erfahrung und die Kooperation

Britta Spanier für die Freiheit und die Unterstützung

Die BoKu für den Kaffee und den Grill und beides in der Sonne

Frau Daniel für das Fördern, das Fordern, die Freiheit und das Vertrauen

Meinen Eltern, weil sie mir den Rücken frei gehalten haben

Meiner Schwester und **Robert** für die kleinen und großen Hilfen in allen Lebenslagen

Marc Kästle, weil mit dir aus A und B ganz einfach „AB“ jetzt wird

Erklärung

Hiermit versichere ich, dass ich die vorliegende Arbeit

Transcriptional regulation of the peptide transporter 1 and its role in development in Caenorhabditis elegans assessed by proteome analysis.

selbständig verfasst und keine anderen als die angegebenen Quellen und Hilfsmittel verwendet habe. Die den benutzten Quellen wörtlich oder inhaltlich übernommenen Stellen sind als solche kenntlich gemacht.

Die Arbeit hat in gleicher oder ähnlicher Form noch keiner anderen Prüfungsbehörde vorgelegen.

Freising, den